A history of solar activity over millennia

Ilya G. Usoskin[1] 📵

Abstract

Here we review present knowledge of the long-term behaviour of solar activity on a multi-millennial timescale, as reconstructed using the indirect proxy method. The concept of solar activity is discussed along with an overview of the dedicated indices used to quantify different aspects of variable solar activity, with special emphasis on sunspot numbers. Over long timescales, quantitative information about past solar activity is historically obtained using a method based on indirect proxies, such as cosmogenic isotopes ^{14}C and ^{10}Be in natural stratified archives (e.g., tree rings or ice cores). We give a historical overview of the development of the proxy-based method for past solar-activity reconstruction over millennia, as well as a description of the modern state of the art. Special attention is paid to the verification and cross-calibration of reconstructions. It is argued that the method of cosmogenic isotopes makes a solid basis for studies of solar variability in the past on a long timescale (centuries to millennia) during the Holocene (the past ~ 12 millennia). A separate section is devoted to reconstructions of extremely rare solar eruptive events in the past, based on both cosmogenic-proxy data in terrestrial and lunar natural archives, as well as statistics of sun-like stars. Finally, the main features of the long-term evolution of

---

Extended author information available on the last page of the article

solar magnetic activity, including the statistics of grand minima and maxima occurrence, are summarized and their possible implications, especially for solar/ stellar dynamo theory, are discussed.

Contents

1 Introduction

The concept of the perfectness and constancy of the sun, postulated by Aristotle, was a strong belief for centuries and an official doctrine of Christian and Muslim countries. However, as people had noticed already before the time of Aristotle, some slight transient changes in the sun can be observed even with the naked eye. Although scientists knew about the existence of "imperfect" spots on the sun since the early 17th century, it was only in the 19th century that the scientific community recognized that solar activity varies in the course of an 11-year solar cycle. Solar variability was later found to have many different manifestations, including the fact that the "solar constant", or the total solar irradiance, TSI, (the amount of total incoming solar electromagnetic radiation in all wavelengths per unit area at one astronomical unit, a.u.) is not a constant. The sun appears much more complicated and active than a static hot plasma ball, with a great variety of nonstationary active processes going beyond the adiabatic equilibrium foreseen in the basic theory of sun-as-star. Such transient nonstationary (often eruptive) processes can be broadly regarded as solar activity, in contrast to the so-called "quiet" sun. Solar activity includes active transient and long-lived phenomena on the solar photosphere and

corona, such as spectacular solar flares, sunspots, prominences, coronal mass ejections (CMEs), etc. Interesting stories on the history of sunspot observations and studies can be found in various books (e.g., Arlt and Vaquero 2020; Brody 2002; Tassoul and Tassoul 2004).

The very fact of the existence of solar activity posed an enigma for solar physics, leading to the development of sophisticated models of the sun's magnetic dynamo. The sun is the only star, which can be studied in great detail and thus can be considered as a proxy for cool stars. On the other hand, a study of the large population of sun-like stars can provide another view of the sun's behaviour. Quite a number of dedicated ground-based and space-borne experiments were and are being carried out to learn more about solar variability. The use of the sun as a paradigm for cool stars leads to a better understanding of the processes driving the broader population of cool sun-like stars. Therefore, studying and modelling solar activity can increase the level of our understanding of nature.

On the other hand, the study of variable solar activity is not of purely academic interest, as it directly affects the terrestrial environment. Although changes in the sun are barely visible without the aid of precise scientific instruments, these changes have a great impact on many aspects of our lives. In particular, the heliosphere (a spatial region of about 200–300 AU across) is mainly controlled by the solar magnetic field. This leads to the modulation of galactic cosmic rays (GCRs) by solar magnetic activity. Additionally, eruptive and transient phenomena in the sun/corona and in the interplanetary medium can lead to a sporadic acceleration of energetic particles with greatly enhanced flux. Such processes can modify the radiation environment on Earth and need to be taken into account for planning and maintaining space missions and even transpolar jet flights. Solar activity can cause, through the coupling of solar wind and the Earth's magnetosphere, strong geomagnetic storms, which may disturb radio-wave propagation and navigation-system stability, or induce dangerous spurious currents in long pipes or power lines. Another important aspect is a potential link between solar-activity variations and the Earth's climate (see, e.g., reviews by Dudok de Wit et al. 2015; Gray et al. 2010; Haigh 2007; Mironova et al. 2015).

It is important to study solar variability on different timescales. The primary basis for such studies is observational (or reconstructed) data. The sun's activity is systematically explored in different ways (solar, heliospheric, interplanetary, magnetospheric, terrestrial), including ground-based and space-borne experiments and dedicated space missions during the last few decades, thus covering 3–4 solar cycles. However, it should be noted that the modern epoch was characterized, until the earlier 2000s by high solar activity dominated by an 11-year cyclicity, and it is not straightforward to extrapolate present knowledge (especially empirical and semi-empirical relationships and models) to a longer timescale. The most recent cycles 23–25 indicate the return to the normal moderate level of solar activity, as manifested, e. g., via the extended and weak solar minimum in 2008–2009 and weak solar and heliospheric parameters, which are unusual for the space era but may be quite typical for the normal activity (see, e.g., Gibson et al. 2011). On the other hand, contrary to some predictions, a grand minimum of activity has not started. Thus, we may

experience, in the near future, interplanetary conditions quite different with respect to those we got used to during the last decades.

Therefore, the behaviour of solar activity in the past, before the era of direct measurements, is of great importance for a variety of reasons. For example, it allows an improved knowledge of the statistical behaviour of the solar-dynamo process, which generates the cyclically-varying solar magnetic field, making it possible to estimate the fractions of time the sun spends in states of very-low activity, called grand minima. Such studies require a long time series of solar-activity data. The longest direct series of solar activity is the 410-year-long sunspot-number series, which depicts the dramatic contrast between the (almost spotless) Maunder minimum and the modern period of very high activity. Thanks to the recent development of precise technologies, including accelerator mass spectrometry, solar activity can be reconstructed over multiple millennia from concentrations of cosmogenic isotopes ^{14}C and ^{10}Be in terrestrial archives. This allows one to study the temporal evolution of solar magnetic activity, and thus of the solar dynamo, on much longer timescales than are available from direct measurements.

This paper gives an overview of the present status of our knowledge of long-term solar activity, covering the period of the Holocene (the last ~ 12 millennia). A description of the concept of solar activity and a discussion of observational methods and indices are presented in Sect. 2. The proxy method of solar-activity reconstruction is described in some detail in Sect. 3. Section 4 gives an overview of what is known about past solar activity. The long-term averaged flux of solar energetic particles (SEPs) is discussed in Sect. 5. Finally, conclusions are summarized in Sect. 6.

2 Solar activity: concept and observations

2.1 The concept of solar activity

The sun is known to be far from a static state, the so-called "quiet" sun described by classical solar-structure theories, but instead goes through various nonstationary active processes. Such nonstationary and nonequilibrium (often eruptive) processes can be broadly regarded as solar activity. The concept of 'solar activity' is used since long (e.g., de La Rue et al. 1871) and is well established. The presence of magnetic activity, including stellar flares, is considered a common typical feature of sun-like stars (Maehara et al. 2012). Although a direct projection of the energy and occurrence frequency of superflares on sun-like stars (e.g., Shibata et al. 2013) does not agree with solar data (Aulanier et al. 2013) and terrestrial proxy (see Sect. 5), the existence of solar/stellar activity is clear. Whereas the concept of solar activity is quite a common term nowadays, it is neither straightforwardly interpreted nor unambiguously defined. For instance, solar-surface magnetic variability, eruption phenomena, coronal activity, radiation of the sun as a star or even interplanetary transients and geomagnetic disturbances can be related to the concept of solar activity. All these manifestations are driven by the solar magnetism. A variety of indices quantifying solar activity have been proposed in order to represent different observables and

caused effects. Most of the indices are highly correlated to each other due to the dominant 11-year cycle, but may differ in fine details and/or long-term trends. In addition to the solar indices, indirect proxy data is often used to quantify solar activity via its presumably known effect on the magnetosphere or heliosphere. The indices of solar activity that are often used for long-term studies are reviewed below.

2.2 Indices of solar activity

Solar (as well as other) indices can be divided into physical and synthetic according to the way, they are obtained/calculated. Physical indices quantify the directly-measurable values of a real physical observable, such as, e.g., the radioflux, and thus have a clear physical meaning as they quantify physical features of different aspects of solar activity and their effects. Synthetic indices (the most common being sunspot number) are calculated (or synthesized) using a special algorithm from observed (often not measurable in physical units) data or phenomena. Additionally, solar activity indices can be either direct (i.e., directly relating to the sun) or indirect (relating to indirect effects caused by solar activity), as discussed in subsequent Sects. 2.2.1 and 2.2.2.

2.2.1 Direct solar indices

The most commonly used index of solar activity is based on sunspot number. Sunspots are dark (as observed in white light) areas on the solar disc (of size up to tens of thousands of km, lifetime up to half a year), characterized by a strong magnetic field, which leads to a lower temperature (about 4000 K compared to 5800 K in the photosphere) and observed as darkening in the visible wavelength. The sunspot number is a synthetic, rather than a physical, index, but it is a useful parameter in quantifying the level of solar activity. This index presents the weighted number of individual sunspots and/or sunspot groups, calculated in a prescribed manner from simple visual solar observations. The use of the sunspot number makes it possible to combine together thousands and thousands of regular and fragmentary solar observations made by earlier professional and amateur astronomers. The technique, initially developed by Rudolf Wolf, yielded the longest series of directly and regularly observed scientific quantities. Therefore, it is common to quantify solar magnetic activity via sunspot numbers. For details see the review on sunspot numbers and solar cycles (Clette and Lefèvre 2016; Clette et al. 2023; Hathaway and Wilson 2004; Hathaway 2015).

Wolf (WSN) and International (ISN) sunspot number series

The concept of the sunspot number was developed by Rudolf Wolf of the Zürich observatory in the middle of the 19th century. The sunspot series, initiated by him, is called the Zürich or Wolf sunspot number (WSN) series. The relative sunspot number R_z is defined as
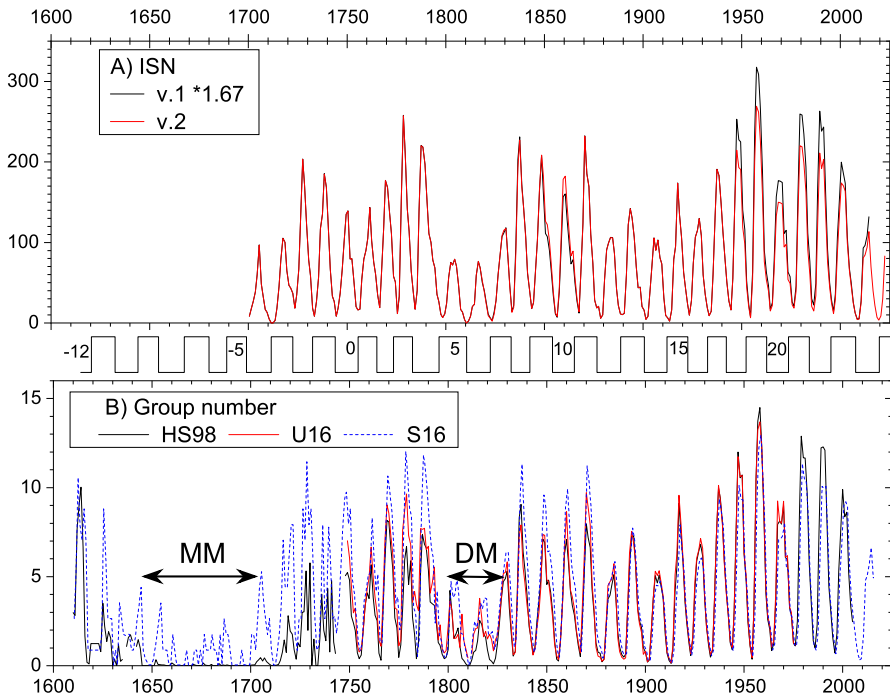
Fig. 1 Annual sunspot activity for the last centuries. **a** International sunspot number series versions 1 and 2 (the former is scaled with a 1.67 factor, see SILSO at http://sidc.be/silso/datafiles). **b** Number of sunspot groups: HS98—(Hoyt and Schatten 1998); U16—(Usoskin et al. 2016b); S16—(Svalgaard and Schatten 2016). Standard (Zürich) cycle numbering is shown between the panels. Approximate dates of the Maunder minimum (MM) and Dalton minimum (DM) are shown in the lower panel

$$R_z = k \cdot (10 \cdot G + N), \tag{1}$$

where G is the number of sunspot groups, N is the number of individual sunspots in all groups visible on the solar disc and k denotes the individual correction factor, which compensates for differences in observational techniques and instruments used by different observers, and is used to normalize different observations to each other.

The value of R_z (see Fig. 1a) is calculated for each day using only one observation made by the "primary" observer (judged as the most reliable observer during a given time) for the day. The primary observers were Staudacher (1749–1787), Flaugergues (1788–1825), Schwabe (1826–1847), Wolf (1848–1893), Wolfer (1893–1928), Brunner (1929–1944), Waldmeier (1945–1980) and Koeckelenbergh (since 1980). If observations by the primary observer are not available for a certain day, the secondary, tertiary, etc. observers are used (see the hierarchy of observers in Waldmeier 1961). The use of only one observer for each day aims to make R_z a homogeneous time series. As a drawback, such an approach ignores all other observations available for the day, which constitute a large fraction of the existing information. Moreover, possible errors of the primary observer cannot be caught or estimated. The observational uncertainties in the monthly R_z can be up to 25% (e.g.,

Vitinsky et al. 1986). The WSN series is based on observations performed at the Zürich Observatory during 1849–1981 using almost the same technique. This part of the series is fairly stable and homogeneous although an offset due to the change of the weighting procedure might have been introduced in 1945–1946 (Clette et al. 2014) but the correction for this effect is not clear and leads to uncertainties (Friedli 2020; Lockwood et al. 2014). However, prior to that, there have been many gaps in the data that were interpolated. If no sunspot observations are available for some period, the data gap is filled, without note in the final WSN series, using interpolation between the available data and by employing some proxy data. In addition, earlier parts of the sunspot series were "corrected" by Wolf using geomagnetic observation (see details in Svalgaard 2012), which makes the series less homogeneous. Therefore, the WSN series is a combination of direct observations and interpolations for the period before 1849, leading to possible errors and inhomogeneities as discussed, e.g, by Vitinsky et al. (1986), Wilson (1998), Letfus (1999), Svalgaard (2012), Clette et al. (2014). The quality of the Wolf series before 1749 is rather poor and hardly reliable (Hathaway and Wilson 2004; Hoyt et al. 1994; Hoyt and Schatten 1998).

The main problem of the WSN was a lack of documentation so that only the final product was available without information on the raw data, which made a full revision of the series hardly possible. Although this information does exist, it was hidden in hand-written notes of Rudolf Wolf and his successors. The situation is being improved now with an effort of the Rudolf Wolf Gesellschaft (http://www.wolfinstitute.ch) to scan and digitize the original Wolf's notes (Friedli 2020).

Note that the sun has been routinely photographed since 1876 so that full information on daily sunspot activity is available (the Greenwich series) with observational uncertainties being small compared to the observed variability, for the last 140 years.

The routine production of the WSN series was terminated in Zürich in 1982. Since then, the sunspot number series is routinely updated as the International sunspot number (ISN) R_i, provided by the Solar Influences Data Analysis Center in Belgium (Clette et al. 2007). The international sunspot number series is computed using the same definition (Eq. 1) as WSN but it has a significant distinction from the WSN: it is based not on a single primary solar observation for each day but instead uses a weighted average of more than 20 approved observers. The ISN (see SILSO at http://sidc.be/silso/datafiles) has been recently updated to version 2 with corrections to some known inhomogeneities (Clette et al. 2014). A potential user should know that the ISN (v.2) is calibrated to Wolfer, in contrast to earlier WSN and ISN (v.1) calibrated to Wolf. As a result, a constant scaling factor of 0.6 should be applied to compare ISN (v.2) to ISN (v.1). The two versions are shown in Fig. 1a. One can see that the ISN v.2 is is very close to v.1 (scaled up by a factor of 1.67) with a small difference after the 1940s, because of the correction for the *Waldmeier discontinuity* (see below).

During the Second World War, production of the sunspot numbers was launched in the US, known as the American relative sunspot number R_A (Shapley 1949). It is continuously updated since then (Schaefer 1997) under the auspices of the Department of Terrestrial Magnetism of the Carnegie Institute and the American Association of Variable Star Observers (AAVSO—https://www.aavso.org/aavso-sunspot-count-data), but is not widely used, since the ISN is considered the reference sunspot series.

In addition to the international sunspot number R_i, there is also a series of hemispheric sunspot numbers R_N and R_S, which account for spots only in the northern and southern solar hemispheres, respectively (note that $R_i = R_N + R_S$). These series are used to study the N-S asymmetry of solar activity (Temmer et al. 2002).

Group sunspot number (GSN) series

Since the WSN series is of lower quality before the 1850s and is hardly reliable before 1750, there was a need to re-evaluate early sunspot data. This tremendous work has been done by Hoyt and Schatten (1996, 1998), who performed an extensive archive search and nearly doubled the amount of original information compared to the Wolf series. They have produced a new series of sunspot activity called the group sunspot numbers (GSN—see Fig. 1b), which includes all available archival records. The daily group sunspot number R_g is defined as follows:

$$R_g = \frac{12.08}{n} \sum_i k_i' G_i, \tag{2}$$

where G_i is the number of sunspot groups recorded by the i-th observer, k_i' is the observer's individual correction factor, n is the number of observers for the particular day, and 12.08 is a normalization number scaling R_g to R_z values for the period of 1874–1976. However, the exact scaling factor 12.08 has recently been questioned due to an inhomogeneity within the RGO data between 1874–1885 (Cliver and Ling 2016; Willis et al. 2016). R_g is more robust than R_z or R_i since it is based on more easily identified sunspot groups and does not include the number of individual spots. By this, the GSN avoids a problem related to the visibility of small sunspots since a group of several small spots would appear as one blurred spot for an observer with a low-quality telescope. Another potential uncertainty may be related to a problem of grouping individual spots into sunspot groups consistently throughout ages (Clette et al. 2014). This uncertainty directly affecting the GSN is also important for WSN/ ISN series since the number of groups composes 50–90% of the WSN/ISN values. Another important advantage of the GSN series is that all the raw data are available. The GSN series includes not only one "primary" observation, but all available observations, and covers the period since 1610, being, thus, 140 years longer than the original WSN series. It is particularly interesting that the period of the Maunder minimum (1645–1715) was surprisingly well covered with daily observations (Hoyt and Schatten 1996; Ribes and Nesme-Ribes 1993) allowing for a detailed analysis of sunspot activity during this grand minimum (see also Sect. 4.2). Systematic uncertainties of the R_g values are estimated to be about 10% before 1640, less than 5% from 1640–1728 and from 1800–1849, 15–20% from 1728–1799, and about 1% since 1849 (Hoyt and Schatten 1998). The GSN series is more homogeneous and transparent than the WSN series before 1849. The two series are nearly identical after the 1870s (Hathaway and Wilson 2004; Hoyt and Schatten 1998; Letfus 1999). However, the GSN series still contains some lacunas, uncertainties and possible inhomogeneities (see, e.g., Cliver and Ling 2016; Letfus 2000; Usoskin et al. 2003a; Vaquero et al. 2012).

Updates of the series

The search for other lost or missing records of past solar instrumental observations has not ended even since the extensive work by Hoyt and Schatten. Archival searches still give new interesting findings of forgotten sunspot observations, often outside major observatories—see a detailed review book by Vaquero and Vázquez (2009) and original papers by Casas et al. (2006), Vaquero et al. (2005, 2007), Arlt (2008), Arlt (2009), Carrasco and Vaquero (2016). Interestingly, not only sunspot counts but also regular drawings, forgotten for centuries, are being restored nowadays in dusty archives. A very interesting work has been done by Rainer Arlt (Arlt 2008, 2009; Arlt and Abdolvand 2011; Arlt et al. 2013) on recovering, digitizing, and analyzing regular drawings by Schwabe of 1825–1867 and Staudacher of 1749–1796. This work led to the extension of the Maunder butterfly diagram for several solar cycles backwards (Arlt 2009; Arlt and Abdolvand 2011; Arlt et al. 2013; Usoskin et al. 2009c). Recently, more research groups joined the effort of the past data recovery, active being groups from Spain (Victor Carrasco and José Vaquero) and Japan (Hisashi Hayakawa). Recent findings of the lost data by several observers made it possible to correct some earlier uncertain data and revise the pattern of the solar variability in the past (e.g., Carrasco et al. 2020a, b, 2021a; Hayakawa et al. 2021a; Vaquero et al. 2011). In particular, the butterfly diagram has been extended, fragmentary covering four hundred years as shown in Fig. 2.

Recent corrections to the group number database have been collected (http://haso.unex.es/?q=content/data) by Vaquero et al. (2016) who updated the database of Hoyt and Schatten (1998) by correcting some errors and inexactitudes and adding more data.

Several inconsistencies and discontinuities have been found in the existing sunspot series. For instance, Leussu et al. (2013) have shown that the values of WSN before 1848 (when Wolf had started his observations) were overestimated by $\approx 20\%$ because of the incorrect $k-$factor ascribed by Wolf to Schwabe. This error, called the "Wolf discontinuity", erroneously alters the WSN/ISN series but does not affect the GSN series. Another reported error is the so-called "Waldmeier discontinuity" around 1947 (Clette et al. 2014), related to the fact that Waldmeier had modified the procedure of counting spots, including 'weighting' sunspot number, without proper noticing which led to a greater sunspot number compared to the standard technique.
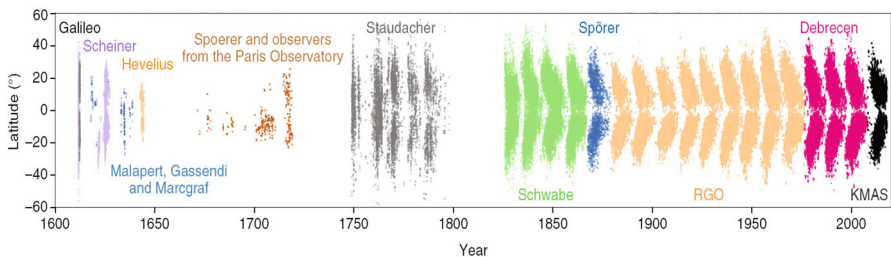

Fig. 2 Maunder butterfly diagram of sunspot occurrence reconstructed from different sources as compiled by Muñoz-Jaramillo and Vaquero (2019)

This suggests that the WSN/ISN may be overestimated by 10–20% past 1947 (Clette et al. 2014; Lockwood et al. 2014), but this does not directly affect the GSN series. As studied by Friedli (2020), this weighting might have been introduced intermittently already in the early 20th century.

Clette et al. (2014) and Cliver and Ling (2016) proposed, based on the ratio of the number of groups reported by Wolfer to that based on the Royal Greenwich Observatory (RGO) data, that there might be a transition in the calibration of GSN around the turn of the 19th to 20th century (or even until 1915) related to the inhomogeneous quality of the RGO data used to build the GSN at that period. On the other hand, Carrasco et al. (2013) and Aparicio et al. (2014), using independent observations of David Hadden from Iowa or Madrid Observatory data found that the problem with RGO data is essential only before the 1880s but not after that. Willis et al. (2016) studied RGO data for the years 1874–1885 and found that the database of Hoyt and Schatten (1998) might have slightly underestimated the RGO number of groups during that time. Sarychev and Roshchina (2009) suggested that the RGO data are erroneous for the period 1874–1880 but quite homogeneous after that. Vaquero et al. (2014) reported that ISN values for the period prior to 1850 are discordant with the number of spotless days, and concluded that the problem could be related to the calibration constants by Wolf (as found by Leussu et al. 2013) and to the non-linearity of ISN for low values. Most of these errors affect the WSN/ISN series, while GSN is more robust.

Thus, such inconsistencies should be investigated, and new series, with corrections of the known problems, need to be produced. Different efforts have been made recently leading to inconsistent solar activity reconstructions. One of the new reconstructions was made by Clette et al. (2014) who introduced a revised version of the ISN (v.2—see Fig. 1a), correcting two apparent discontinuities, Wolf and Waldmeier, as described above. In addition, the entire series was rescaled to the reference level of Wolfer, while the 'classic' WSN/ISN series was scaled to Wolf. This leads to a constant scaling with the factor $1.667 = ^1/_{0.6}$ of the ISN_v.2 series with respect to other series. Keeping this scaling in mind, the ISN_v2 series is systematically different from the earlier one after the 1940s, and for a few decades in the mid-19th century. This was not a fundamental revision by a scaling correction for a couple of errors.

A full revision of the GSN series was performed by Svalgaard and Schatten (2016) who used the number of sunspot groups by Hoyt and Schatten (1998) but applied a different method to construct the new GSN series. They also used a daisy-chain linear regression to calibrate different observers but did it in several steps. A few key observers, called the 'backbones', were selected, and other observers were re-normalized to the 'backbones' using linear regressions. Then the 'backbones' were calibrated to each other, again using linear scaling. Before 1800, when the daisy-chain calibration cannot be directly applied, two other methods, the 'high-low' (observers reporting a larger number of groups were favoured over those reporting a smaller number of groups) and 'brightest star' (only the highest daily number of sunspot groups per year was considered) methods. This GSN series, called S16, is shown in Fig. 1b as the blue dotted curve. It suggests a much higher than usually
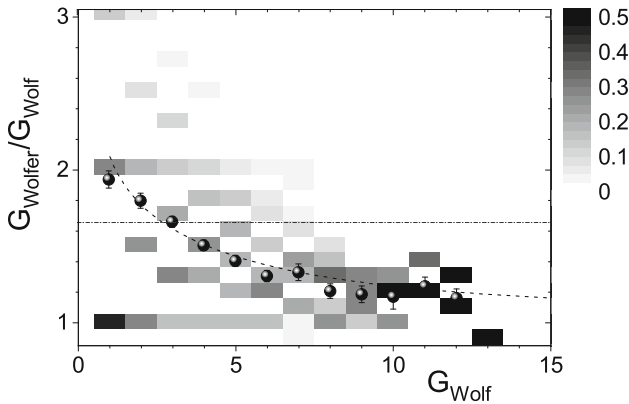
Fig. 3 Correction c−factor of Wolf to Wolfer. The grey scale represents the probability density function (PDF) of the ratio of the number of groups reported by Wolfer for days, when Wolf reported a given number of groups. The big dots with error bars depict the mean values. The dashed line is a functional exponential fit. The horizontal dot-dashed line represents the constant correction k−factor 1.667 (Clette et al. 2014). Modified after Usoskin et al. (2016b)

thought, level of solar activity in the 19th and especially 18th centuries, comparable to that during the mid-20th century. As a result of the 'brightest star' method, it yields moderate values during the Maunder minimum in contrast to the present paradigm of virtually no sunspots (Eddy 1976; Ribes and Nesme-Ribes 1993; Hoyt and Schatten 1996; Usoskin et al. 2015; Vaquero et al. 2015). On the contrary, many recent studies confirmed, using the revised and newly found sunspot observations, the very low level of solar activity during the Maunder minimum (e.g., Carrasco et al. 2021b; Hayakawa et al. 2021b).

The use of the traditional k−factor method of linear scaling for the inter-calibration of solar observers has been found invalid (Dudok de Wit et al. 2016; Lockwood et al. 2016c, b; Usoskin et al. 2016b), and a need for a modern non-parametric method had emerged. This is illustrated by Fig. 3 which shows the ratio of the sunspot group number reported by Wolfer, G_{Wolfer}, to that by Wolf, G_{Wolf}, for days where both reports are available. This ratio obviously depends on the level of activity, being about two for low-activity days ($G_{Wolfer} = 1$) and only ≈ 1.2 for high-activity days. The ratio is strongly non-linear due to the fact that large sunspot groups dominate during periods of high activity. The horizontal dash-dotted line denotes the constant scaling k−factor of 1.667 used earlier (Clette et al. 2014) between Wolf and Wolfer. One can see that the use of the k−factor leads to a significant, by $\approx 40\%$, over-correction of the numbers from Wolf when scaling them to Wolfer, especially during the solar-cycle maximum. This has led to the concept of the c-factor which depends on the level of activity (Fig. 3).

Several new methods, free of the linear assumption, have been proposed recently. An advanced method was proposed by Chatzistergos et al. (2017), also based on the daisy-chain procedure of the observer calibration (e.g., S16) but replacing a linear scaling by the observer's acuteness quantified in the minimum observable sunspot-group size.

Table 1 Values of the observational acuity threshold for the key observers of the 18–19th centuries (after Willamo et al. 2017)

Observer	T_{obs}	N	S_{th}
RGO	1874−1976	28124	0
Broger	1896−1935	8600	$8\binom{11}{5}$
Quimby	1889−1921	7428	$23\binom{31}{17}$
Winkler	1882−1910	4813	$60\binom{71}{51}$
Wolfer	1880−1928	7165	$6\binom{11}{1}$
Tacchini	1871−1900	6256	$18\binom{22}{13}$
Leppig	1867−1881	2463	$50\binom{61}{43}$
Spörer	1861−1893	5409	$0\binom{2}{0}$
Weber	1859−1883	6983	$25\binom{31}{20}$
Wolf	1848−1893	8122	$45\binom{49}{36}$
Shea	1847−1866	5538	$25\binom{31}{20}$
Schmidt	1841−1883	6970	$10\binom{12}{7}$
Schwabe	1825−1866	8297	$8\binom{12}{4}$
Pastorff	1819−1833	1462	$3\binom{9}{0}$
Derfflinger	1802−1824	374	$50\binom{80}{40}$
Herschel	1794−1818	372	$20\binom{40}{10}$
Horrebow	1761−1776	1365	$70\binom{87}{54}$
Schubert	1754−1758	446	$20\binom{23}{14}$

Columns are: Name of the observer; Period of observation T_{obs}; Number of observational days N; The threshold area A_{th} in uncorrected msd; values in parentheses denote the upper and lower 1σ bound

Another method called the ADF-method (Usoskin et al. 2016b, 2021a), is based on a comparison of statistics of the active-day fraction (ADF) in the sunspot (group) records of an observer with that of the reference data-set (the RGO record of sunspot groups for the period 1900–1976). By comparing them, the observational acuity threshold A_{th} can be found and defined so that the observer is supposed to report all the sunspot groups with an area greater than the threshold and to miss all smaller groups. This threshold characterizes the quality of the observer and is further used to calibrate his/her records. The values of the defined thresholds for some principal observers of the 18–19th century are given in Table 1. This method tends to slightly underestimate the high activity and essentially overestimate the lower activity (Willamo et al. 2018). Based on the defined observational acuity thresholds for each observer, a new GSN series was constructed (Usoskin et al. 2016b), called U16, which is depicted in Fig. 1b as the red curve. It was slightly updated by Usoskin et al. (2021a). It lies lower than GSN S16 around solar maxima but slightly higher than HS98, in the 18-19th centuries.

Another new method was proposed by Friedli (2020) who revised the WSN series based on recently digitized Wolf's original notes and using the relation between the numbers of groups and individual spots. This series appears consistent with the GSN

Us16 series and close to the classical ISN series but is lower than the GSN S16 series.

Several attempts to test/validate different sunspot reconstructions using indirect proxies yielded indicative results: tests based on cosmogenic radionuclides (Asvestari et al. 2017b), including ^{44}Ti measured in the fallen meteorites (see Fig. 19) as well as geomagnetic and heliospheric proxies (Lockwood et al. 2016a, b) favor the 'lower' reconstructions (Hoyt and Schatten 1998; Usoskin et al. 2016b) against the 'high' reconstructions (Svalgaard and Schatten 2016). On the other hand, comparison with the solar open-magnetic-field models (Owens et al. 2016) cannot distinguish between different series.

The current situation with the sunspot number series is still developing and can hardly be resolved now. The old 'classical' WSN and GSN series need to be corrected for apparent inhomogeneities. Yet, newly emerging revisions of the sunspot series are mutually inconsistent and require efforts of the solar community on a consensus approach. On the other hand, the scientific community needs a 'consensus' series of solar activity and the work in this direction is underway (Clette et al. 2023). This Review will be updated as the situation progresses.

Other indices

An example of a synthetic index of solar activity is the *flare index*, representing solar-flare activity (e.g., Kleczek 1952; Özgüç et al. 2003). The flare index quantifies daily flare activity in the following manner; it is computed as a product of the flare's relative importance I in the H_α-range and duration t, $Q = I \cdot t$, thus being a rough measure of the total energy emitted by the flare. The daily flare index is produced by Bogazici University (Özgüç et al. 2003) and is available since 1936.

A traditional physical index of solar activity is related to the radioflux of the sun in the wavelength range of 10.7 cm and is called the *F10.7 index* (e.g., Tapping and Charrois 1994). This index represents the flux (in solar flux units, $1\mathrm{sfu} = 10^{-22}\ \mathrm{Wm}^{-2}\ \mathrm{Hz}^{-1}$) of solar radio emission at a centimetric wavelength. There are at least two sources of 10.7 cm flux—free-free emission from hot coronal plasma and gyromagnetic emission from active regions (Tapping 1987). It is a good quantitative measure of the level of solar activity, which is not directly related to sunspots. A close correlation between the F10.7 index and sunspot number indicates that the latter is a good index of general solar activity, including coronal activity. The solar F10.7 cm record has been measured continuously since 1947.

Another physical index is the *coronal index* (e.g., Rybanský et al. 2005), which is a measure of the irradiance of the sun as a star in the coronal green line. Computation of the coronal index is based on observations of green corona intensities (Fe XIV emission line at 530.3 nm wavelength) from coronal stations all over the world, the data being transformed to the Lomnický Štit photometric scale. This index is considered a basic optical index of solar activity. A synthesized homogeneous database of the Fe XIV 530.3 nm coronal-emission line intensities has existed since 1943.

Often *sunspot area* is considered as a physical index representing solar activity (e. g., Baranyi et al. 2001; Balmaceda et al. 2005). This index gives the total area of visible spots on the solar disc in units of millionths of the sun's visible hemisphere,

corrected for apparent distortion due to the curvature of the solar surface. The area of individual groups may vary between tens of millionths (for small groups) up to several thousands of millionths for huge groups. This index has a physical meaning related to the solar magnetic flux emerging at sunspots. Sunspot areas are available since 1874 in the Greenwich series obtained from daily photographic images of the sun. Sunspot group areas were routinely produced by the Royal Greenwich Observatory from daily photographic images of the sun for the period between 1874–1976 and after 1976 extended by the SOON network. Note, that the quality of the RGO data before 1880–1890s may be uneven (see discussion in Sect. 2.2.1). Sunspot areas can be reconstructed even before that using drawing of the sun by H. Schwabe for the years 1826–1867 (Arlt et al. 2013; Senthamizh Pavai et al. 2015) and images by Spörer for the period 1861–1894 (Diercke et al. 2015). In addition, some fragmentary solar drawings exist even for earlier periods, including the Maunder minimum in the 17th century (Fig. 2).

An important quantity is the solar irradiance, total and spectral (Fröhlich 2012). Irradiance variations are physically related to solar magnetic variability (e.g., Solanki et al. 2000), and are often considered manifestations of solar activity, which is of primary importance for solar-terrestrial relations.

Other physical indices include spectral sun-as-star observations, such as the *Ca II-K* index (e.g., Donnelly et al. 1994; Foukal 1996), the space-based *Mg II core-to-wing ratio* as an index of solar UVI (e.g., Donnelly et al. 1994; Snow et al. 2005; Viereck and Puga 1999) and many others.

All the above indices are closely correlated to sunspot numbers on the solar-cycle scale, but may depict quite different behaviour on short or long timescales.

2.2.2 Indirect indices

Sometimes quantitative measures of solar-variability effects are also considered as indices of solar activity. These are related not to solar activity *per se*, but rather to its effect on different environments. Accordingly, such indices are called indirect and can be roughly divided into terrestrial/geomagnetic and heliospheric/interplanetary.

Geomagnetic indices quantify different effects of geomagnetic activity ultimately caused by solar variability, mostly by variations of solar-wind properties and the interplanetary magnetic field. For example, the *aa*-index, which provides a global index of geomagnetic activity relative to the quiet-day curve for a pair of antipodal magnetic observatories (in England and Australia), is available from 1868 (Mayaud 1972). An extension of the geomagnetic series is available from the 1840s using the Helsinki *Ak(H)* index (Nevanlinna 2004a, b). Although the homogeneity of the geomagnetic series is compromised (e.g., Love 2011; Lukianova et al. 2009), it still remains an important indirect index of solar activity. A review of the geomagnetic effects of solar activity can be found, e.g., in Pulkkinen (2007). It is noteworthy that geomagnetic indices, in particular low-latitude aurorae (Silverman 2006), are associated with coronal/interplanetary activity (high-speed solar-wind streams, interplanetary transients, etc.) that may not be directly related to the sunspot-cycle phase and amplitude, and therefore serve only as an approximate index of solar activity. One of the earliest instrumental geomagnetic indices is related to the daily

magnetic declination range, the range of diurnal variation of magnetic needle readings at a fixed location, and is available from the 1780s (Nevanlinna 1995). However, this data exists as several fragmentary sets, which are difficult to combine into a homogeneous data series.

Several geomagnetic activity indices have been proposed recently. One is the IDV (inter-diurnal variability) index (Lockwood et al. 2013; Svalgaard and Cliver 2005) based on Bartels' historical u-index of geomagnetic activity, related to the difference between successive daily values of the horizontal or vertical component of the geomagnetic field. Another index is IHV (inter-hourly variability) calculated from the absolute differences between successive hourly values of the horizontal component of the geomagnetic field during night hours to minimize the effect of the daily curve (Mursula and Martini 2006; Svalgaard et al. 2004). Some details of the derivation and use of these indirect indices for long-term solar-activity studies can be found, e.g., in the Living Review by Lockwood (2013).

Heliospheric indices are related to features of the solar wind or the interplanetary magnetic field measured (or estimated) in interplanetary space. For example, the time evolution of the total (or open) solar magnetic flux is extensively used (e.g., Krivova et al. 2007, 2021; Linker et al. 2021; Lockwood et al. 1999; Wang et al. 2005).

A special case of heliospheric indices is related to the galactic cosmic-ray intensity recorded in natural terrestrial archives. Since this indirect proxy is based on data recorded naturally throughout the ages and revealed now, it makes possible the reconstruction of solar activity changes on long timescales, as discussed in Sect. 3.

2.3 Solar activity observations in the pre-telescopic epoch

Instrumental solar data is based on regular observation (drawings or counting of spots) of the sun using optical instruments, e.g., the telescope used by Galileo in the early 17th century. These observations have mostly been made by professional astronomers whose qualifications and scientific thoroughness were doubtless. They form the basis of the group sunspot number series (Hoyt and Schatten 1998), which can be more-or-less reliably extended back to 1610 (see discussion in Sect. 2.2.1). However, some fragmentary records of qualitative solar and geomagnetic observations exist even for earlier times, as discussed below (Sects. 2.3.1–2.3.2).

2.3.1 Instrumental observations: Camera obscura

The invention of the telescope revolutionized astronomy. However, another solar astronomical instrument, the camera obscura, also made it possible to provide relatively good solar images and was still in use until the late 18th century. Camera obscura was known from early times, as they have been used in major cathedrals to define the sun's position (see the review by Heilbron 1999; Vaquero 2007; Vaquero and Vázquez 2009). The earliest known drawing of the solar disc was made by Frisius, who observed the solar eclipse in 1544 using a camera obscura. That observation was performed during the Spörer minimum and no spots were observed on the sun. The first known observation of a sunspot using a camera obscura was done by Kepler in May 1607, who erroneously ascribed the spot on the sun to a

transit of Mercury. Although such observations were sparse and related to other phenomena (solar eclipses or transits of planets), there were also regular solar observations by camera obscura. For example, about 300 pages of logs of solar observations made in the cathedral of San Petronio in Bologna from 1655–1736 were published by Eustachio Manfredi in 1736 (see the full story in Vaquero 2007). Therefore, observations and drawings made using camera obscura can be regarded as instrumental observations (e.g., Tovar et al. 2021).

2.3.2 Naked-eye observations

Even before regular professional observations performed with the aid of specially-developed instruments (what we now regard as scientific observations) people were interested in unusual phenomena. Several historical records exist based on naked-eye observations of transient phenomena in the sun or in the sky.

From even before the telescopic era, a large amount of evidence of spots being observed on the solar disc can be traced back as far as the middle of the 4th century BC (Theophrastus of Athens). The earliest known drawing of sunspots is dated to December 8, 1128 AD as published in "The Chronicle of John of Worcester" (Willis and Stephenson 2001). However, such evidence from occidental and Moslem sources is scarce and mostly related to observations of transits of inner planets over the sun's disc, probably because of the dominance of the dogma on the perfectness of the sun's body, which dates back to Aristotle's doctrine (Bray and Loughhead 1964). Oriental sources are much richer for naked-eye sunspot records, but that data is also fragmentary and irregular (see, e.g., Clark and Stephenson 1978; Wittmann and Xu 1987; Yau and Stephenson 1988). Spots on the sun are mentioned in official Chinese and Korean chronicles from 165 BC to 1918 AD. While these chronicles are fairly reliable, the data is not straightforward to interpret since it can be influenced by meteorological phenomena, e.g., dust loading in the atmosphere due to dust storms (Willis et al. 1980) or volcanic eruptions (Scuderi 1990) can facilitate sunspots observations. Direct comparison of Oriental naked-eye sunspot observations and European telescopic data shows that naked-eye observations can serve only as a qualitative indicator of sunspot activity, but can hardly be quantitatively interpreted (see, e.g., Willis et al. 1996, and references therein). Moreover, as a modern experiment of naked-eye observations (Mossman 1989) shows, Oriental chronicles contain only a tiny ($^1/_{200} - ^1/_{1000}$) fraction of the number of sunspots potentially visible with the naked eye (Eddy et al. 1989). This indicates that records of sunspot observations in the official chronicles were highly irregular (Eddy 1983) and probably dependent on dominating traditions during specific historical periods (Clark and Stephenson 1978). Although naked-eye observations tend to qualitatively follow the general trend in solar activity according to *a posteriori* information (e.g., Vaquero et al. 2002), extraction of any independent quantitative information from these records is very difficult as potentially influenced by the meteorological, astronomical and political factors at the time of observations..

Visual observations of aurorae Borealis at middle latitudes form another proxy for solar activity (e.g., Basurah 2004; Hayakawa et al. 2019b; Křivský 1984; Lee et al.

2004; Schove 1983; Schröder 1992; Silverman 1992; Siscoe 1980; Vázquez and Vaquero 2010). Fragmentary records of aurorae can be found in both occidental and oriental sources since antiquity. The first known dated notations of an aurora are from Babylon in 567 BCE and 660 BCE (Hayakawa et al. 2019a; Stephenson et al. 2004). Aurorae may appear at middle latitudes as a result of enhanced geomagnetic activity due to transient interplanetary phenomena. Of particular interest are 'sporadic' and 'equatorial' aurorae (e.g., Hayakawa et al. 2018; He et al. 2021). Although auroral activity reflects coronal and interplanetary features rather than magnetic fields on the solar surface, there is a strong correlation between long-term variations of sunspot numbers and the frequency of aurora occurrences. Because of the phenomenon's short duration and low brightness, the probability of seeing an aurora is severely affected by other factors such as the weather (sky overcast, heat lightning), the Moon's phase, season, etc. The fact that these observations were not systematic in early times (before the beginning of the 18th century) makes it difficult to produce a homogeneous data set. Moreover, the geomagnetic latitude of the same geographical location may change quite dramatically over centuries, due to the migration of the geomagnetic axis, which also affects the probability of watching aurorae (Oguti and Egeland 1995; Siscoe and Verosub 1983). For example, the geomagnetic latitude of Seoul (37.5° N 127° E), which is currently less than 30°, was about 40° a millennium ago (Kovaltsov and Usoskin 2007). This dramatic change alone can explain the enhanced frequency of aurorae observations recorded in oriental chronicles.

2.3.3 Mathematical/statistical extrapolations

Due to the lack of reliable information regarding solar activity in the pre-instrumental era, it seems natural to try extending the sunspot series back in time, before 1610 AD, by means of extrapolating its statistical properties. Indeed, numerous attempts of this kind have been made even recently (e.g., de Meyer 1998; Nagovitsyn 1997; Rigozo et al. 2001; Zharkova et al. 2015). Such models aim to find the main feature of the actually-observed sunspot series, e.g., a modulated carrier frequency or a multi-harmonic representation, which is then extrapolated backwards in time. The main disadvantage of this approach is that it is not a reconstruction based upon measured or observed quantities, but rather a "post-diction" based on extrapolation. This method is often used for short-term predictions, but it can hardly be used for the reliable long-term reconstruction of solar activity. In particular, it assumes that the sunspot time series is stationary, i.e., a limited-time realization contains full information on its future and past. Clearly, such models cannot include periods exceeding the time span of observations upon which the extrapolation is based. Hence, the pre- or post-diction becomes increasingly unreliable with growing extrapolation time, and its accuracy is hard to estimate.

Sometimes a combination of the above approaches is used, i.e., a fit of the mathematical model to indirect qualitative proxy data. In such models, a mathematical extrapolation of the sunspot series is slightly tuned and fitted to some proxy data for earlier times. For example, Schove (1955, 1979) fitted the slightly variable but phase-locked carrier frequency (about 11 years) to fragmentary data from naked-eye sunspot observations and auroral sightings. Phase locking was

achieved by assuming exactly nine solar cycles per calendar century. This series, known as *Schove* series, reflects qualitative long-term variations of the solar activity, including some grand minima, but cannot pretend to be a quantitative representation of solar activity level. The Schove series played an important historical role in the 1960s. In particular, a comparison of the $\Delta^{14}C$ data with this series succeeded in convincing the scientific community that secular variations of ^{14}C in tree rings have solar and not climatic origins (Stuiver 1961). This formed a cornerstone of the precise method of solar-activity reconstruction, which uses cosmogenic isotopes from terrestrial archives. However, attempts to reconstruct the phase and amplitude of the 11-year cycle, using this method were unsuccessful. For example, Schove (1955) made predictions of forthcoming solar cycles up to 2005, which failed. We note that all these works are not able to reproduce, for example, the Maunder minimum (which cannot be represented as a result of the superposition of different harmonic oscillations), yielding too high sunspot activity compared to that observed. From the modern point of view, the Schove series can be regarded as archaic.

The main source of data on the past solar activity before the era of direct observations is related to cosmogenic-isotope data measured in terrestrial archives (see Sect. 3).

2.4 The solar cycle and its variations

The sunspot-number series based on telescopic observations since 1610 covers the full range of solar variability, from the grand Maunder minimum in the 17th century to the Modern grand maximum in the second half of the 20th century (e.g., Acero et al. 2018). Accordingly, it allows us to study typical features of solar variability on a multi-centennial timescale.

2.4.1 Quasi-periodicities

11-yr Schwabe cycle
The main feature of solar activity is its pronounced quasi-periodicity with a period of about 11 years, known as the Schwabe cycle, which varies in both amplitude and duration. The first observation of possible regular variability in sunspot numbers was made by the Danish astronomer Christian Horrebow in the 1770s on the basis of his sunspot observations from 1761–1769 (see details in Gleissberg 1952; Vitinsky 1965), but the results were forgotten. It took over 70 years before the amateur astronomer Heinrich Schwabe announced in 1844 that sunspot activity varies cyclically with a period of about 10 years (Schwabe 1844). This cycle, called the 11-year or Schwabe cycle, is the most prominent variability in the sunspot-number series. The length and amplitude of the Schwabe cycle vary essentially, from 8 to 15 years in duration and by a few orders of magnitude in size. There are also empirical rules relating different parameters of the solar cycle, most known being the *Waldmeier* relation (Waldmeier 1935, 1939) relating the cycle height and the length of the ascending phase (strong cycles raise fast), and the *Gnevyshev–Ohl* rule (Gnevyshev and Ohl 1948) clustering cycles to pairs of an even-numbered cycle

followed by a stronger odd-numbered cycle. The use of cosmogenic data has confirmed the robustness of the Waldmeier rule but was unable to reproduce the Gnevyshev–Ohl rule on the 1000-yr timescale (Usoskin et al. 2021). A detailed review of solar cyclic variability can be found in Hathaway (2015).

Solar cycles are consequently numbered since 1749 which was solar cycle #1 according to the Wolf numbering. Presently, solar cycle #25 is in progress.

The Schwabe cycle is recognized now as a fundamental feature of solar activity originating from the solar-dynamo process. This 11-year cyclicity is prominent in many other parameters including solar, heliospheric, geomagnetic, space weather, climate and others. The background for the 11-year Schwabe cycle is the 22-year Hale magnetic polarity cycle. George Hale found that the polarity of sunspot magnetic fields changes in both hemispheres when a new 11-year cycle starts (Hale et al. 1919). This relates to the reversal of the global magnetic field of the sun with the period of ≈22 years. It is often considered that the 11-year Schwabe cycle is the modulo of the sign-alternating Hale cycle (e.g., Bracewell 1986; de Meyer 1998; Kurths and Ruzmaikin 1990; Mininni et al. 2001; Sonett 1983), but this is only a mathematical representation.

Phase catastrophe?

Sometimes the regular time evolution of solar activity is broken up by periods of greatly depressed activity called grand minima. The last grand minimum (and the only one covered by direct solar observations) was the famous Maunder minimum from 1645–1715 (Eddy 1976, 1983). Other grand minima in the past, known from cosmogenic isotope data, include, e.g., the Spörer minimum around 1450–1550 and the Wolf minimum around the 14th century (see the detailed discussion in Sect. 4.2). Sometimes the Dalton minimum (ca. 1790–1820) is also considered to be a grand minimum. As suggested by Schüssler et al. (1997), this can be a separate, intermediate state of the dynamo between the grand minimum and normal activity, or an unsuccessful attempt of the sun to switch to the grand minimum state (Frick et al. 1997; Sokoloff 2004). This is observed as the "phase catastrophe" (disrupted smooth evolution of a dynamical system in the phase space) of solar-activity evolution (e.g., Kremliovsky 1994; Vitinsky et al. 1986). A peculiarity in the phase evolution of sunspot activity around 1800 was also noted by Sonett (1983), who ascribed it to a possible error in Wolf sunspot data, and by Wilson (1988a), who reported on a possible misplacement of sunspot minima for cycles 4–6 in the WSN series. It has been also suggested that the phase catastrophe can be related to a tiny cycle, which might have been lost at the end of the 18th century because of very sparse observations (Usoskin et al. 2001a, 2002b, 2003b). Independent evidence of the existence of the lost cycle has been proposed based on the reconstructed sunspot butterfly diagram for that period (Usoskin et al. 2009c). However, it is impossible to conclude, without the magnetic-polarity data, whether it was a full new (lost) cycle or an unusual burst of activity at the declining phase of the previous cycle as proposed by Zolotova and Ponyavin (2011). Cosmogenic-isotope data cannot resolve the existence of a full separate lost cycle (Jiang et al. 2011; Usoskin et al. 2021b).

Centennial Gleissberg cycle

The long-term change (trend) in the Schwabe cycle amplitude is known as the secular Gleissberg cycle (Gleissberg 1939) with a mean period of about 90 years. However, the Gleissberg cycle is not a cycle in the strict periodic sense but rather a modulation of the cycle envelope with a varying timescale of 60–140 years (e.g., Gleissberg 1971; Kuklin 1976; Ogurtsov et al. 2002).

See more discussion of this and longer cycles in Sect. 4.1 using cosmogenic data.

2.4.2 Randomness versus regularity

The short-term (days–months) variability of sunspot numbers is greater than the observational uncertainties indicating the presence of random fluctuations (noise). As typical for most real signals, this noise is not uniform (white), but rather red or correlated noise (e.g., Frick et al. 1997; Ostryakov and Usoskin 1990; Oliver and Ballester 1996), namely, its variance depends on the level of the signal. While the existence of regularity and randomness in sunspot series is apparent, their relationship is not clear (e.g., Wilson 1994)—are they mutually independent or intrinsically tied together? Moreover, the question of whether randomness in sunspot data is due to chaotic or stochastic processes, is still open.

Earlier it was common to describe sunspot activity as a *multi-harmonic process* with several basic harmonics (e.g., Sonett 1983; Vitinsky 1965; Vitinsky et al. 1986) with the addition of random noise, which plays no role in the solar-cycle evolution. However, it has been shown (e.g., Charbonneau 2001; Mininni et al. 2002; Rozelot 1994; Weiss and Tobias 2000) that such an oversimplified approach depends on the chosen reference time interval and does not adequately describe the long-term evolution of solar activity. A multi-harmonic representation is based on an assumption of the stationarity of the benchmark series, but this assumption is broadly invalid for solar activity (e.g., Kremliovsky 1994; Polygiannakis et al. 2003; Sello 2000). Moreover, a multi-harmonic representation cannot, for an apparent reason, be extrapolated to a timescale larger than that covered by the benchmark series. The fact that purely mathematical/statistical models cannot give good predictions of solar activity (as discussed below) implies that the nature of the solar cycle is not a multi-periodic or other purely deterministic process, but chaotic or stochastic processes play an essential role in sunspot cycle formation (e.g., Moss et al. 2008; Käpylä et al. 2012).

An old idea of the possible planetary influence on the dynamo has received a new pulse recently with some unspecified torque effect proposed to act on the assumed quasi-rigid non-axisymmetric tahocline (Abreu et al. 2012). However, this result was criticized by Poluianov and Usoskin (2014) as being an artefact of an inappropriate analysis (aliasing effect of incorrect smoothing). In addition, Cauquoin et al. (2014) have shown that such periodicities were not observed in ^{10}Be data 330 kyr ago. Another speculated planetary effect is a tidal locking of the dynamo (Stefani et al. 2019). However, that work was reported to be methodologically flawed (Nataf 2022). Moreover, a theoretical consideration suggests that these effects are too weak per se and require an unknown strong amplification mechanism to become observable (Charbonneau 2022).

The question of whether solar cycles are independent of each other (short memory) or are synchronised by an internal/external clock is crucially important for the solar dynamo. This can be straightforwardly distinguished with a statistical test since the dispersions of the cycle period and phase would grow with the number of solar cycles if the cycles are independent (random walk), but remain constant for the synchronized cycles (clock). An analysis of the directly observed sunspot numbers series (e.g., Gough 1981) favoured the random-walk hypothesis but the synchronized clock could not be rejected because of the two short series (about 20 cycles). The recent 1000-year-long solar cycle reconstruction (Sect. 3.6.1) has greatly the statistic to 96 solar cycles that made it possible to finally resolve this ambiguity. As shown by Weisshaar et al. (2023), the dispersion linearly grows with the number of solar cycles analyzed, and the 'clock' hypothesis can be rejected with very high confidence. Thus, the idea of internal or external synchronisation of the solar cycle contradicts the available data.

Different numeric tests, such as an analysis of the Lyapunov exponents (Kremliovsky 1995; Mundt et al. 1991; Ostriakov and Usoskin 1990; Sello 2000), Kolmogorov entropy (Carbonell et al. 1994; Sello 2000) and Hurst exponent (Oliver and Ballester 1998; Ruzmaikin et al. 1994), confirm the irregular and unpredictable nature of the solar-activity time evolution (see, e.g., a review by Panchev and Tsekov 2007).

It was suggested quite a while ago that the variability of the solar cycle may be a temporal realization of a *low-dimensional chaotic system* (e.g., Ruzmaikin 1981). This concept became popular in the early 1990s when many authors considered solar activity as an example of low-dimensional deterministic chaos, described by a strange attractor (e.g., Kurths and Ruzmaikin 1990; Morfill et al. 1991; Mundt et al. 1991; Ostriakov and Usoskin 1990; Rozelot 1995; Salakhutdinova 1999; Serre and Nesme-Ribes 2000; Hanslmeier et al. 2013). Such a process naturally contains randomness, which is an intrinsic feature of the system rather than an independent additive or multiplicative noise. However, although this approach easily produces features seemingly similar to those of solar activity, quantitative parameters of the low-dimensional attractor varied greatly as obtained by different authors. Later it was realized that the analyzed data set was too short (Carbonell et al. 1993, 1994), and the results were strongly dependent on the choice of filtering methods (Price et al. 1992). Developing this approach, Mininni et al. (2000, 2001) suggested that one can consider sunspot activity as an example of a 2D Van der Pol relaxation oscillator with an intrinsic stochastic component.

Such phenomenological or basic principles models, while succeeding in reproducing (to some extent) the observed features of solar-activity variability, do not provide insight into the physical nature of regular and random components of solar variability. In this sense, efforts to understand the nature of randomness in sunspot activity in the framework of dynamo theory are more advanced. Corresponding theoretical dynamo models have been developed (see reviews by Charbonneau 2020; Ossendrijver 2003), which include stochastic or chaotic processes (e.g., Brandenburg and Sokoloff 2002; Brooke and Moss 1994; Charbonneau and Dikpati 2000; Feynman and Gabriel 1990; Hoyng 1993; Lawrence et al. 1995; Moss et al. 1992; Schmalz and Stix 1991; Schmitt et al. 1996; Weiss et al. 1984). For example, Feynman and Gabriel (1990) suggested that the transition from a regular to a chaotic dynamo passes through bifurcation. Charbonneau and Dikpati

(2000) studied stochastic fluctuations in a Babcock–Leighton dynamo model and succeeded in the qualitative reproduction of the anti-correlation between cycle amplitude and length (Waldmeier rule). Their model also predicts a phase-lock of the Schwabe cycle, i.e., that the 11-year cycle is an internal "clock" of the sun. Most often the idea of fluctuations is related to the α-effect, which is the result of the electromotive force averaged over turbulent vortices, and thus can contain a fluctuating contribution (e.g., Brandenburg and Spiegel 2008; Hoyng 1993; Moss et al. 2008; Ossendrijver et al. 1996). Note that a significant fluctuating component (with an amplitude greater than 100% of the regular component) is essential in all these models.

2.4.3 A note on solar activity predictions

Randomness (see Sect. 2.4.2) in the SN series is directly related to the predictability of solar activity. Forecasting solar activity has been a subject of intense study for many years (e.g., Gleissberg 1948; Newton 1928; Vitinsky 1965; Yule 1927) and has greatly intensified recently with hundreds of journal articles being published to predict the solar cycles No. 24 and 25 maxima (see, e.g., reviews by Jiang et al. 2023; Nandy 2021; Pesnell 2012, 2016; Pesnell and Schatten 2018), following the boost of space-technology development and increasing debates on solar-terrestrial relations. A systematic analysis (Nandy 2021) of the predictions published recently for cycles 24 and 25 implies that, while statistical and mathematical methods produce widely diverse results, physics-based predictions for the current cycle 25 converge and predict a moderately weak sunspot cycle, as confirmed by the developing solar cycle. The convergence of the physics-based models implies progress in the understanding of solar cycle evolution, in contrast to purely mathematical methods. As concluded by Nandy (2021), predictions for a solar cycle at around the end of the proceeding cycle as based on the observed polar field (flux) are fairly reliable. However, uncertainties in the observed magnetograms and sunspot emergence may affect the results (Jiang et al. 2023). Longer-scale predictions are hardly possible because of the random fluctuations (mostly related to the tilt-angle distribution of bipolar sunspot pairs) in the solar-cycle dynamo mechanism. Detailed reviews of the solar activity prediction methods and results have been recently provided by Petrovay (2020); Nandy (2021).

Note that several 'predictions' of the general decline of the coming solar activity have been made recently (Abreu et al. 2008; Lockwood et al. 2011; Solanki et al. 2004), however, these are not really true predictions but rather acknowledgements of the fact that the Modern Grand maximum (Solanki et al. 2004; Usoskin et al. 2003c) has ceased. Similar caution can be made about predictions of a grand minimum (e.g., Lockwood et al. 2011; Miyahara et al. 2010)—a grand minimum should appear soon or later, but presently we are hardly able to predict its occurrence.

2.5 Summary

In this section, the concept of solar activity and quantifying indices is discussed, as well as the main features of solar-activity temporal behaviour.

The concept of solar activity is quite broad and covers non-stationary and non-equilibrium (often eruptive) processes, in contrast to the "quiet" sun concept, and their effects upon the terrestrial and heliospheric environment. Many indices are used to quantify different aspects of variable solar activity. Quantitative indices include direct (i.e., related directly to solar variability) and indirect (i.e., related to terrestrial and interplanetary effects caused by solar activity) ones, they can be physical or synthetic. While all indices depict the dominant 11-year cyclic variability, their relationships on other timescales (short scales or long-term trends) may vary to a great extent.

The most common and the longest available direct index of solar activity is the sunspot number, which is a synthetic index and is useful for the quantitative representation of overall solar activity outside the grand minimum. During the grand Maunder minimum, however, it may give only a clue about solar activity whose level may drop below the sunspot formation threshold. The sunspot number series is available for the period from 1610 AD, after the invention of the telescope, and covers, in particular, the Maunder minimum in the late 17th century. However, this series has big uncertainties before 1900 (Sect. 2.2.1). Fragmentary non-instrumental observations of the sun before 1610, while giving a possible hint of relative changes in solar activity, cannot be interpreted in a quantitative manner.

Solar activity in all its manifestations is dominated by the 11-year Schwabe cycle, which has, in fact, a variable length of 9–14 years for individual cycles. The amplitude of the Schwabe cycle varies greatly—from the almost spotless Maunder minimum to the very high cycle 19, possibly in relation to the Gleissberg or secular cycle. Longer super-secular characteristic times can also be found in various proxies of solar activity, as discussed in Sect. 4.

Solar activity contains essential chaotic/stochastic components, that lead to irregular variations and make the prediction of solar activity for a timescale exceeding one solar cycle impossible.

3 Proxy method of past solar-activity reconstruction

In addition to direct solar observations, described in Sect. 2.2.1, there are also indirect solar proxies, which are used to study solar activity in the pre-telescopic era. Unfortunately, we do not have any reliable data that could give a direct index of solar variability before the beginning of the sunspot-number series. Therefore, one must use indirect proxies, i.e., quantitative parameters, which can be measured nowadays but represent different effects of solar magnetic activity in the past. It is common to use, for this purpose, signatures of terrestrial indirect effects induced by variable solar-magnetic activity, that are stored in natural archives. Such traceable signatures can be related to nuclear (used in the cosmogenic-isotope method) or chemical (used, e.g., in the nitrate method) effects caused by cosmic rays (CRs) in the Earth's atmosphere, lunar rocks or meteorites.

The most common proxy of solar activity is formed by the data on cosmogenic radionuclides (e.g., ^{10}Be, ^{14}C and ^{36}Cl), which are produced by cosmic rays in the

Earth's atmosphere (e.g, Bard et al. 1997; Beer et al. 1990, 2012; Stuiver and Quay 1980; Usoskin 2017).

Other cosmogenic nuclides, which are used in geological and paleomagnetic dating, are less suitable for studies of solar activity (see e.g., Beer et al. 2012). Cosmic rays are the main source of cosmogenic nuclides in the atmosphere (excluding anthropogenic factors during the last decades) with the maximum production being in the lower stratosphere. After a complicated transport in the atmosphere, the cosmogenic isotopes are stored in natural archives such as polar ice, trees, marine sediments, etc. This process is also affected by changes in the geomagnetic field and climate. Cosmic rays experience heliospheric modulation due to solar wind and the frozen-in solar magnetic field. The intensity of modulation depends on solar activity and, therefore, cosmic-ray flux and the ensuing cosmogenic isotope intensity depends inversely on solar activity. An important advantage of cosmogenic data is that primary archiving is done naturally in a similar manner throughout the ages, and these archives are measured nowadays in laboratories using modern techniques. If necessary, the measurements can be repeated and improved, as has been done for some radiocarbon samples. In contrast to fixed historical archival data (such as sunspot or auroral observations) this approach makes it possible to obtain homogeneous data sets of stable quality and to improve the quality of data with the invention of new methods (such as accelerator mass spectrometry). However, it only allows reconstructions of long-term variability with annual resolution at best, or even decadal, or extreme SEP events. Cosmogenic-isotope data is the main regular indicator of solar activity on a very long-term scale. The redistribution of nuclides in terrestrial reservoirs and archiving may be affected by local and global climate/circulation processes, which are, to a large extent, unknown in the past. However, a combined study of different nuclides data, whose responses to terrestrial effects are very different, may allow for disentangling external and terrestrial signals.

3.1 The physical basis of the method

3.1.1 Heliospheric modulation of cosmic rays

The flux of cosmic rays (highly energetic fully ionized nuclei) is considered roughly constant (at least at the time scales relevant to the present study) in the vicinity of the Solar system. However, before reaching the vicinity of Earth, galactic cosmic rays experience complicated transport in the heliosphere that leads to modulation of their flux. Heliospheric transport of GCR is described by Parker's theory (Parker 1965; Toptygin 1985) and includes four basic processes (Potgieter 2013): the diffusion of particles due to their scattering on magnetic inhomogeneities, the convection of particles by the out-blowing solar wind, adiabatic energy losses in expanding solar wind, drifts of particles in the magnetic field, including the gradient-curvature drift in the regular heliospheric magnetic field, and the drift along the heliospheric current sheet, which is a thin magnetic interface between the two heliomagnetic hemispheres. Because of variable solar-magnetic activity, CR flux in the vicinity of Earth is strongly modulated (see Fig. 4). The most prominent feature in CR modulation is the
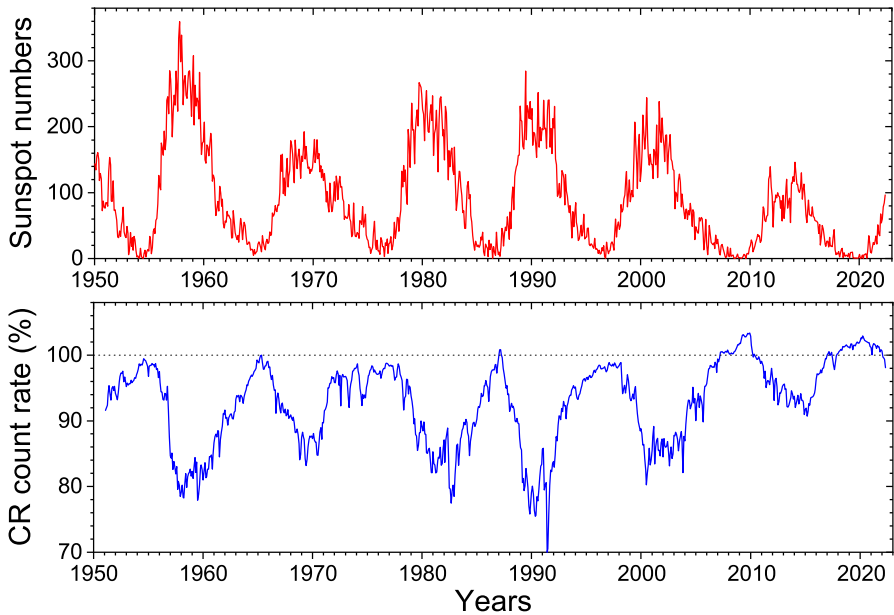
Fig. 4 Cyclic variations since 1951. *Panel a:* Time profiles of International sunspot number v.2 (http://sidc.be/silso/datafiles); *Panel b:* Cosmic-ray flux as the count rate of a subpolar neutron monitor (Oulu NM http://cosmicrays.oulu.fi, Climax NM data used before 1964), 100% NM count rate corresponds to May 1965

11-year cycle, which is in inverse relation to solar activity. The 11-year cycle in CR is delayed with a variable delay (from a month up to two years) with respect to the sunspots (e.g., Koldobskiy et al. 2022a). The time profile of cosmic-ray flux as measured by a neutron monitor (NM) is shown in Fig. 4 (panel b) together with the sunspot numbers (panel a). Besides the inverse relation between them, some other features can also be noted. A 22-year cyclicity manifests itself in cosmic-ray modulation through the alteration of sharp and flat maxima in cosmic-ray data, originating from the charge-dependent drift mechanism (Jokipii and Levy 1977). One may also note short-term fluctuations, which are not directly related to sunspot numbers but are driven by interplanetary transients caused by solar eruptive events, e.g., flares or CMEs or by fast solar-wind streams. An interesting feature is related to the recent decades. The CR flux in 2009 was the highest ever recorded by NMs (Moraal and Stoker 2010), as caused by the favourable heliospheric conditions (unusually weak heliospheric magnetic field and the flat heliospheric current sheet). On the other hand, the sunspot minimum was comparable to other minima. The level of CR modulation during the cycle 24 was moderate, shallower than for the previous cycles, reflecting the weak solar cycle 24. For the previous 50 years of high and roughly-stable solar activity, no trends have been observed in CR data; however, as will be discussed later, the overall level of CR has changed significantly on the centurial-millennial timescales.

A full solution to the problem related to CR transport in the heliosphere is a complicated task and requires sophisticated 3D time-dependent self-consistent modelling. However, the problem can be essentially simplified for applications at a long timescale. An assumption on the azimuthal symmetry (requires times longer than the solar-rotation period of ≈ 27 days synodic) and quasi-steady changes reduce it to a 2D quasi-steady problem. A further assumption of the spherical symmetry of the heliosphere reduces the problem to a 1D case. This approximation can be used only for rough estimates since it neglects the drift effect, but it is useful for long-term studies when the heliospheric parameters cannot be evaluated independently. Further, but still reasonable, assumptions (constant solar-wind speed, roughly power-law CR energy spectrum, slow spatial changes of the CR density) lead to the force-field approximation (Caballero-Lopez and Moraal 2004; Gleeson and Axford 1968), which can be solved analytically in the form of characteristic curves. The differential intensity J_i of the cosmic-ray nuclei of type i with kinetic energy T at 1 AU is given in this case as

$$J_i(T, \phi) = J_{\mathrm{LIS},i}(T + \Phi_i) \frac{(T)(T + 2T_r)}{(T + \Phi_i)(T + \Phi_i + 2T_r)} , \qquad (3)$$

where $\Phi_i = (Z_i e / A_i)\phi$ for cosmic nuclei of i-th type (charge and mass numbers are Z_i and A_i), T and ϕ are expressed in MeV/nucleon and in MV, respectively, and $T_r = 938$ MeV is the proton's rest mass. T is the CR particle's kinetic energy, and ϕ is the modulation potential.

The local interstellar spectrum (LIS) J_{LIS} forms the boundary condition for the heliospheric transport problem. Recent data from Voyager 1 and 2 spacecraft travelling beyond the termination shock give a clue for the lower-energy (<100 MeV/nuc) range of LIS (Bisschoff and Potgieter 2016; Webber et al. 2008), although the residual modulation beyond the heliopause may still affect this (Herbst et al. 2012). The high-energy tail of LIS can be evaluated using near-Earth measurements, e.g., with the AMS-02 detector (Aguilar et al. 2021). However, the LIS is not well known in the energy range affected by the heliospheric modulation, between 0.1–20 GeV/nuc. Presently-used and historical approximations for LIS (e.g., Burger et al. 2000; Garcia-Munoz et al. 1975; Vos and Potgieter 2015; Webber and Higbie 2009) agree with each other for energies above 20 GeV but may contain uncertainties of up to a factor of 1.5 around 1 GeV (Asvestari et al. 2017a). These uncertainties in the boundary conditions make the results of the modulation theory slightly model-dependent (see discussion in Herbst et al. 2010; Usoskin et al. 2005) and require the LIS model to be explicitly cited.

This approach gives results, which are at least dimensionally consistent with the full theory and can be used for long-term studies (Caballero-Lopez and Moraal 2004; Usoskin et al. 2002a). Differential CR intensity is described by the only time-variable parameter, called the modulation potential ϕ, which is mathematically interpreted as the averaged rigidity (i.e., the particle's momentum per unit of charge) loss of a CR particle in the heliosphere. However, it is only a formal spectral index whose physical interpretation is not straightforward, especially on short timescales and during active periods of the sun (Caballero-Lopez and Moraal 2004). Despite its cloudy physical

meaning, this force-field approach provides a very useful and simple single-parametric approximation for the differential spectrum of GCR, since the spectrum of different GCR species directly measured near the Earth can be well fitted by Eq. (3) using only the parameter ϕ in a wide range of solar activity levels (Usoskin et al. 2011, 2017). Therefore, changes in the whole energy spectrum (in the energy range from 100 MeV/nucleon to 100 GeV/nucleon) of cosmic rays due to the solar modulation can be described by this single number within the framework of the adopted LIS.

Since protons compose about 90% of GCR in the particle numbers, heavier species were sometimes neglected earlier, but this can lead to an essential error. Helium and heavier nuclei compose about 1/3 of GCR in the number of nucleons and since they are less modulated than protons in the heliosphere and magnetosphere, they can contribute up to 50% into atmospheric processes (Koldobskiy et al. 2019; Webber and Higbie 2003).

3.1.2 Geomagnetic shielding

Cosmic rays are charged particles and therefore are affected by the Earth's magnetic field. Thus the geomagnetic field puts an additional shielding on the incoming flux of cosmic rays. It is usually expressed in terms of the cutoff rigidity P_c, which is the minimum rigidity a vertically incident CR particle must possess (on average) in order to reach the top of the atmosphere at a given location and time (Cooke et al. 1991). Neglecting such effects as the East-West asymmetry, which is roughly averaged out for the isotropic particle flux, or nondipole magnetic momenta, which decay rapidly with distance, one can come to a simple approximation called Störmer's equation, which describes the vertical geomagnetic cutoff rigidity P_c:

$$P_c \approx 1.9\,M\,(R_o/R)^2\,\cos^4 \lambda_G\;[\mathrm{GV}]\,, \tag{4}$$

where M is the geomagnetic dipole moment (in 10^{22} A m^2), R_o is the Earth's mean radius, R is the distance from the given location to the dipole center, and λ_G is the geomagnetic latitude. The cutoff concept works like a Heaviside step function so that all cosmic rays whose rigidity is below the cutoff are not allowed to enter the atmosphere while all particles with higher rigidity can penetrate. This approximation provides a good compromise between simplicity and reality (Nevalainen et al. 2013), especially when using the eccentric dipole description of the geomagnetic field (Fraser-Smith 1987). The eccentric dipole has the same dipole moment and orientation as the centred dipole, but the dipole's centre and consequently the poles, defined as crossings of the axis with the surface, are shifted with respect to geographical ones.

The shielding effect is the strongest at the geomagnetic equator, where the present-day value of P_c may reach up to 17 GV in the region of the Bay of Bengal. There is almost no cutoff in the geomagnetic polar regions ($|\lambda_G| \geq 60°$). However, even in the latter case, the atmospheric cutoff becomes important, i.e., particles must have rigidity above 0.5 GV in order to initiate the atmospheric cascade which can reach the ground (see Sect. 3.1.3).

The geomagnetic field is seemingly stable on the short-term scale, but it changes essentially on centurial-to-millennial timescales (e.g., Korte and Constable 2006; Licht et al. 2013; Pavón-Carrasco et al. 2014). Such past changes can be evaluated based on measurements of the residual magnetization of independently-dated samples. These can be paleo- (i.e., natural stratified archives such as lake or marine sediments or volcanic lava) or archaeological (e.g., clay bricks that preserve magnetization upon baking) samples. Most paleo-magnetic data preserve not only the magnetic field intensity but also the direction of the local field, while archeo-magnetic samples provide information on the intensity only. Using a large database of such samples, it is possible to reconstruct (under reasonable assumptions) the large-scale magnetic field of the Earth. Data available provides good global coverage for the last three millennia, allowing for a reliable paleomagnetic reconstruction of the true dipole moment (DM) or virtual dipole moment[1] (VDM) and its orientation (Licht et al. 2013). Less precise, but still reliable reconstructions of the DM and its orientation are possible for the last ten (Knudsen et al. 2008; Usoskin et al. 2016a) or even a hundred millennia (Panovska et al. 2019). Directional paleomagnetic reconstructions are less reliable on a longer timescale, because of the spatial sparseness of the paleo/archeo-magnetic samples in the earlier part of the Holocene (Korte et al. 2011). Some paleomagnetic reconstructions are shown in Fig. 5. All paleomagnetic models depict a similar long-term trend—an enhanced intensity during the period between 1500 BC and 500 AD and a significantly lower field before that.

Changes in the dipole moment M inversely modulate the flux of CR at Earth, with strong effects in tropical regions and globally. The migration of the geomagnetic axis, which changes the geomagnetic latitude λ_G of a given geographical location is also important; while not affecting the global flux of CR, it can dramatically change the CR effect regionally, especially at middle and high latitudes. These changes affect the flux of CR impinging on the Earth's atmosphere both locally and globally and must be taken into account when reconstructing solar activity from terrestrial proxy data (e.g., Usoskin et al. 2010; Wu et al. 2018b). Accounting for these effects is quite straightforward provided the geomagnetic changes in the past are known independently, e.g., from archeo- and paleo-magnetic studies (Donadini et al. 2010). However, because of progressively increasing uncertainties of paleomagnetic reconstructions back in time, it presently forms an important difficulty for the proxy method on the long-term scale (Snowball and Muscheler 2007), especially in the early part of the Holocene. On the other hand, the geomagnetic field variations are relatively well known for the last few millennia (Genevey et al. 2008; Korte and Constable 2008; Knudsen et al. 2008; Licht et al. 2013).

---

[1] The concept of VDM assumes that the geomagnetic dipole is centred at the planet's centre and its axis is aligned with the true magnetic axis, while the VADM (virtual axial DM) assumes that the dipole axis is aligned with the Earth's rotational axis.
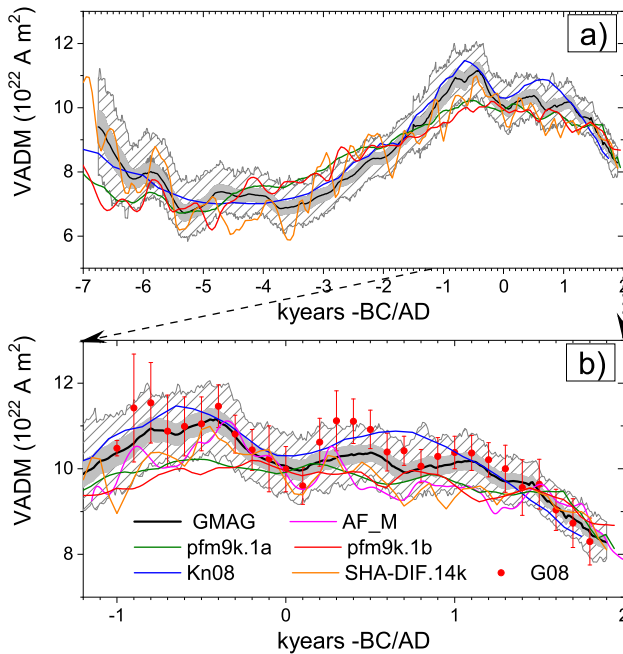
Fig. 5 Geomagnetic field intensity over millennia: VADM reconstructions over past 9000 years (panel a), with zoom for the last 3200 years (panel b). Notations are: GMAG.9k (Usoskin et al. 2016a) with 1σ (gray shading) and the full range variability (hatching); AF_M (Licht et al. 2013); G08 (Genevey et al. 2008); pfm9k.1b and pfm9k.1a (Nilsson et al. 2014); Kn08 (Knudsen et al. 2008); and SHA-DIF.14k (Pavón-Carrasco et al. 2014). Modified after Usoskin et al. (2016a)

3.1.3 Cosmic-ray–induced atmospheric cascade

When an energetic CR particle enters the atmosphere, it first moves straight in the upper layers, suffering mostly from ionization energy losses that lead to the ionization of the ambient rarefied air and gradual deceleration of the particles. However, after traversing some amount of matter (the nuclear interaction mean-free path is on the order of 100 g/cm^2 for a proton in the air) the CR particle may collide with a nucleus in the atmosphere, producing a number of secondaries. These secondaries have their own fate in the atmosphere, in particular, they may suffer further collisions and interactions forming an atmospheric cascade (e.g., Dorman 2004). Because of the thickness of the Earth's atmosphere (1033 g/cm^2 at sea level) the number of subsequent interactions can be large, leading to a fully-developed cascade (also called an air shower) consisting of secondary rather than primary particles. A schematic view of the atmospheric cascade is shown in Fig. 6.

Three main components can be separated in the cascade:

– The *"hadronic" nucleonic* component is formed by the products of nuclear collisions of primary cosmic rays and their secondaries with the atmospheric nuclei, and consists mostly of superthermal protons and neutrons.
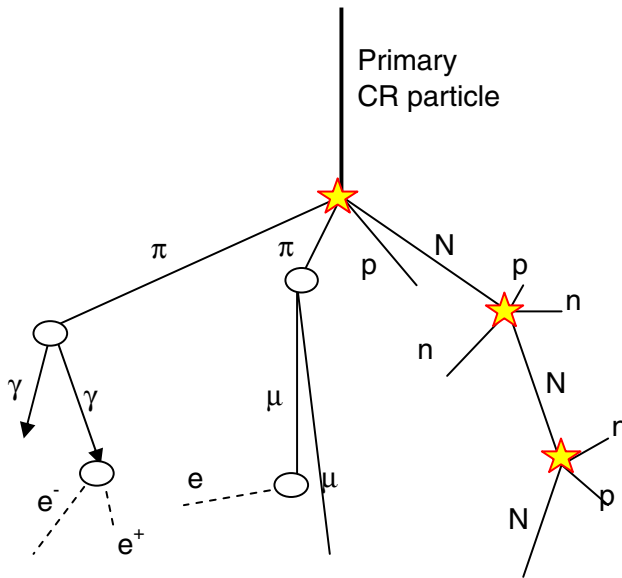
Fig. 6 Schematic view of an atmospheric cascade caused by energetic cosmic rays in the atmosphere. Left-to-right are denoted, respectively, the soft, muon and hadronic components of the cascade. Symbols "N, p, n, μ, π, e^-, e^+, and γ" denote nuclei, protons, neutrons, muons, pions, electrons, positrons, and photons, respectively. Stars denote nuclear collisions, ovals—decay processes. This sketch does not represent the full development of the cascade and serves solely as an illustration of the processes discussed in the text. Image reproduced by permission from Usoskin (2011), copyright by SAIt

– The *"soft"* or electromagnetic component consists of electrons, positrons and photons.
– The *"hard"* or muon component consists mostly of muons; pions are short-lived and decay almost immediately upon production, feeding muons and the "soft" component.

The development of the cascade depends mostly on the amount of matter traversed and is usually linked to residual atmospheric depth, which is very close to the static barometric pressure, rather than to the actual altitude, that may vary depending on the exact atmospheric density profile.

Cosmogenic isotopes are a by-product of the hadronic branch of the cascade (details are given below). Accordingly, in order to evaluate cosmic-ray flux from the cosmogenic isotope data, one needs to know the physics of cascade development. Several models have been developed for this cascade, in particular, its hadronic branch with emphasis on the generation of cosmogenic isotope production. The first models were simplified quasi-analytical (e.g., Lingenfelter 1963; O'Brien and Burke 1973) or semi-empirical models (e.g., Castagnoli and Lal 1980). With the fast advance of computing facilities, it became possible to exploit the best numerical method suitable for such problems—Monte-Carlo (e.g., Argento et al. 2013; Kovaltsov and Usoskin 2010; Kovaltsov et al. 2012; Masarik and Beer 1999, 2009; Poluianov et al. 2016; Usoskin and Kovaltsov 2008; Webber and Higbie 2003;
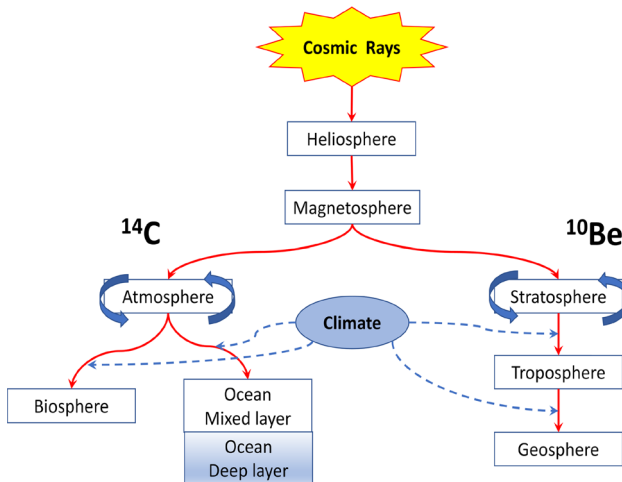
Fig. 7 Schematic representation of ^{14}C (left) and ^{10}Be (right) production chains. The flux of cosmic rays impinging on the Earth is affected by both heliospheric modulation and geomagnetic field changes. The climate may affect the redistribution of the isotopes between different reservoirs. The dashed line denotes a possible influence of solar activity on climate

Webber et al. 2007). The fact that models, based on different independent Monte-Carlo packages, namely, a general GEANT tool (Agostinelli et al. 2003, – https://geant4.web.cern.ch/) and a specific CORSIKA code (Heck et al. 1998, – https://www.iap.kit.edu/corsika/), yield similar results and provides additional verification of the approach.

3.1.4 Transport and deposition

A scheme for the transport and redistribution of the two most useful cosmogenic isotopes, ^{14}C and ^{10}Be, is shown in Fig. 7. After a more-or-less similar production, the two isotopes follow different fates, as discussed in detail in Sects. 3.2.3 and 3.3.3. Therefore, expected terrestrial effects are quite different for the isotopes and comparing them with each other can help in disentangling solar and climatic effects (see Sect. 3.7.3). A reader can find great detail also in a book by Beer et al. (2012).

3.2 Radioisotope ^{14}C

The most commonly used cosmogenic isotope is radiocarbon ^{14}C. This radionuclide is an unstable isotope of carbon with a half-life $\left(T_{1/2}\right)$ of about 5730 years. Since the radiocarbon method is extensively used in other science disciplines where accurate dating is a key issue (e.g., archaeology, palaeoclimatology, quaternary geology), it was developed primarily for this task. The solar-activity–reconstruction method, based on radiocarbon data, was initially developed as a by-product of the dating techniques used in archaeology and Quaternary geology, in an effort to improve the quality of the dating by means of better information on the ^{14}C variable source

function. The present-day radiocarbon calibration curve, based on a dendrochronological scale, uninterruptedly covers the whole Holocene (and extending to 50 000 BP—Reimer et al. 2020) and provides a solid quantitative basis for studying solar activity variations on the multi-millennial time scale.

3.2.1 Measurements

Radiocarbon is usually measured in tree rings, which allows an absolute dating of the samples by means of dendrochronology. Using a complicated technique, the ^{14}C activity[2] A is measured in an independently dated sample, which is then corrected for age as

$$A^* = A \cdot \exp\left(\frac{0.693\,t}{T_{1/2}}\right),\qquad(5)$$

where t and $T_{1/2}$ are the age of the sample and the half-life of the isotope, respectively. Then the relative deviation from the standard activity A_o of oxalic acid (the National Bureau of Standards) is calculated:

$$\delta^{14}C = \left(\frac{A^* - A_o}{A_o}\right) \cdot 1000\,.\qquad(6)$$

After correction for the carbon isotope fractionating (account for the ^{13}C isotope) of the sample, the radiocarbon value of Δ^{14}C is calculated (see details in Stuiver and Pollach 1977).

$$\Delta^{14}C = \delta^{14}C - (2 \cdot \delta^{13}C + 50) \cdot (1 + \delta^{14}C/1000)\,,\qquad(7)$$

where δ^{13}C is the per mille deviation of the ^{13}C content in the sample from that in the standard belemnite sample calculated similarly to Eq. (6). The value of Δ^{14}C (measured in per mille ‰) is further used as the index of radiocarbon relative activity. The series of Δ^{14}C for the Holocene is presented in Fig. 8a as published by the IntCal collaboration of 21 dating laboratories as a result of systematic precise measurements of dated samples from around the world (Reimer et al. 2020) http://intcal.org/. Panel b depicts the production rate Q_{14C} reconstructed by Roth and Joos (2013) using the most up-to-date carbon cycle model.

A potentially interesting approach has been made by Lal et al. (2005), who measured the amount of ^{14}C directly produced by CR in polar ice. Although this method is free of the carbon-cycle influence, the first results, while being in general agreement with other methods, are not precise.

---

[2] Isotope's activity quantifies (a) in the radiometric ^{14}C technique its decay rate, and is usually given in terms of disintegrations per minute per gram of carbon, and (b) in the AMS technique, the ^{14}C/^{12}C ratio, all normalized to the standard.
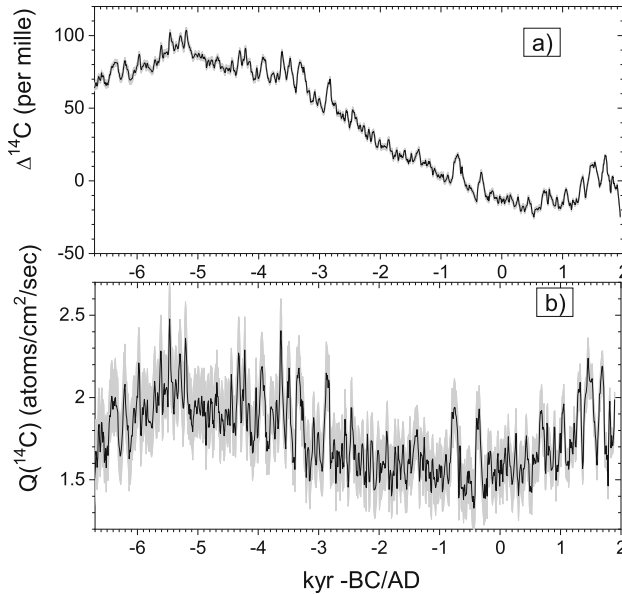
Fig. 8 Radiocarbon series for the Holocene. *Upper panel:* Measured content of Δ^{14}C in tree rings by IntCal13 collaboration (Reimer et al. 2013) (http://www.radiocarbon.org/IntCal13.htm). The long-term trend is caused by the geomagnetic field variations and the slow response of the oceans. *Lower panel:* Production rate of ^{14}C in the atmosphere, reconstructed from the measured Δ^{14}C, along with the 95% confidence interval (Roth and Joos 2013)

3.2.2 Production

The main source of radioisotope ^{14}C (except anthropogenic sources during the last decades) is cosmic rays in the atmosphere. It is produced as a result of the *np*-reaction often called the capture of a thermal neutron by atmospheric nitrogen

$$^{14}\text{N} + n \rightarrow {}^{14}\text{C} + p \,. \tag{8}$$

Neutrons are always present in the atmosphere as a product of the cosmic-ray–induced cascade (see Sect. 3.1.3) but their flux varies in time along with the modulation of cosmic-ray flux. This provides a continuous source of the isotope in the atmosphere, while the sinks are isotope decay and transport into other reservoirs as described below (the carbon cycle).

The connection between the cosmogenic-isotope–production rate, Q, at a given location (quantified via the geomagnetic latitude λ_{G}) and the cosmic-ray flux at a given time t is

$$Q(t) = \int_{P_{\text{c}}(\lambda_{\text{G}})}^{\infty} S(P,t) \, Y(P) \, dP \,, \tag{9}$$

where P_{c} is the local cosmic-ray–rigidity cutoff (see Sect. 3.1.2), $S(P, t)$ is the differential energy spectrum of CR, either galactic (see Sect. 3.1.1) or solar origin,
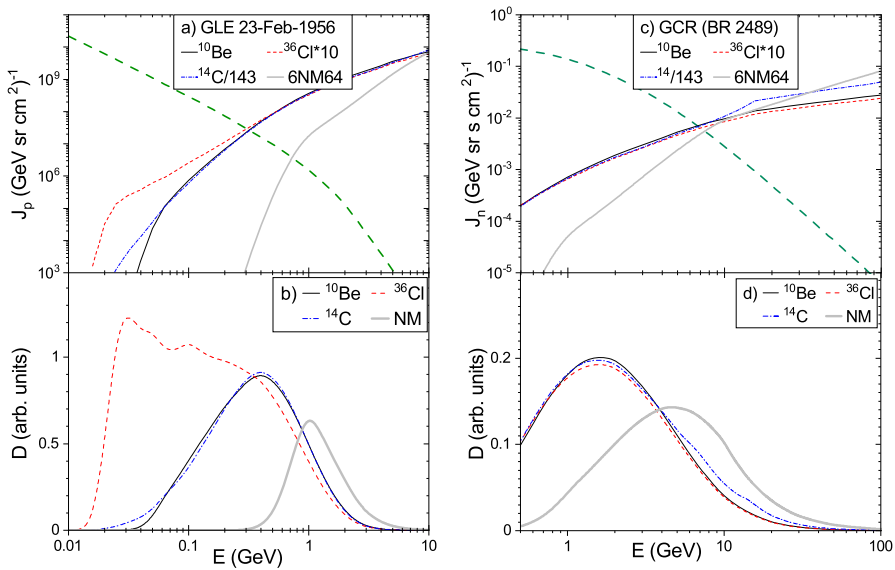
Fig. 9 *Panel a:* Differential energy spectrum of SEP for GLE#5 of 23-Feb-1956 (green dashed curve—Koldobskiy et al. 2021) as well as the production/deposition (yield) functions of a polar 6NM64 neutron monitor (Mishev et al. 2020) and cosmogenic isotopes (Poluianov et al. 2016) ^{10}Be and ^{36}Cl (scaled up with a factor of 10) in polar ice as well as global ^{14}C (scaled down by a factor of 143), as denoted in the legend. The yield functions are shown for primary cosmic-rays protons and given in arbitrary units and the modern geomagnetic field strength ($M = 7.75 \times 10^{22}$ A m^2). *Panel b:* differential response functions (viz. a product of the energy spectrum and yield functions shown in panel a) for the three isotopes and a polar sea-level NM for GLE#5. *Panel c:* Similar to panel a but for the GCR spectrum for Bartel rotation BR 2489 (10-Jan-2016 through 05-Feb-2016). *Panel d:* Similar to panel b but for the GCR spectrum shown in panel c. The plot is based on computations of Koldobskiy et al. (2022b)

and $Y(P)$ is the differential yield function of cosmogenic isotope production, calculated using a Monte-Carlo simulation of the cosmic-ray–induced atmospheric cascade (Kovaltsov et al. 2012; Poluianov et al. 2016). Because of the global nature of the carbon cycle and its long attenuation time, the radiocarbon is globally mixed before the final deposition, and Eq. (9) should be integrated over the globe. The yield function $Y(P)$ of the ^{14}C production is shown in Fig. 9a together with those for ^{10}Be (see Sect. 3.3.2) and for a ground-based neutron monitor (NM), which is the main instrument for studying cosmic-ray variability during the modern epoch. One can see that the yield function increases with the energy of CR. On the other hand, the energy spectrum of CR decreases with energy. Accordingly, the differential production rate (i.e., the product of the yield function and the spectrum, $F = Y \cdot S$—the integrand of Eq. (9)), shown in Fig. 9b, is more informative. The differential production rate reflects the sensitivity to cosmic rays, and the total production rate is simply an integral of F over energy above the geomagnetic threshold.

Thanks to the development of atmospheric cascade models (Sect. 3.1.3), there are numerical models that allow one to compute the radiocarbon production rate as a
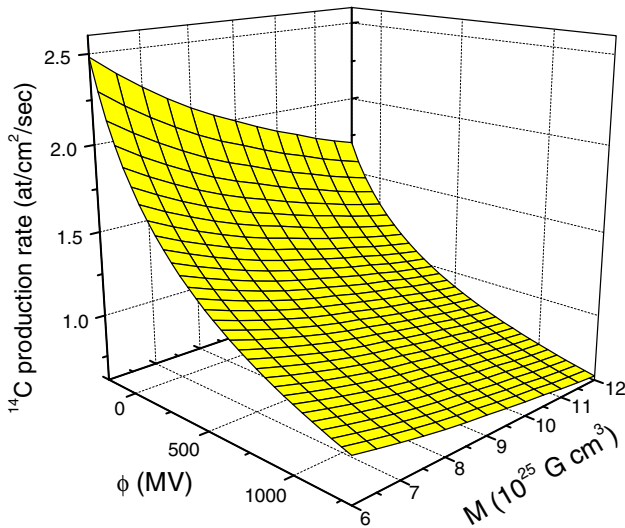
Fig. 10 Globally-averaged production rate of ^{14}C as a function of the modulation potential ϕ and geomagnetic dipole moment M, computed using the yield function by Kovaltsov et al. (2012), LIS by Burger et al. (2000) and cosmic-ray–modulation model by Usoskin et al. (2005). Other models (Masarik and Beer 2009; Poluianov et al. 2016) yield a similar result

function of the modulation potential ϕ and the geomagnetic dipole moment M. The overall production of ^{14}C is shown in Fig. 10.

The production rate of radiocarbon, Q_{14C}, can vary as affected by different factors (see, e.g., Damon and Sonett 1991):

– Variations of the cosmic-ray flux on a geological timescale due to the changing galactic background (e.g., a nearby supernova explosion or crossing the dense galactic arm).
– Secular-to-millennial variations are caused by the slowly-changing geomagnetic field. This is an important component of the variability, which needs to be independently evaluated from paleo and archeo-magnetic studies.
– Modulation of cosmic rays in the heliosphere by solar magnetic activity. This variation is the primary aim of the present method.
– Short-term variability of CR on a daily scale (suppression due to interplanetary transients or enhancement due to solar energetic-particle events) can be hardly resolved in radiocarbon data.
– Extremely strong SEP events can produce strong spikes in the isotope production detectable in annually resolved data (Sect. 5).

Therefore, the production rate of ^{14}C in the atmosphere can be modelled for a given time (namely, the modulation potential and geomagnetic dipole moment) and location. The global production rate Q is then obtained as a result of global averaging.

Table 2 Effective energies (in GeV/nuc) of cosmogenic isotope production by GCR and SEP. Details of computations are available from Koldobskiy et al. (2022b)

Isotope	GCR	SEP
^{14}C	2.48 ± 0.02	0.234 ± 0.018
^{10}Be	2.00 ± 0.02	0.236 ± 0.016
^{36}Cl	1.95 ± 0.02	0.06 ± 0.007

Present-day models excellently agree with the measurements. For example, the mean global-averaged ^{14}C production rate for the period 1750–1900 is estimated from measurements as 1.75 ± 0.01 atoms cm^{-2} s^{-1} (Roth and Joos 2013). The production model (Poluianov et al. 2016) yields for the same period theoretical production rate 1.71–1.76 atoms cm^{-2} s^{-1}, depending on the solar activity and geomagnetic field reconstructions used, being thus in an excellent agreement with the data. The most updated model of radiocarbon production is CRAC:14C (Poluianov et al. 2016).

Effective energy of ^{14}C production is about 2.5 GeV/nuc for GCR and 234 MeV for SEPs (Koldobskiy et al. 2022b). Effective energies are summarized in Table 2.

3.2.3 Transport and deposition

Upon production, cosmogenic radiocarbon gets quickly oxidized to carbon dioxide CO_2 and takes part in the regular carbon cycle of interrelated systems: atmosphere-biosphere-ocean (Fig. 11). Because of the long residence time, radiocarbon becomes globally mixed in the atmosphere and involved in an exchange with the ocean. It is common to distinguish between an upper layer of the ocean, which can directly exchange CO_2 with the air and deeper layers. The measured Δ^{14}C comes from the biosphere (trees), which receives radiocarbon from the atmosphere. Therefore, the processes involved in the carbon cycle are quite complicated. The carbon cycle is usually described using a box model (Oeschger et al. 1974; Siegenthaler et al. 1980), where it is represented by fluxes between different carbon reservoirs and mixing within the ocean reservoir(s), as shown in Fig. 11. Production and radioactive decay are also included in box models. Free parameters in a typical box model are the ^{14}C production rate Q, the air-sea exchange rate (expressed as turnover rate κ), and the vertical–eddy-diffusion coefficient K, which quantifies ocean ventilation. Starting from the original representation (Oeschger et al. 1974), a variety of box models have been developed, which take into account subdivisions of the ocean reservoir and direct exchange between the deep ocean and the atmosphere at high latitudes. The most recent box-diffusion model (Güttler et al. 2015) includes 22 boxes and is suitable to study even fast changes in ^{14}C. More complex models, including a diffusive approach, are able to simulate more realistic scenarios, but they require knowledge of a large number of model parameters. These parameters can be evaluated for the present time using the bomb test—studying the transport and
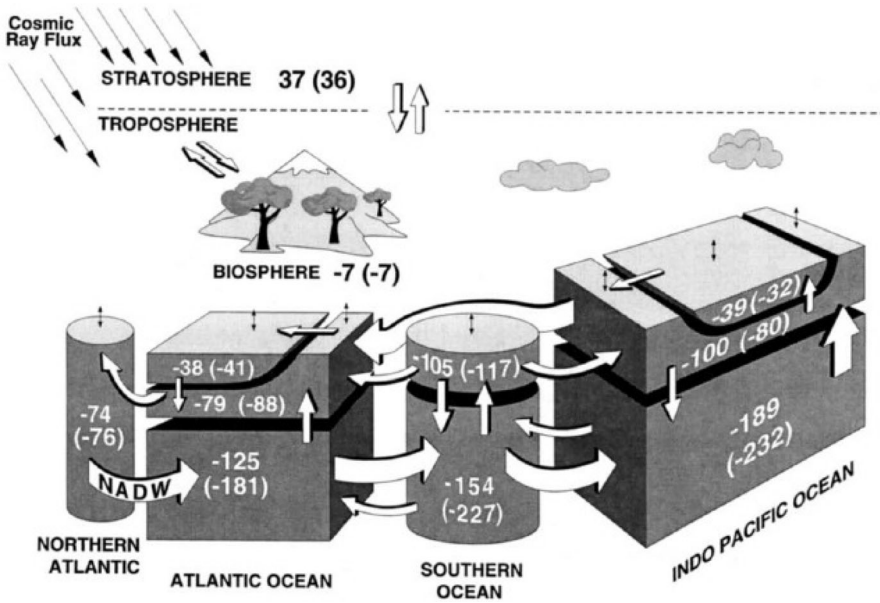
Fig. 11 A 12-box model of the carbon cycle (Broeker and Peng 1986; Siegenthaler et al. 1980). The number on each individual box is the steady-state $\Delta^{14}C$ of this particular reservoir expressed in per mil. Image reproduced by permission from Bard et al. (1997), copyright by Elsevier

distribution of the radiocarbon produced during the atmospheric nuclear tests. However, for long-term studies, only the production rate is considered variable, while the gas-exchange rate and ocean mixing are kept constant. Under such assumptions, there is no sense in subdividing reservoirs or processes, and a simple carbon-box model is sufficient.

Using the carbon cycle model and assuming that all its parameters are constant in time, one can evaluate the production rate Q from the measured $\Delta^{14}C$ data. This assumption is well validated for the Holocene (Damon et al. 1978; Stuiver et al. 1991) as there is no evidence of considerable oceanic change or another natural variability of the carbon cycle (Gerber et al. 2002), and accordingly all variations of $\Delta^{14}C$ predominantly reflect the production rate. This is supported by the strong similarity of the fluctuations of the ^{10}Be data in polar ice cores (Sect. 3.3) compared to ^{14}C, despite their completely different geochemical fate (Bard et al. 1997; Steinhilber et al. 2012). However, the changes in the carbon cycle during the last glaciation and deglaciation were dramatic, especially regarding ocean ventilation; this and the lack of independent information about the carbon cycle parameters, make it hardly possible to qualitatively estimate solar activity from ^{14}C before the Holocene.

A new-generation carbon cycle model has been developed moving from static box-exchange models to a dynamic model. Roth and Joos (2013) presented a fully featured model of intermediate complexity, named Bern3D-LPJ, which includes in addition to the dynamical atmosphere, a 3D dynamic ocean, ocean sediments, and

vegetation models. So far this is the most sophisticated and complete radiocarbon cycle model. A multi-millennial reconstruction of the ^{14}C production rate, obtained as a result of the application of this model to the IntCal09 radiocarbon data (Reimer et al. 2009) is shown in Fig. 8b.

First attempts to extract information on production-rate variations from measured $\Delta^{14}C$ were based on simple frequency separations of the signals. All slow changes were ascribed to climatic and geomagnetic variations, while short-term fluctuations were believed to be of solar origin. This was done by removing the long-term trend from the $\Delta^{14}C$ series and claiming the residual as being a series of solar variability (e. g., Peristykh and Damon 2003). This oversimplified approach was natural at earlier times, before the development of carbon cycle models, but later it was replaced by the inversion of the carbon cycle (i.e., the reconstruction of the production rate from the measured ^{14}C concentration). Although mathematically this problem can be solved correctly as a system of linear differential equations, the presence of fluctuating noise with large magnitude makes it not straightforward since the time derivative cannot be reliably identified leading thus to possible amplification of the high-frequency noise in $\Delta^{14}C$ data. One traditional approach (e.g., Stuiver and Quay 1980) is based on an iterative procedure, first assuming a constant production rate, and then fitting the calculated $\Delta^{14}C$ variations to the actual measurements using a feedback scheme. A concurrent approach based on the presentation of the carbon cycle as a Fourier filter (Usoskin and Kromer 2005) produces similar results. Roughly speaking, the carbon cycle acts as an attenuating and delaying filter for the ^{14}C signal (see Fig. 12). The higher the frequency is, the greater the signal is attenuated. In particular, the large 11-year solar cycle expected in the ^{14}C is attenuated by a factor of hundred in the measured $\Delta^{14}C$ data, making it difficult to detect. Because of the slow oceanic response, the ^{14}C data is also delayed with respect to the production signal. The production rate $Q_{^{14}C}$ for the Holocene is shown in Fig. 8 and depicts both short-term fluctuations as well as slower variations, mostly due to geomagnetic field changes (see Sect. 3.2.5).
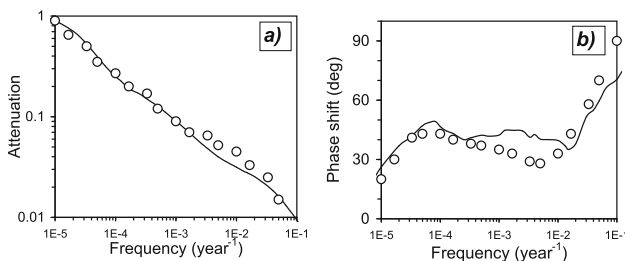

Fig. 12 The frequency characteristics of the carbon cycle: attenuation (left-hand panel) and phase shift (right-hand panel) as a function of the frequency of the ^{14}C production signal. Lines stand for a classical Oeschger–Siegenthaler box model (Siegenthaler et al. 1980), and open circles for a sophisticated PANDORA model (Bard et al. 1997)

3.2.4 The Suess effect and nuclear bomb tests

Unfortunately, cosmogenic ^{14}C data cannot be easily used for the last century, primarily because of the extensive burning of fossil fuels. Since fossil fuels do not contain ^{14}C, the produced CO_2 dilutes the atmospheric $^{14}CO_2$ concentration with respect to the pre-industrial epoch. Therefore, the measured Δ^{14}C cannot be straightforwardly translated into the production rate Q after the late 19th century, and a special correction for fossil fuel burning is needed. This effect, known as the Suess effect (e.g., Suess 1955), can be up to $-25‰$ in Δ^{14}C in 1950 (Tans et al. 1979), which is an order of magnitude larger than the amplitude of the 11-year cycle of a few ‰. Moreover, while the cosmogenic production of ^{14}C is roughly homogeneous over the globe and time, the use of fossil fuels is highly nonuniform (e.g., de Jong and Mook 1982) both spatially (developed countries, in the northern hemisphere) and temporarily (World Wars, Great Depression, industrialization, etc.). This makes it very difficult to perform an absolute normalization of the radiocarbon production to the direct measurements. Sophisticated numerical models (e.g., Mikaloff Fletcher et al. 2006; Sabine et al. 2004) aim to account for the Suess effect and make good progress. However, the results obtained indicate that the determination of the Suess effect does not yet reach the accuracy required for the precise modelling and reconstruction of the ^{14}C production for the industrial epoch. Note that the atmospheric concentration of another carbon isotope ^{13}C is partly affected by land use, which has also been modified during the last centuries.

Another anthropogenic activity greatly disturbing the natural variability of ^{14}C is related to the atmospheric nuclear bomb tests actively performed in the 1960s. For example, the radiocarbon concentration nearly doubled in the early 1960s in the northern hemisphere after nuclear tests performed by the USSR and the USA in 1961 (Damon et al. 1978). On one hand, such sources of momentary spot injections of radioactive tracers (including ^{14}C) provide a good opportunity to verify and calibrate the exchange parameters for different carbon-cycle reservoirs and circulation models (e.g., Bard et al. 1987; Sweeney et al. 2007). Thus, the present-day carbon cycle is more or less known. On the other hand, the extensive additional production of isotopes during nuclear tests makes it hardly possible to use the ^{14}C as a proxy for solar activity after the 1950s (Joos 1994).

These anthropogenic effects do not allow one to make a straightforward link between pre-industrial data and direct experiments performed during more recent decades.

3.2.5 The effect of the geomagnetic field

As discussed in Sect. 3.1.2, knowledge of geomagnetic shielding is an important aspect of the cosmogenic isotope method. Since radiocarbon is globally mixed in the atmosphere before deposition, its production is affected by changes in the geomagnetic dipole moment M, while magnetic-axis migration plays hardly any role in ^{14}C data.

The crucial role of paleomagnetic reconstructions has long been known (e.g., Elsasser et al. 1956; Kigoshi and Hasegawa 1966). Many earlier corrections for possible geomagnetic-field changes were performed by detrending the measured $\Delta^{14}C$ abundance or production rate Q (Peristykh and Damon 2003; Stuiver and Quay 1980; Voss et al. 1996), under the assumption that geomagnetic and solar signals can be disentangled from the production in the frequency domain. Accordingly, the temporal series of either measured $\Delta^{14}C$ or its production rate Q was decomposed into the slow-changing trend and faster oscillations. The trend is supposed to be entirely due to geomagnetic changes, while the oscillations are ascribed to solar variability. Such a method, however, obliterates all information on possible long-term variations of solar activity. On the other hand, this also misinterprets the short-term (centennial timescale) variations of the geomagnetic field which are essential (e.g., Licht et al. 2013; Pavón-Carrasco et al. 2018). Accordingly, the frequency-domain decomposition may lead to erroneous results. A direct correction for the geomagnetic field effect should be used instead.

Simplified empirical correction factors were also often used (e.g., Stuiver and Quay 1980; Stuiver et al. 1991). The modern approach is based on a physics-based model (e.g., Solanki et al. 2004; Vonmoos et al. 2006; Wu et al. 2018b) and allows the quantitative reconstruction of solar activity, explicitly using independent reconstructions of the geomagnetic field. In this case, the major source of errors in solar activity reconstructions is related to uncertainties in the paleomagnetic data (Snowball and Muscheler 2007). These errors are insignificant for the last several millennia (Licht et al. 2013; Usoskin et al. 2016a), but become increasingly important in earlier times.

3.3 Cosmogenic isotope ^{10}Be

3.3.1 Measurements

The cosmogenic isotope ^{10}Be is useful for long-term studies of solar activity because of its long half-life of around 1.4×10^6 years. Its concentration is usually measured in stratified ice cores allowing for independent dating. The ^{10}Be/^{9}Be ratio needs to be precisely measured at an accuracy better than 10^{-13}. This can be done using AMS (Accelerator Mass Spectrometry) technique, which makes the measurements complicated and expensive. Correction for the decay is straightforward and does not include isotope fractionating. From the measured samples, first the ^{10}Be concentration is defined, usually in units of 10^4 atoms/g. Sometimes, a correction for the snow precipitation amount is considered leading to the observable ^{10}Be flux, which is the number of atoms, precipitating to the surface per cm^2 per second.

There exist different ^{10}Be series suitable for studies of long-term solar activity, coming from ice cores in Greenland and Antarctica. They have been obtained from different cores with different resolutions, and include data from Milcent, Greenland (Beer et al. 1983); Camp Century, Greenland (Beer et al. 1988); Dye 3, Greenland (Beer et al. 1990); Dome Concordia and South Pole, Antarctica (Raisbeck et al. 1990); GRIP, Greenland (Yiou et al. 1997); GISP2, Greenland (Finkel and

Nishiizumi 1997); Dome Fuji, Antarctica (Horiuchi et al. 2007, 2008; Miyake et al. 2015); Dronning Maud Land, Antarctica (Ruth et al. 2007); NGRIP (North Greenland Ice Core Project), Greenland (Berggren et al. 2009); NEEM (North Greenland Eemian Ice Drilling), Greenland (Sigl et al. 2015); West Antarctic Ice Sheet Divide Ice Core (WAIS/WDC), Antarctica (Sigl et al. 2015), etc.

We note that data on ^{10}Be in other archives, e.g., lake sediments, is usually more complicated to interpret because of the potential influence of the climate (Belmaker et al. 2008; Horiuchi et al. 1999).

Details of the ^{10}Be series and their comparison with each other can be found in Beer (2000), Muscheler et al. (2007), and Beer et al. (2012).

3.3.2 Production

The isotope ^{10}Be is produced as a result of the spallation of atmospheric nitrogen and oxygen by the nucleonic component of the cosmic-ray–induced atmospheric cascade (Sect. 3.1.3).

A small contribution may also exist from photo-nuclear reactions (Bezuglov et al. 2012). The cross-section (a few mbar) of the spallation reactions is almost independent of the energy of impacting particles and has a threshold of about 15 MeV. Thus, the production of ^{10}Be is defined mostly by the multiplicity of the nucleonic component, which increases with the energy of primary cosmic rays (see Fig. 9). Maximum production occurs at an altitude of 10–15 km due to a balance between the total energy of the cascade (which increases with altitude) and the number of secondaries (decreasing with altitude). Slightly more than half of global ^{10}Be is produced in the stratosphere (50–60%) and the rest in the troposphere (Golubenko et al. 2022; Heikkilä et al. 2013; Kovaltsov and Usoskin 2010; Usoskin and Kovaltsov 2008). For SEPs, the production is mostly ($> 90\%$) in the polar stratosphere.

Computation of ^{10}Be isotope production is straightforward, provided a model of the atmospheric cascade is available. The first consistent model was developed by Lal et al. (Bhandari et al. 1966; Lal and Peters 1967; Lal and Suess 1968), using an empirical approach based on fitting simplified model calculations to measurements of the isotope concentrations and "star" (inelastic nuclear collisions) formations in the atmosphere. Next was an analytical model by O'Brien (1979), who solved the problem of the GCR-induced cascade in the atmosphere using an analytical stationary approximation in the form of the Boltzmann equation. Those models were based on calculating the rate of inelastic collisions or "stars" and then applying the mean spallation yield per "star". A new step in the modelling of isotope production was made by Masarik and Beer (1999), who performed a full Monte Carlo simulation of a GCR-initiated cascade in the atmosphere and used cross-sections of spallation reactions directly instead of the average "star" efficiency. Modern models (Kovaltsov and Usoskin 2010; Poluianov et al. 2016; Usoskin and Kovaltsov 2008; Webber and Higbie 2003; Webber et al. 2007) are based on a full Monte-Carlo simulation of the atmospheric cascade, using improved cross sections. The global production rate of ^{10}Be is about 0.02–0.04 atoms cm^{-2} s^{-1} (Kovaltsov and Usoskin 2010; Masarik and

Beer [1999]; Poluianov et al. [2016]; Webber et al. [2007]), which is lower than that for ^{14}C (about 2 atoms cm^{-2} s^{-1}; see Sect. 3.2.2) by two orders of magnitude. The yield function of ^{10}Be production is shown in Fig. 9. The peak of ^{10}Be sensitivity is very similar to that of ^{14}C and lower than that for a neutron monitor. The effective energy of ^{10}Be production is close to that of ^{14}C for both GCR and SEP (see Table 2). Comparison of model computations with direct beryllium production experiments (Kovaltsov and Usoskin [2010]; Usoskin and Kovaltsov [2008]), and also the results of modelling of the short-living ^{7}Be isotope (Golubenko et al. [2021]; Usoskin et al. [2009a]) suggest that earlier numerical models (Masarik and Beer [1999]; Webber and Higbie [2003]; Webber et al. [2007]) tend to underestimate the production.

Although the production of ^{10}Be can be more or less precisely modelled, a simple normalization "surface", similar to that shown in Fig. 10 for ^{14}C, is not easy to produce because of partial mixing in the atmosphere (see Sect. 3.3.3). Simplified models, assuming either only global (e.g., Beer [2000]) or polar production (Bard et al. [1997]; Usoskin et al. [2004]), have been used until recently. However, it has been recognized that a more realistic model of the limited atmospheric mixing should be used. Without detailed knowledge of ^{10}Be transport in the atmosphere, it is impossible to relate the quantitatively-measured concentration to the production (as done for ^{14}C using the carbon cycle), and one has to assume that the measured abundance is proportional (with an unknown coefficient) to the production rate in a specific geographical region (see Sect. 3.3.3).

3.3.3 Atmospheric transport

After production, the ^{10}Be isotope has a seemingly simple (Fig. 7) but difficult-to-account-for fate in the atmosphere. Its atmospheric residence time depends on scavenging, stratosphere-troposphere exchange and inter-tropospheric mixing (e.g., McHargue and Damon [1991]). Soon after production, the isotope is thought to become attached to atmospheric aerosols and follows their fate (Beer et al. [2012]). In addition, it may be removed from the lower troposphere by wet deposition (rain and snow). The mean residence time of the aerosol-bound radionuclide in the atmosphere is quite different for the troposphere, being a few weeks, and stratosphere, where it is one to two years (Raisbeck et al. [1981]). Accordingly, ^{10}Be produced in the troposphere is deposited mostly locally, i.e., in the polar regions, while stratospheric ^{10}Be can be partly or totally mixed. In addition, because of the seasonal (usually Spring) intrusion of stratospheric air into the troposphere at mid-latitudes, there is an additional contribution of stratospheric ^{10}Be. Therefore, the measured ^{10}Be concentration (or flux) in polar ice is modulated not only by production but also by climate/precipitation effects (e.g., Bard et al. [1997]; Steig et al. [1996]). This led Lal ([1987]) to the extreme conclusion that variations of polar ^{10}Be reflect a meteoro-logical, rather than solar signal. However, comparison between Greenland and Antarctic ^{10}Be series and between ^{10}Be and ^{14}C data (e.g., Bard et al. [1997]; Beer et al. [2012]; Horiuchi et al. [2008]; Steinhilber et al. [2012]; Usoskin et al. [2009b]; Wu et al. [2018b]) suggests that the beryllium data mostly depicts production variations (i.

e., solar signal) on top of which some meteorological effects can be superposed (see also Sect. 3.7.3).

Since both assumptions of the global and purely-local polar production of ^{10}Be archived in polar ice are over-simplified, several attempts have been made to overcome this problem. For instance, Vonmoos et al. (2006) assumed that the production of ^{10}Be recorded in Greenland is related to the entire hemisphere in the stratosphere (i.e, global stratospheric mixing) but is limited to latitudes above 40° latitude in the troposphere (partial tropospheric mixing). This approach uses either semi-empirical or indirect arguments in choosing the unknown degree of mixing.

Recent efforts in employing modern atmospheric 3D circulation models for simulations of ^{10}Be transport and deposition, including realistic air-mass transport and dry-vs-wet deposition (Field et al. 2006; Golubenko et al. 2021; Heikkilä et al. 2008, 2009), look more promising. An example of ^{10}Be deposition computed on the world grid using the NASA GISS model (Field et al. 2006) is shown in Fig. 13. The
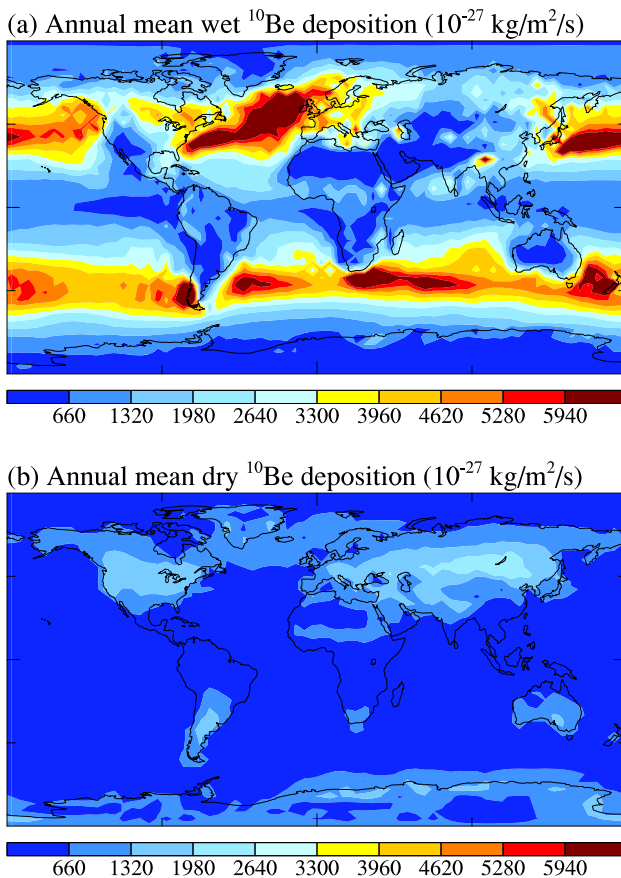
(a) Annual mean wet ^{10}Be deposition (10^{-27} kg/m^2/s)

(b) Annual mean dry ^{10}Be deposition (10^{-27} kg/m^2/s)

Fig. 13 Wet (panel a) and dry (panel b) deposition of ^{10}Be, computed using the NASA GISS model (Field et al. 2006) for a fixed sea-surface temperature

precision of the models allows one to distinguish local effects, e.g., for Greenland (Heikkilä et al. 2008). A simulation performed by combining a detailed ^{10}Be-production model with an air-dynamics model can result in an absolute model relating the production and deposition of the radionuclide. The validity and usefulness of this approach have been recently demonstrated by Usoskin et al. (2009a), who directly modelled production (using the CRAC model – Usoskin and Kovaltsov 2008) and transport (using the GISS ModelE—Koch et al. 2006) of a short-living beryllium isotope ^{7}Be and showed that such a combined model is able to correctly reproduce both the absolute level and temporal variations of the ^{7}Be concentration measured in near-ground air around the globe. Keeping in mind the similarity between the production and transport of the two beryllium isotopes, ^{7}Be and ^{10}Be, this serves as a support for the advanced modelling of ^{10}Be transport. Similar agreement between measured and modelled seasonal variability has been confirmed by other models, ECHAM5-HAM (Pedro et al. 2011) and SOCOL (Golubenko et al. 2021) suggesting that the modern models can catch sufficient accuracy of beryllium transport.

3.3.4 Effect of the geomagnetic field

In order to properly account for geomagnetic changes (Sect. 3.1.2), one needs to know the effective region in which the radionuclide is produced before being stored in the archive analyzed. For instance, if the concentration of ^{10}Be measured in polar ice reflects mainly the isotope's production in the polar atmosphere (as, e.g., assumed by Usoskin et al. 2003c), no strong geomagnetic signal is expected to be observed, since the geographical poles are mostly related to high geomagnetic latitudes. On the other hand, assuming global mixing of atmospheric ^{10}Be before deposition in polar ice (e.g., Masarik and Beer 1999), one expects that only changes in the geomagnetic dipole moment affect the signal. However, because of partial mixing, which can be different in the stratosphere and troposphere, taking into account migration and displacement of the geomagnetic dipole axis may be essential for a reliable reconstruction of solar variability from ^{10}Be data (McCracken 2004). Therefore, only a full combination of the transport and production models, the latter explicitly including geomagnetic effects estimated from paleomagnetic reconstructions, can adequately account for geomagnetic changes and separate the solar signal. These form a new generation of physics-based models for the cosmogenic-isotope proxy method. We note that paleomagnetic data should ideally not only provide the dipole moment (VADM or VDM) but should also provide estimates of the geomagnetic axis attitude and displacement of the dipole centre (Korte et al. 2011).

3.4 Cosmogenic isotope ^{36}Cl

Another useful isotope is chlorine-36 (^{36}Cl) which has a half-life time of about 301300 years. It is produced by the spallation of atmospheric argon by cosmic-ray particles and secondaries of the atmospheric cascades (Poluianov et al. 2016). Because of the much smaller production rate (argon is much less abundant than

nitrogen and oxygen), it is very difficult to measure. Accordingly, ^{36}Cl is not used to study long-term solar activity. On the other hand, as seen in Fig. 9, production of ^{36}Cl is much more sensitive to lower-energy cosmic rays than other isotopes. This makes chlorine-36 very important to study extreme SEP events (Sect. 5) as it allows us to estimate the energy spectrum of such events (e.g., Mekhaldi et al. 2015; Paleari et al. 2022).

The chlorine-36 isotope takes part in the global chlorine cycle but often is considered to be similar in transport to the beryllium isotope (Heikkilä et al. 2013). It cannot be used after the 1950s because of the large amount of ^{36}Cl produced during the bomb tests.

3.5 Towards a quantitative physical model

Several methods have been developed historically to convert measured cosmogenic-isotope data into a solar activity index, ranging from very simple regressions to physics-based models. The proxy method in which physics-based models are used instead of a phenomenological regression is being developed to link SN series with cosmogenic-isotope production (Muscheler et al. 2007; Solanki et al. 2004; Steinhilber et al. 2012; Usoskin et al. 2003c, 2007, 2014, 2016a; Vonmoos et al. 2006; Wu et al. 2018b). Due to recent theoretical developments, it is now possible to construct a full chain of physical models for the entire relationship between solar activity and cosmogenic data.

The physics-based reconstruction of solar activity (in terms of sunspot numbers) from cosmogenic proxy data includes several steps (e.g., Wu et al. 2018b):

1. Computation of the isotope's production rate in the atmosphere from the measured concentration in the archive (Sects. 3.2.2 and 3.3.2);
2. Computation, considering independently known secular geomagnetic changes (see Sect. 3.2.5) and a model of the CR-induced atmospheric cascade, of the GCR spectrum parameter quantified via the modulation potential ϕ (Sect. 3.5.2), some reconstructions being terminated at this point, some others skip this step going directly to the next one;
3. Computation of a physical heliospheric index, whether of the open solar magnetic flux or the average heliospheric magnetic field (HMF) intensity at the Earth's orbit (Sect. 3.5.2);
4. Computation of a solar index (sunspot number series), corresponding to the above-derived heliospheric parameter (Sect. 3.5.3).

Presently, all these steps can be completed using appropriate models. Some models stop after computations of the modulation potential as its translation into the solar index may include additional uncertainties. Although the uncertainties of the models may be considerable, the models allow a full basic quantitative reconstruction of solar activity in the past. Modern models (Usoskin et al. 2021b; Wu et al. 2018b) lead to pseudo-sunspot-number reconstructions that are consistent with the direct solar observation during the period of their overlap.
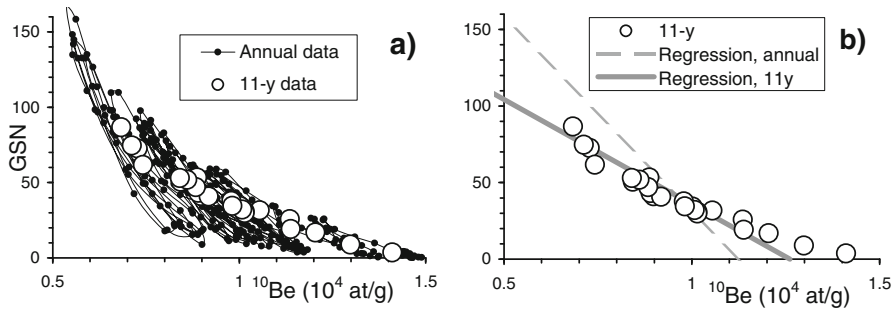
Fig. 14 Scatter plot of smoothed group sunspot numbers versus (2-year delayed) ^{10}Be concentration. **a** Annual (connected small dots) and 11-year averaged (big open dots) values. **b** Best-fit linear regressions between the annual (dashed line) and 11-year averaged values (solid line). The dots are the same as in panel (a). (After Usoskin and Kovaltsov 2004)

3.5.1 Regression models

Mathematical regression is the most apparent and often used (until recently) method of solar-activity reconstruction from proxy data (see, e.g., Ogurtsov 2004; Stuiver and Quay 1980). The reconstruction of solar activity is performed in two consecutive steps. First, a phenomenological regression (either linear or nonlinear) is built between a proxy data set and a direct solar-activity index for the available "training" period (e.g., since 1750 for WSN/ISN or since 1610 for GSN). Then this regression is extrapolated backwards to evaluate SN from the proxy data. The main shortcoming of the regression method is that it depends on the time resolution and choice of the "training" period. The former is illustrated by Fig. 14, which shows the scatter plot of the ^{10}Be concentration versus GSN for the annual and 11-year smoothed data.

One can see that the slope of the ^{10}Be-vs-GSN relation (about −500 g/atom) within individual cycles is significantly different from the slope of the long-term relation (about −100 g/atom), i.e., individual cycles do not lie on the line of the 11-year averaged cycles. Moreover, the slope of the regression for individual 11-year cycles varies essentially depending on the solar activity level. Therefore, a formal regression built using the annual data for 1610–1985 yields a much stronger GSN-vs-^{10}Be dependence than for the cycle-averaged data (see Fig. 14b), leading to a potentially-erroneous evaluation of the sunspot number from the ^{10}Be proxy data.

It is equally dangerous to evaluate other solar/heliospheric/terrestrial indices from sunspot numbers by extrapolating an empirical relation obtained for the last few decades back in time. This is because the last decades (after the 1950s) were well covered by direct observations of solar, terrestrial and heliospheric parameters, corresponding to a very high level of solar activity. After a steep rise in the activity level between the late 19th and mid-20th centuries, the activity remained at a roughly constant high level, being totally dominated by the 11-year cycle without a long-term trend. Accordingly, all empirical relations built based on data for this period are focused on the 11-year variability and can overlook possible long-term trends (Mursula et al. 2003). This may affect all regression-based reconstructions, whose results cannot be independently (directly or indirectly) tested. In particular, this may

be related to solar irradiance reconstructions, which are often based on regression-like models, built and verified using data from the last three solar cycles, when there was no strong trend in solar activity.

Regression models are not in use in the modern state of the art.

3.5.2 Reconstruction of heliospheric parameters

The modulation potential ϕ (see Sect. 3.1.1) is directly related to cosmogenic isotope production in the atmosphere. It is a parameter describing the spectrum of galactic cosmic rays (see the definition and full description of this index in Usoskin et al. 2005) in the force-field approximation and is sometimes used as a stand-alone index of solar (or, actually, heliospheric) activity. We note that, provided the isotope production rate Q is estimated and geomagnetic changes can be properly accounted for, it is straightforward to obtain a time series of the modulation potential, using, e. g., the relation shown in Fig. 10. Reconstructions of solar activity often end at this point, representing solar activity by the modulation potential, as some authors (e.g., Beer et al. 2003; Brehm et al. 2021; Muscheler et al. 2007; Vonmoos et al. 2006) believe that further steps (see Sect. 3.5.3) may introduce additional uncertainties. However, since ϕ is a heliospheric, rather than solar, index, the same uncertainties remain when using it as an index of solar activity. Moreover, the modulation potential is a model-dependent quantity (see discussion in Sect. 3.1.1) and therefore does not provide an unambiguous measure of heliospheric activity. In addition, the modulation potential is not a physical index but rather a formal fitting parameter to describe the GCR spectrum near Earth and, thus, is not a universal solar-activity index.

Modulation of GCR in the heliosphere (see Sect. 3.1.1) is mostly defined by the turbulent HMF, which ultimately originates from the sun and is thus related to solar activity. It has been shown, using a theoretical model of the heliospheric transport of cosmic rays (e.g., Usoskin et al. 2002a), that on the long-term scale (beyond the 11-year solar cycle) the modulation potential ϕ is closely related to the open solar magnetic flux F_o, which is a physical quantity describing the solar magnetic variability (e.g., Krivova et al. 2021; Lockwood 2013). An example of F_o reconstruction for the last 1000 years is shown in Fig. 15.

Sometimes, instead of the open magnetic flux, the mean HMF intensity at Earth orbit, B, is used as a heliospheric index (Caballero-Lopez and Moraal 2004; McCracken 2007; Steinhilber et al. 2010). Note that B is linearly related to F_o assuming constant solar-wind speed, which is valid on long-term scales. In addition, the count rate of a "pseudo" neutron monitor (i.e., a count rate of a neutron monitor if it was operated in the past) is considered as a solar/heliospheric index (e.g., Beer 2000; McCracken and Beer 2007).

3.5.3 A link to sunspot numbers

The open solar magnetic flux F_o described above is related to the magnetic phenomena on the Sun such as sunspots or faculae. Modern physics-based models allow one to calculate the open solar magnetic flux from data of solar observation, in
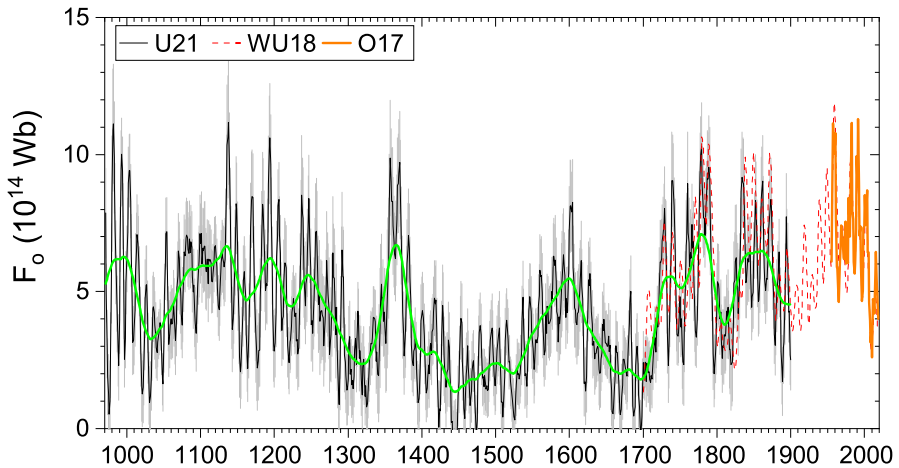
Fig. 15 An example of reconstruction of the open solar flux from the ¹⁴C high-resolution data for the last 1000 years (black U21 curve—Usoskin et al. 2021b). Direct opens solar flux estimates from sunspot numbers since 1700 (red W18 curve—Wu et al. 2018b) and from measurements since 1955 (orange O17 curve—Owens et al. 2017)

particular sunspots (Krivova et al. 2007, 2021; Owens et al. 2012; Solanki et al. 2000, 2002) or geomagnetic activity indices (Lockwood et al. 2014). Besides the solar active regions, the model includes ephemeral regions. Although these models are based on physical principles, they contain some unknowns like the decay time of the open flux, which cannot be measured or theoretically calculated and has to be found by means of fitting the model to data. This free parameter has been determined by requiring the model output to reproduce the best available data sets for the last 30 years with the help of a genetic algorithm. Inversion of the model, i.e., the computation of sunspot numbers for given F_o values is formally a straightforward solution of a system of linear differential equations, however, the presence of noise in the real data makes it only possible in a numerical-statistical way (see, e.g., Usoskin et al. 2004, 2007, 2021b). By inverting this model one can compute the sunspot-number series corresponding to the reconstructed open flux, thus forging the final link in a chain quantitatively connecting solar activity to the measured cosmogenic isotope abundance. An example of the quality of the sunspot reconstruction by inverting the SN–F_o relation is shown in Fig. 16 for the last decades when there are measurements of cosmic-ray variability by neutron monitors. The agreement between the cosmic-ray-based reconstruction of sunspot numbers (black dashed curve) and the actual ISN values is generally good, confirming the validity of the approach. However, there are two short periods of disagreement: around 1972, due to the so-called 'mini-cycle' in the cosmic-ray modulation caused by an unusual heliospheric structure (e.g., Benevolenskaya 1998); and around 1990 when a series of exceptionally strong Forbush decreases took place. During both periods, the regular relationship between sunspot numbers and GCR modulation was distorted, but in the ooposite directions.
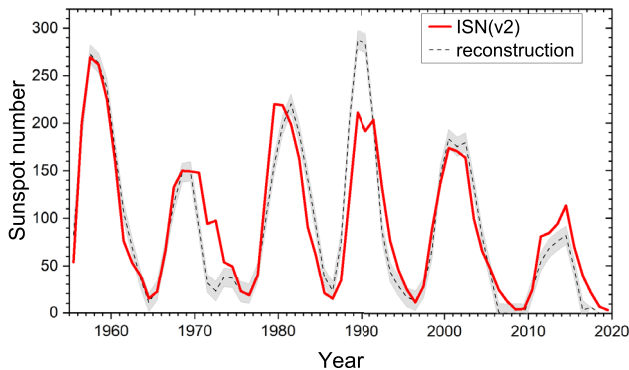
Fig. 16 Annual sunspot number since 1955 as provided by the ISN (v2—red curve) and reconstructed from cosmic-ray data measured by neutron monitors (black dashed curve with 1σ uncertanties—Usoskin et al. 2021b)

As very important for climate research, the variations of the total solar irradiance (TSI) are sometimes reconstructed from the solar proxy data (Steinhilber et al. 2009; Vieira et al. 2011; Wu et al. 2018a). However, the absolute range of the TSI variability on the centennial-millennial time scales still remains unknown (Schmutz 2021).

3.6 Solar activity reconstructions

Detailed computational models of cosmogenic isotope production in the atmosphere (e.g., Masarik and Beer 1999) have opened up a new possibility for long-term solar-activity reconstruction (e.g., Beer 2000). The first quantitative reconstructions of solar activity from cosmogenic proxy appeared in the early 2000s based on ^{10}Be deposited in polar ice (Beer et al. 2003; Usoskin et al. 2003c).

Beer et al. (2003) reconstructed the modulation potential on a multi-millennial timescale using the model computations by Masarik and Beer (1999) and the ^{10}Be data from the GISP2 core in Greenland. This result was extended, including also the ^{14}C data set, and covers the whole Holocene (Steinhilber et al. 2010, 2012; Vonmoos et al. 2006).

Usoskin et al. (2003c) presented a reconstruction of sunspot activity over the last millennium, based on ^{10}Be data from both Greenland and Antarctica, using a physics-based model described in detail in Usoskin et al. (2004). This result reproduces the four known grand minima of solar activity—Maunder, Spörer, Wolf and Oort minima (see Sect. 4.2). Later Solanki et al. (2004) reconstructed 10-year–averaged sunspot numbers from the ^{14}C content in tree rings throughout the Holocene and estimated its uncertainties. The most recent (for the moment of writing this review) full physics-based reconstruction of sunspot numbers based on multi-proxy data (all available long-running ^{14}C and ^{10}Be records) and exploiting a Bayesian approach has been performed by Wu et al. (2018b) as shown in Fig. 17.

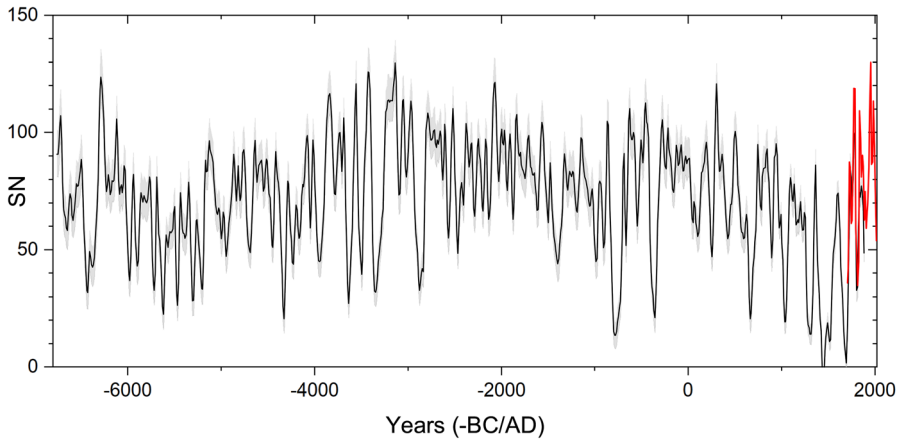The obtained results are discussed in Sect. 4.

Fig. 17 Long-term multip-proxy sunspot-number reconstruction with 1σ uncertainties (after Wu et al. 2018b). ISN (v.2) are shown in red
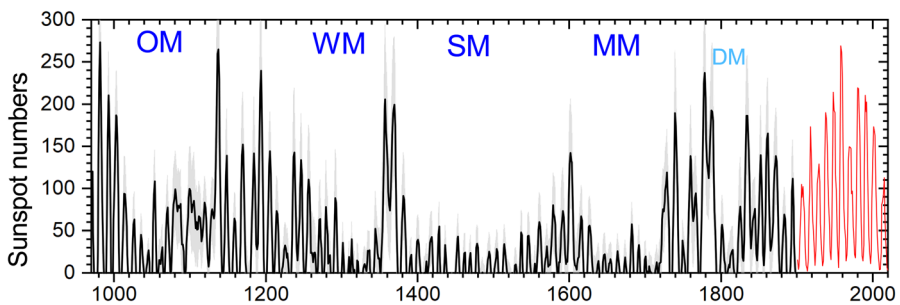

Fig. 18 Annual sunspot numbers reconstructed from ^{14}C (black curve with 1σ uncertainties) since 970 AD (Usoskin et al. 2021b). The red curve depicts ISN(v.2) since 1900. Blue letters denote grand minima of solar activity: Oort (OM), Wolf (WM), Spörer (SM) and Maunder (MM) minima. The Dalton minimum ca. 1800 (denoted as light-blue DM) is a low of the secular Gleissberg cycle and is not usually considered as a grand minimum (see text)

3.6.1 11-year solar cycles resolved

Until recently, it was thought that cosmogenic-isotope data can hardly resolve individual solar cycles because of the low signal-to-noise ratio and also insufficiently accurate dating of ice cores. Some indication of the ≈ 11-year cycles can be obtained by statistical methods, such as wavelet analysis (e.g., Miyahara et al. 2006a) or heavy band-pass filtering of data (Beer et al. 1998). A major breakthrough has been made recently thanks to high-precision annual measurements of ^{14}C in tree rings since 970 AD performed by Brehm et al. (2021). The highest accuracy of the data made it possible to perform the first proxy-based reconstructions of individual solar cycles continuously covering the last millennium (Usoskin et al. 2021b). This has nearly tripled the amount of known solar cycles from 24 in WSN and 35 in GSN to 96 solar cycles, of which 50 are well-resolved (Fig. 18). The full list of cycles, including their

parameters (dates of minima and maxima, amplitude) can be found in Table 1 of Usoskin et al. (2021b).

3.7 Verification of reconstructions

Because of the diversity of the methods and results of solar-activity reconstruction, it is vitally important to verify them. Even though full verification is not possible, there are different means of indirect or partial verification, as discussed below. Several solar-activity reconstructions on the millennium timescale that differ from each other to some degree and are based on terrestrial cosmogenic isotope data have been published by various groups. Also, they may suffer from systematic effects. Therefore, there is a need for an independent method to verify/calibrate these results in order to provide a reliable quantitative estimate of the level of solar activity in the past, prior to the era of direct observations.

3.7.1 Comparison with direct data

As a direct verification of solar-activity reconstructions, a comparison with the actual sunspot data for the last few centuries can serve. However, regression-based models (see Sect. 3.5.1) cannot be tested in this way, since it would require a long set of independent direct data outside the "training" interval. It is usual to include all available data in the "training" period to increase the statistics of the regression, which rules out the possibility of testing the model. On the other hand, such a comparison to the actual sunspot data can be regarded as a direct test for a physics-based model since it does not include phenomenological links over the same time interval. The period of the last four centuries is pretty good for testing purposes since it includes the whole range of solar activity levels from the nearly spotless Maunder minimum to the Modern grand maximum. However, because of the uncertainties in the sunspot number series (see Sect. 2.2.1), this method shows only an approximate agreement, and direct sunspot numbers cannot serve as the ultimate basis to verify the cosmogenic-based reconstructions. Moreover, the difference may be real for some periods since the two methods reflect different aspects of solar activity—see, e. g., Fig. 16.

Models focused on the reconstruction of heliospheric parameters (HMF or the modulation potential ϕ) cannot be verified in this manner since no direct heliospheric data exists before the middle of the 20th century and indirect data since the middle of the 19th century. Comparison to direct cosmic-ray data after the 1950s (or, with caveats, after the 1930s—McCracken and Beer 2007) is less conclusive since the latter are of shorter length and correspond to a period of high solar activity, leading to larger uncertainties during grand minima. Moreover, ^{14}C data cannot be tested in this way because of the anthropogenic (Suess) effect and nuclear tests (Sect. 3.2.4).

It is important that some (semi)empirical relations, forming the basis for the proxy method, are established for the recent decades of high solar activity. The end of the Modern grand maximum of activity and the current moderate level of activity, characterized by the highest ever observed cosmic ray flux as recorded by ground-

based neutron monitors, the very low level of the HMF and geomagnetic activity should help to verify the connections between solar activity, cosmic ray fluxes, geomagnetic activity, the heliospheric magnetic field, and open magnetic flux.

3.7.2 Meteorites and lunar rocks: A direct probe of the galactic cosmic-ray flux

Another test of solar/heliospheric activity in the past comes from cosmogenic isotopes measured in lunar rock or meteorites. Cosmogenic isotopes, produced in meteoritic or lunar rocks during their exposure to CR in interplanetary space, provide a direct measure of cosmic-ray flux. Uncertainties due to imprecisely known terrestrial processes, including the geomagnetic shielding and atmospheric redistribution, are naturally avoided in this case, since the nuclides are directly produced by cosmic rays in the body of the rock, where they remain until they are measured, without any transport or redistribution. The activity of a cosmogenic isotope in meteorite/lunar rock corresponds to an integral of the balance between the isotope's production and decay, thus representing the time-integrated CR flux over a period determined by the mean life of the radioisotope. The results of different analyses of measurements of cosmogenic isotopes in meteoritic and lunar rocks show that the average GCR flux remained roughly constant—within 10% over the last million years and within a factor of 1.5 for longer periods of up to 10^9 years (e.g., Grieder 2001; Poluianov et al. 2018; Vogt et al. 1990).

By means of measuring the abundance of relatively short-lived cosmogenic isotopes in meteorites, which fell through the ages, one can evaluate the variability of the CR flux, since the production of cosmogenic isotopes ceases after the fall of the meteorite. A nearly ideal isotope for studying centurial-scale variability is ^{44}Ti with a half-life of 59.2 ± 0.6 yr (a lifetime of about 85 years). The isotope is produced in nuclear interactions of energetic CR with nuclei of iron and nickel in the body of a meteorite (Bonino et al. 1995; Taricco et al. 2006). Because of its mean life, ^{44}Ti is relatively insensitive to variations in cosmic-ray flux on decadal (11-year Schwabe cycle) or shorter timescales, but is very sensitive to the level of CR flux and its variations on a centurial scale. Using a full model of ^{44}Ti production in a stony meteorite (Michel and Neumann 1998) and data on the measured activity of cosmogenic isotope ^{44}Ti in meteorites, which fell during the past 235 years (Taricco et al. 2006), provides a method to test, in a straightforward manner, reconstructions of solar activity after the Maunder minimum. First, the expected ^{44}Ti activity needs to be calculated from the reconstructed series using the modulation potential, and then compared with the results of actual measurements (see Fig. 19). Since the lifetime of the ^{44}Ti is much longer than the 11-year cycle, this method does not allow for the reconstruction of solar/heliospheric activity, but it serves as a direct way to test existing reconstructions independently. As shown by Usoskin et al. (2006c), the ^{44}Ti data confirms significant secular variations of the solar magnetic flux during the last century (cf. Lockwood et al. 1999; Solanki et al. 2000; Wang et al. 2005). Moreover, the recent sunspot number reconstructions with relatively high solar activity during the 17th and 18th centuries, appear inconsistent with the data of ^{44}Ti in meteorites (Fig. 19).
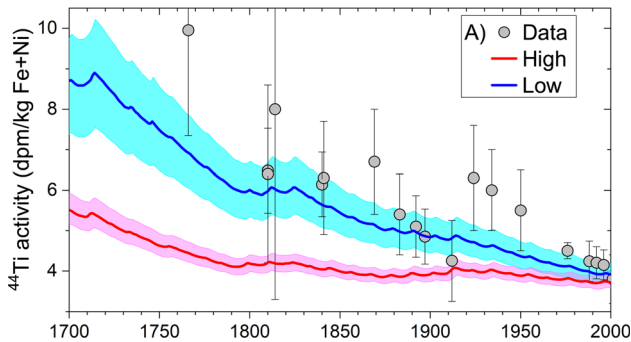
Fig. 19 Time profile of the ^{44}Ti activity measured (grey dots with error bars) in the meteorites fallen during the last 250 years (Taricco et al. 2006). The red and blue coloured curves with the 1σ model uncertainties (hatched areas) depict the modelled ^{44}Ti activity computed for "high" (e.g., Svalgaard and Schatten 2016) and "low" (e.g., Hoyt and Schatten 1998; Usoskin et al. 2016b) reconstructions of solar activity, respectively. Modified after Asvestari et al. (2017b)

3.7.3 Comparison between isotopes

As an indirect test of the solar-activity reconstruction, one can compare different isotopes. The idea behind this test is that the two main isotopes, ^{14}C and ^{10}Be, have essentially different terrestrial fates, so that only the production signal, namely, solar modulation of cosmic rays can be regarded as common in the two series. Processes of transport/deposition are different (moreover, the ^{14}C series is obtained as an average of the worldwide–distributed samples). The effect of changing geomagnetic fields is also slightly different for the two isotopes since radiocarbon is globally mixed, while ^{10}Be is only partly mixed before being stored in an archive. Even comparison between data of the same ^{10}Be isotope, but measured in far-spaced ice cores (e.g., Greenland and Antarctica), may help in separating climatic and extraterrestrial factors, since meteorology in the two opposite polar areas is quite different.

The first thorough consistent comparison between ^{10}Be and ^{14}C records for the last millennium was performed by Bard et al. (1997). They assumed that the measured ^{10}Be concentration in Antarctica is directly related to CR variations. Accordingly, ^{14}C production was considered as proportional to ^{10}Be data. Then, applying a 12-box carbon-cycle model, Bard et al. (1997) computed the expected Δ^{14}C synthetic record. Finally, these ^{10}Be-based Δ^{14}C variations were compared with the actual measurements of Δ^{14}C in tree rings, which depicted a close agreement in the profile of temporal variation (coefficient of linear correlation $r = 0.81$ with exact phasing). Despite some fine discrepancies, which can indicate periods of climatic influence in either (or both) of the series, that result has clearly proven the dominance of solar modulation of cosmogenic nuclide production variations during the last millennium. This conclusion has been confirmed (e.g., Muscheler et al. 2007; Usoskin et al. 2003c) in the sense that quantitative solar-activity reconstructions, based on ^{10}Be and ^{14}C data series for the last millennium, yield very similar results, which differ only in small details. However, a longer comparison over the entire

Holocene timescale suggests that while centennial variations of solar activity reconstructed from the two isotopes are very close to each other, there might be a discrepancy in the very long-term trend (Inceoglu et al. 2015; Usoskin et al. 2016a; Vonmoos et al. 2006), whose nature is not clear (climate changes, geomagnetic effects or model uncertainties).

More recently, Usoskin et al. (2009b) studied the dominance of the solar signal in different cosmogenic isotope data on different time scales. They compared the expected ^{10}Be variations computed from ^{14}C-based reconstruction of cosmic ray intensity with the actually measured ^{10}Be abundance at the sites and found that:

– There is good agreement between the ^{14}C and ^{10}Be data sets, on different timescales and at different locations, confirming the existence of a common solar signal in both isotope data;
– The ^{10}Be data are driven by the solar signal on timescales from about centennial to millennial time scales;
– The synchronization is lost on short (<100 years) timescales, either due to local climate or chronological uncertainties (Delaygue and Bard 2011) but the solar signal becomes important even at short scales during periods of grand minima of solar activity,
– There is an indication of a possible systematic uncertainty in the early Holocene (cf. Inceoglu et al. 2015; Usoskin et al. 2016a; Vonmoos et al. 2006), likely due to a not-perfectly-stable thermohaline circulation.

Overall, both ^{14}C- and ^{10}Be-based records are consistent with each other over a wide range of timescales and time intervals.

Thus, a comparison of the results obtained from different sources implies that the variations of cosmogenic nuclides on the long-term scale (centuries to millennia) during the Holocene are primarily defined by the solar modulation of CR.

3.8 Composite reconstruction

Most of the earlier solar activity reconstructions are based on single proxy records, either ^{14}C or ^{10}Be. Although they are dominated by the same production signal, viz. solar activity, (see Sect. 3.7.3), they still contain essential fractions of noise which is related to either measurement errors or to the local/regional climate.

An important first step in the direction of extracting the common solar signal from different proxy records was made by Steinhilber et al. (2012) who combined, in a composite reconstruction, different ^{10}Be ice core records from Greenland and Antarctica with the global ^{14}C tree ring record. The composite was made in a mathematical way, using the principal component analysis as a numerical tool. This analysis formally finds the common variability in different series, which is assumed to be the solar signal. However, since the used mathematical tool can only work with relative variability, the reconstruction also yields relative values rather than absolute values, and it is not available in the terms of sunspot numbers. A particular problem with the composite series is related to the dating uncertainty of ^{10}Be. While ^{14}C data

are 'absolutely' dated via dendrochronology, the uncertainties in the ice core dating make the ^{10}Be series lose by up to 80 years in the earlier Holocene (Adolphi and Muscheler 2016). Accordingly, the series should be either heavily smoothed, as done by Steinhilber et al. (2012) or corrected for the dating errors, before applying a composite analysis.

The composite reconstruction method was greatly advanced by Wu et al. (2018b) who applied a Bayesian approach to multi-proxy data. They used a Monte Carlo search for the most probable values of the parameters including the CR modulation potential, scalings of the ^{10}Be depositional fluxes as well as the unknown dating uncertainties of ice cores. For a set of the model parameters, the discrepancy between the modelled and the measured datasets was computed in the form of the χ^2 values, then a new set of parameters was randomly selected, and so on. Finally, the optimum set of the parameters was found, along with uncertainties, to minimize the χ^2 statistics. In contrast to the inverted reconstruction scheme, the method is based on direct modelling, making it more robust and allowing it to provide a straightforward estimate of the related uncertainties. Using six ^{10}Be series from Greenland and Antarctica, and the global 14C production series, Wu et al. (2018b) made the first fully consistent reconstruction of solar activity over the last nine millennia quantified via the most probable values of decadal sunspot numbers and their realistic uncertainties (Fig. 17). Presently, this is the most accurate solar-activity reconstruction over the Holocene that also led to a full physics-based reconstruction of the TSI over the Holocene (Wu et al. 2018a).

3.9 Summary

In this section, a proxy method of past–solar-activity reconstruction is described in detail. This method is based on the use of indirect proxies of solar activity, i.e., quantitative parameters, which can be measured now, but represent signatures, stored in natural archives, of the different effects of solar magnetic activity in the past. Such traceable signatures can be related to nuclear or chemical effects caused by cosmic rays in the Earth's atmosphere, lunar rocks or meteorites. This approach allows one to obtain homogeneous datasets with stable quality and to improve the accuracy of data when new measurement techniques become available (Brehm et al. 2021). It provides the only known regular indicator of solar activity on a very long-term scale.

The most common proxy of solar activity is formed by data from cosmogenic radionuclides, ^{10}Be and ^{14}C, produced by cosmic rays in the Earth's atmosphere. After a complicated transport in the atmosphere, these cosmogenic isotopes are stored in natural archives such as polar ice, trees, or marine sediments, from where they can be measured nowadays. This process is also affected by changes in the geomagnetic field and the climate. Because of the latter, solar-activity reconstructions are presently limited to the time span of the Holocene (10–12 kyrs) with a stable warm climate.

Radioisotope ^{14}C, measured in independently dated tree rings, forms a very useful proxy for long-term solar-activity variability. It participates in the complicated carbon cycle, which smoothes out spatial and short-term variability of isotope production.

For the Holocene period, with its stable climate, it provides a useful tool for studying solar activity in the past. Existing models allow for the quantitative conversion between the measured relative abundance of ^{14}C and the production rate in the atmosphere. The use of radiocarbon for earlier periods, the glacial and deglaciation epochs, is limited by severe climate and ocean-ventilation changes. Radiocarbon data cannot be used after the end of the 19th century because of the Suess effect and atmospheric nuclear tests.

Another solar activity proxy is the cosmogenic ^{10}Be isotope measured in stratified polar ice cores. Atmospheric transport of ^{10}Be is relatively straightforward, but its details are yet unresolved, leading to the lack of a reliable quantitative model relating the measured isotope concentration in ice to the atmospheric production. Presently, it is common to assume that the production rate is proportional, with an unknown coefficient, to the measured concentration. However, a newly-developed generation of models, which include 3D atmospheric-circulation models, will hopefully solve this problem soon.

Modern physics-based models make it possible to build a chain, which quantitatively connects isotope production rate and sunspot activity, including subsequently the GCR flux quantified via the heliospheric index, the open solar magnetic flux, solar modulation potential or the average HMF intensity at the Earth's orbit, and finally the sunspot-number series. Presently, all these steps can be made using appropriate models allowing for a full basic quantitative reconstruction of solar activity in the past. The main uncertainties in the solar-activity reconstruction arise from paleo-magnetic models (Snowball and Muscheler 2007).

Independent verification of the reconstructions, including direct comparison with sunspot numbers, cosmogenic isotopes in meteorites and the comparison of different models with each other, confirms their veracity in both relative variations and the absolute level. It also implies that the variations in cosmogenic nuclides on the long-term scale (centuries to millennia) during the Holocene are primarily defined by the solar modulation of CR.

4 Variability of solar activity over millennia

Several reconstructions of solar activity on multi-millennial timescales have been performed recently using physics-based models (see Sect. 3) from measurements of ^{14}C in tree rings and ^{10}Be in polar ice. In this section, we discuss the temporal quasi-cyclic variability of thus-reconstructed solar activity on a longer scale. Figure 20 shows the wavelet analysis of the 1000-year-long sunspot number reconstruction shown in Fig. 18 and allows us to analyze cycles shorter than about 250 years. Figure 21 depicts the wavelet power spectrum of the decadal sunspot numbers reconstructed over the Holocene (Fig. 17) to analyze cycles with up to 4000 years periods. The global wavelet power spectrum of that is shown in Fig. 22. All these cycles are believed to be of solar origin since they are not present in the geomagnetic field variations (e.g., González-López et al. 2021).
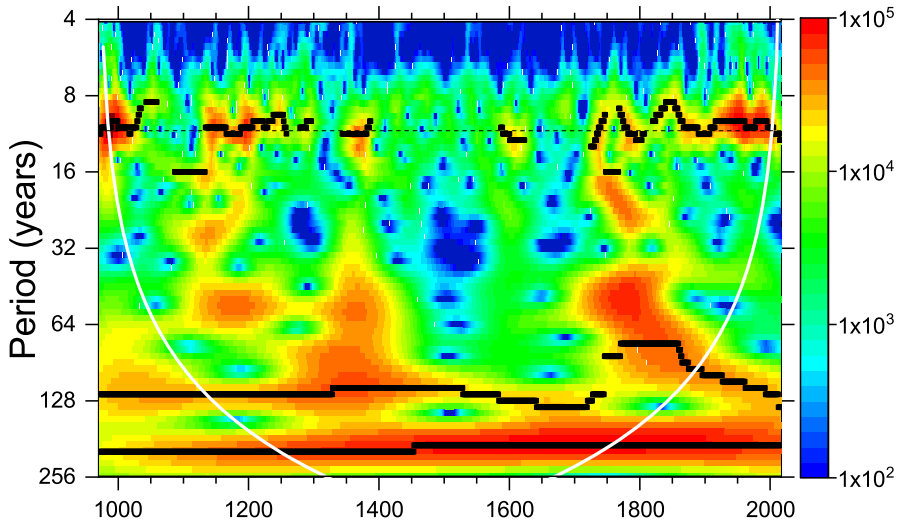
Fig. 20 Wavelet power spectrum (Morelt basis, scale factor $k = 3$) of the 1000-year long sunspot number reconstruction shown in Fig. 18 (Usoskin et al. 2021b). Thick black lines mark the power ridges corresponding to the cycle lengths around 11 years (indicated by the horizontal dashed line), 100 years and 210 years. White curves mark the cone of influence. The plot is modified after Usoskin et al. (2021b)
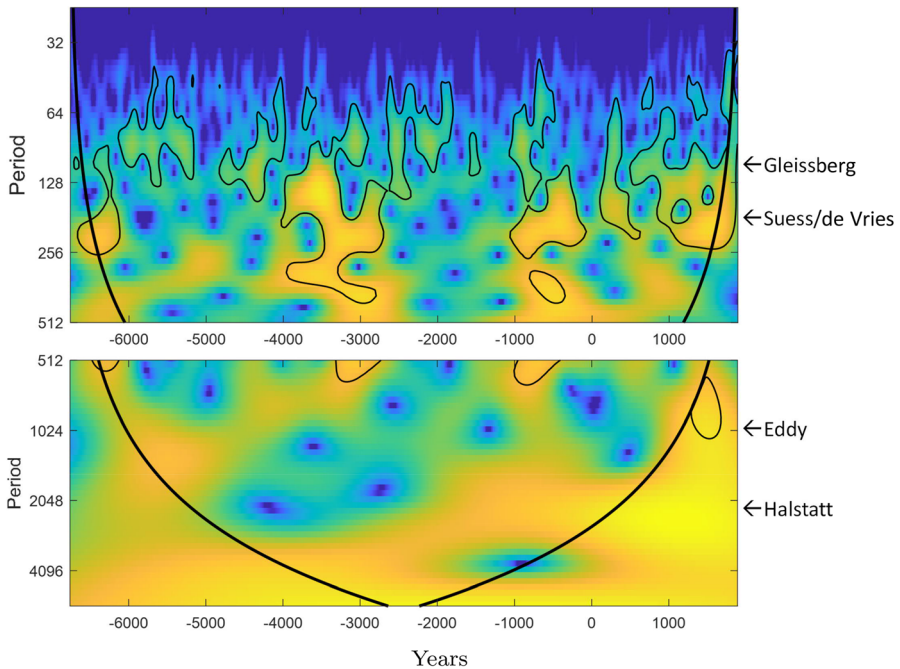

Fig. 21 Wavelet power spectrum (Morlet basis, scale-factor $k = 6$ and 3 for the upper and lower panels, respectively) for decadal sunspot number (Fig. 17) reconstructed for the Holocene (Wu et al. 2018b). Time is given in years (−BC/AD). Contours bound the 95% confidence level, thick black curves mark the cone of influence. Approximate ranges of quasi-periodicities discussed in Sect. 2.4.1 are indicated by arrows on the right
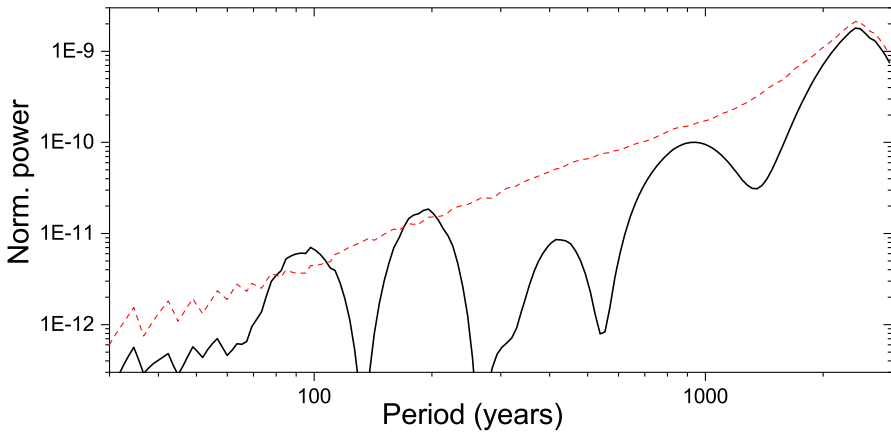
Fig. 22 Global wavelet (Morlet basis) power spectrum (black curve) of the long-term sunspot-number series (Fig. 17). Red-dashed line bounds the 95% confidence level estimated using the AR1 auto-regressive noise (Grinsted et al. 2004)

4.1 Quasi-periodicities and characteristic times

Longer (super-secular) cycles cannot be studied using direct solar observations, but only indicatively by means of indirect proxies such as cosmogenic isotopes discussed in Sect. 3.

As seen in Fig. 20, the 11-year Schwabe cycle is persistent throughout the entire millennium except for deep phases of the grand minima but, it varies in length between 8–17 years (see Table 1 in Usoskin et al. 2021b). This is consistent with the Schwabe cycle variability observed during the last centuries in sunspot numbers. The analysis of these cycles confirms that they are stochastic and not phase-locked (Weisshaar et al. 2023).

Centennial Gleissberg cycle

Another prominent feature visible in the wavelet plot is the Gleissberg cycle which is also variable in length from 70–130 years. Gleissberg cycle was known already from the direct sunspot data (Gleissberg 1939) but the question of its stability could only be studied with the proxy data. As seen, it is unstable with a floating instant period (cf. Ogurtsov 2004) but significant in the global wavelet power spectrum (Fig. 22).

210-yr Suess / de Vries cycle

A cycle with a period of 205–210 years, called the de Vries or Suess cycle in different sources, is a prominent feature, observed in various cosmogenic data (e.g., Sonett and Finney 1990; Steinhilber et al. 2012; Suess 1980; Usoskin et al. 2004; Zhentao 1990). It appears amazingly stable over the last millennium (Fig. 20) but intermittent over the Holocene period (Fig. 21). This cycle also appears highly significant in the global wavelet power spectrum (Fig. 22). As discussed by Usoskin et al. (2014), the Suess/de Vries cycle mostly manifests itself as the recurrence period of grand minima within their clusters.

Millennial Eddy cycle

Sometimes variations with a characteristic time of 600–700 years or 1000–1200 years are discussed (e.g., Abreu et al. 2012; Steinhilber et al. 2012; Sonett and Finney 1990; Vasiliev and Dergachev 2002; Vitinsky et al. 1986), but they are intermittent and insignificant, see Fig. 21. As seen in Fig. 22, they are not statistically significant as being below the noise-related level. Sometimes it is called the Eddy cycle (Steinhilber et al. 2012).

≈ 2400-yr Hallstatt cycle

A 2000–2400-year cycle is also noticeable in radiocarbon data series (see, e.g., Damon and Sonett 1991; Vasiliev and Dergachev 2002; Vitinsky et al. 1986). It can be studied only using a very long series, covering the whole Holocene. It was traditionally ascribed to climatic or geomagnetic variability (Vasiliev and Dergachev 2002; Vasiliev et al. 2012) but a recent joint study (Usoskin et al. 2016a) of ^{14}C and ^{10}Be data-sets has shown that the Hallstatt cycle is of solar origin and is manifested through the clustered occurrence of grand minima and maxima around its lows and highs, respectively. The Hallstatt cycle is barely significant (Fig. 22) and cannot be robustly confirmed from a 10-millennia-long time series (only four cycles).

Only these periodicities (or characteristic timescales) can be considered (barely) significant and stable, other timescales are not stable (Chol-jun and Kyong-phyong 2022).

4.2 Grand minima of solar activity

Let us consider the ^{14}C-based decade reconstruction (Usoskin et al. 2016a) of sunspot numbers (shown in Fig. 23) highlighting the identified grand minima and
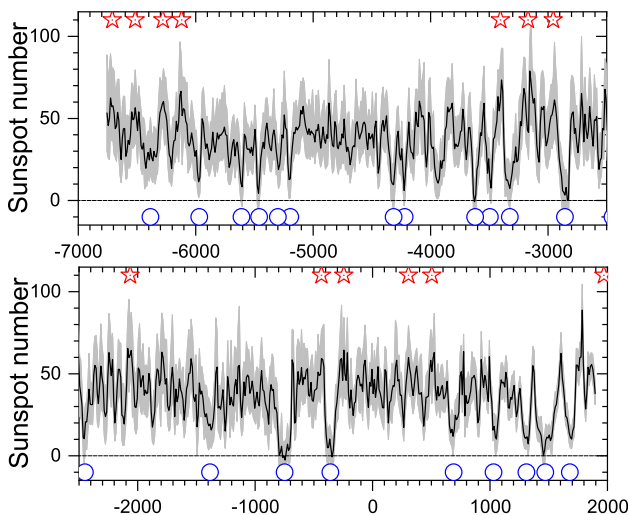

Fig. 23 Sunspot activity (decadal data) throughout the Holocene, reconstructed from ^{14}C by Usoskin et al. (2016a). Blue circles and red stars denote grand minima and maxima, respectively

maxima of solar activity. This result is similar to that based on the reconstruction by Wu et al. (2018b) (Fig. 17).

A very particular type of solar activity is the grand minimum when solar activity is greatly reduced. The most famous is the Maunder minimum in the late 17th century, which is discussed below in some detail (for details see Carrasco et al. 2021b; Soon and Yaskell 2003; Usoskin et al. 2015). Grand minima are believed to correspond to a special state of the dynamo (Käpylä et al. 2016; Moss et al. 2008; Passos et al. 2014; Sokoloff 2004), and their very existence poses a challenge for the solar-dynamo theory. It is noteworthy that dynamo models do not agree on how often such episodes occur in the sun's history and whether their appearance is regular or random. For example, the commonly used mean-field dynamo yields a fairly-regular 11-year cycle (Charbonneau 2020), while dynamo models including a stochastic driver predict the intermittency of solar magnetic activity (Charbonneau 2001; Choudhuri 1992; Mininni et al. 2001; Ossendrijver 2000; Schmitt et al. 1996; Schüssler et al. 1994; Weiss and Tobias 2000). Most of the models predict the purely random occurrence of the grand minima, without any intrinsic long-term memory (Moss et al. 2008). Although cosmogenic isotope data suggest the possible existence of such memory (Usoskin et al. 2007), statistics is not sufficient to distinguish between the two cases (Usoskin et al. 2009d).

4.2.1 The Maunder minimum

The Maunder minimum (MM) is a representative of grand minima in solar activity (e.g., Eddy 1976), when sunspots have almost completely vanished from the solar surface, while the solar wind kept blowing, although at a reduced pace (Cliver et al. 1998; Owens et al. 2012; Usoskin et al. 2001b). As proposed by Lockwood and Owens (2014), the solar wind was uniform and slow, 250–275 km/s, nearly half of the modern time velocity. This is consistent with the quiet corona observed during solar eclipses taking place during the MM (Hayakawa et al. 2021b). There is some uncertainty in the definition of the duration of MM: the "formal" duration is 1645–1715 (Eddy 1976), while its deep phase with the absence of apparent sunspot cyclic activity is often considered as 1645–1700, with the low but clear solar cycle of 1700–1712 being ascribed to a recovery or transition phase (Usoskin et al. 2000). For example, Vaquero and Trigo (2015) proposed the concept of the "extended" MM of 1618–1723. MM was amazingly well covered by direct sunspot observations (Hoyt and Schatten 1996)—more than 95% of days have formal records (however many of them are generic) and 30–50% of days have explicit data (Vaquero et al. 2015). The late part of MM after the 1680s is particularly well covered with direct data from the French school of astronomy (Ribes and Nesme-Ribes 1993). On the other hand, sunspots appeared rarely (during ∼ 2% of the days) and seemingly sporadically, without an indication of the 11-year cycle.

Some recent studies proposed that the sunspot activity level might have been underestimated during MM: Zolotova and Ponyavin (2015) claimed that the annual number of sunspot groups was as high as 3–8 (the sunspot number 50–100) during MM, Svalgaard and Schatten (2016) claimed more modest peak annual numbers of sunspot groups as 2–3 (25–40 in sunspot number) but still too high. These claims

were based on the fact that original data include many generic statements of the absence of sunspots for long periods of time, and could be dismissed. However, these statements made by professional astronomers in dedicated monitoring of the sun, should be considered seriously. A thorough analysis of all the available sunspot data made by applying 'filters' of different degrees of strictness was made by Vaquero et al. (2015) who concluded that the level of sunspot activity was indeed very low during MM, even if considering only explicit records. This analysis was more recently confirmed by Carrasco et al. (2021b). The low level of activity during MM was confirmed also by an aggregate study of other indirect data for that period (Usoskin et al. 2015): while there are known auroral observations during MM, they all are limited to high latitudes (close to the auroral oval), where polar lights occur even without strong geomagnetic storms; data of cosmogenic isotopes ^{14}C measured in tree trunks and ^{44}Ti in fallen meteorites clearly indicate a very high flux of cosmic rays (low solar activity) during MM.

Such a low level of activity makes it almost impossible to apply standard methods of time-series analysis to sunspot data during MM (e.g., Frick et al. 1997). Therefore, special methods such as the distribution of spotless days versus days with sunspots (e.g., Carrasco et al. 2021b; Harvey and White 1999; Kovaltsov et al. 2004; Vaquero et al. 2014) or an analysis of sparsely-occurring events (Usoskin et al. 2000) should be applied in this case. Using these methods, Usoskin et al. (2001b) have shown that sunspot occurrence during the Maunder minimum was gathered into two major clusters (1652–1662 and 1672–1689), with the mass centres of these clusters being in 1658 and 1679–1680. Together with the sunspot maxima before (1640) and after (1705) the deep Maunder minimum, this implies a dominant 22-year periodicity in sunspot activity throughout the Maunder minimum (Mursula et al. 2001), with a subdominant 11-year cycle emerging towards the end of the Maunder minimum (Mendoza 1997; Ribes and Nesme-Ribes 1993; Usoskin et al. 2000; Vaquero et al. 2015) and becoming dominant again after 1700. Similar behaviour of a dominant 22-year cycle and a weak subdominant Schwabe cycle during the Maunder minimum was found in other indirect solar proxy data: auroral occurrence (Křivský and Pejml 1988; Schlamminger 1990; Silverman 1992) and ^{14}C data (Kocharov et al. 1995; Miyahara et al. 2006b; Peristykh and Damon 1998; Stuiver and Braziunas 1993). This is in general agreement with the concept of "immersion" of 11-year cycles during the Maunder minimum (Vitinsky et al. 1986, and references therein). This concept means that full cycles cannot be resolved and sunspot activity only appears as pulses around cycle-maximum times.

An analysis of ^{10}Be data (Beer et al. 1998) implied that the 11-year cycle was weak but fairly regular during the Maunder minimum, but its phase was inverted (Usoskin et al. 2001b). Theoretical studies (Owens et al. 2012; Wang and Sheeley Jr 2012) confirm that such a phase change between cosmic rays and solar activity can indeed appear for very weak cycles due to the mechanism producing open solar flux that modulates cosmic rays.

It was believed earlier (Miyahara et al. 2006b; Ribes and Nesme-Ribes 1993; Sokoloff and Nesme-Ribes 1994; Usoskin et al. 2000, 2001b; Vitinsky et al. 1986) that transition from the normal high activity to the deep minimum did not have any apparent precursor before MM. However, newly recovered data suggest that the start

of the Maunder minimum might have been not very sudden but via regular cycles of reduced height (Vaquero et al. 2011). There is an indication that the length of the solar cycle may slightly extend during and already slightly before a grand minimum (Miyahara et al. 2004; Nagaya et al. 2012), which is in agreement (note that the possible cycle maximum in 1650 discussed there was based on an erroneous data point and should be dismissed) with the results by Vaquero et al. (2015).

The 11-year Schwabe cycle started dominating solar activity after 1700. Recovery of sunspot activity from the deep minimum to normal activity was gradual, passing through a period of nearly-linear amplification of the 11-year cycle.

Although the Maunder minimum is the only one with available direct sunspot observations, its predecessor, the Spörer minimum from 1450–1550, is covered by precise (bi)annual measurements of ^{14}C (Brehm et al. 2021; Miyahara et al. 2006a). An analysis of this data (Miyahara et al. 2006a, b) reveals a similar pattern with the dominant 22-year cycle and suppressed 11-year cycle, thus supporting the idea that the above general scenario may be typical for a grand minimum. A similar pattern has been also found for an un-named grand minimum in the 4th century BC (Nagaya et al. 2012).

A very important feature of sunspot activity during the Maunder minimum was its strong north-south asymmetry, as sunspots were only observed in the southern solar hemisphere during the end of the Maunder minimum (Ribes and Nesme-Ribes 1993; Sokoloff and Nesme-Ribes 1994). This observational fact has led to intensive theoretical efforts to explain a significant asymmetry of the sun's surface magnetic field in the framework of the dynamo concept (e.g., Sokoloff 2004). Note that the discovery (Arlt 2008, 2009) of Staudacher's original drawings of sunspots in the late 18th century shows that similarly asymmetric sunspot occurrence existed also at the beginning of the Dalton minimum in 1790s (Usoskin et al. 2009c). However, the northern hemisphere dominated during that period contrary to the situation during the Maunder minimum, implying that the dominant hemisphere is random, as predicted by many dynamo models (see, e.g., Nandy et al. 2021, and references therein).

4.2.2 Grand minima on a multi-millennial timescale

The presence of grand minima in solar activity on the long-term scale has been mentioned numerously (e.g., Eddy 1977b; Inceoglu et al. 2015; Solanki et al. 2004; Steinhilber et al. 2012; Usoskin et al. 2007; Wu et al. 2018b), using the radioisotope data of ^{14}C in tree rings and ^{10}Be in ice cores. For example, Eddy (1977a) identified major excursions in the detrended ^{14}C record as grand minima and maxima of solar activity and presented a list of six grand minima and five grand maxima for the last 5000 years (see Table 3). Stuiver and Braziunas (1989) and Stuiver et al. (1991) also studied grand minima as systematic excesses of the high-pass filtered ^{14}C data and suggested that the minima are generally of two distinct types: short minima of duration 50–80 years (called Maunder-type) and longer minima collectively called Spörer-like minima. Using the same method of identifying grand minima as significant peaks in high-pass filtered Δ^{14}C series, Voss et al. (1996) provided a list of 29 such events for the past 8000 years. A similar analysis of bumps in the ^{14}C production rate was presented by Goslar (2003). However, such studies retained a

Table 3 Conservative list with approximate dates (in –BC/AD) of grand minima in reconstructed solar activity (1—listed in Usoskin et al. (2007); 2—listed in Inceoglu et al. (2015); 3—listed in Usoskin et al. (2016a))

Center (−BC/AD)	Duration (years)	Comment
1680	80	Maunder[†]
1470	160	Spörer
1310	80	Wolf
1030	80	Oort
690	80	1–3 Horrebow[‡]
−360	80	1–3
−750	120	1–3
−1385	70	1–3
−2450	40	2, 3
−2855	90	1–3
−3325	90	1–3
−3495	50	1–3
−3620	50	1–3
−4220	30	1–3
-4315	50	1–3
−5195	50	2, 3
−5300	50	1–3
−5460	40	1–3
−5610	40	1–3
−6385	130	1–3
−7035	50	1
−7305	30	1
−7515	150	1
−8215	110	1
−9165	150	1

[†] independently known.

[‡] proposed to be named after Christian Horrebow (Kaiser Kudsk et al. 2022)

qualitative element, since they are based on high-pass–filtered ^{14}C data and thus implicitly assume that ^{14}C variability can be divided into short-term solar variations and long-term changes attributed solely to the slowly-changing geomagnetic field. This method ignores any possible long-term changes in solar activity on timescales longer than 500 years (Voss et al. 1996). The modern approach, based on physics-based modelling (Sect. 3), allows for the quantitative reconstruction of the solar activity level in the past, and thus, for a more realistic definition of the periods of grand minima or maxima.

A list of 25 grand minima, identified in the quantitative solar-activity reconstruction of the last 11 000 years, shown in Fig. 23, is presented in Table 3 (after Inceoglu et al. 2015; Usoskin et al. 2007, 2016a). The cumulative duration of the grand minima is about 1900 years, indicating that the sun in its present evolutionary stage
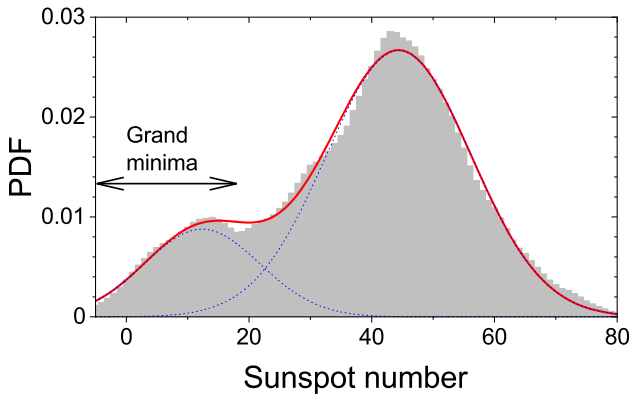
Fig. 24 Probability density function of the reconstructed decadal sunspot numbers (corresponding to ISN, v.1) for the last three millennia (grey histogram). Shown is also the best-fit bimodal Gaussian distribution (red curve with the two modes shown by dotted blue lines). The grand minimum mode is indicated by the arrow. The plot is modified after Usoskin et al. (2014)

spends $\approx {}^1/_6$ (17%) of its time in a quiet state, corresponding to grand minima. Note that the definition of grand minima is quite robust.

It is shown, using the cosmogenic-proxy data for the past millennia, that grand minima correspond to a special mode of the solar dynamo which is statistically significantly separated from the main mode of moderate activity (Usoskin et al. 2014; Wu et al. 2018b). The probability density function (PDF) of the occurrence of decadal sunspot numbers in the reconstruction based on ^{14}C for the last three millennia (Usoskin et al. 2014) is shown in Fig. 24. One can see that the PDF has a clear bimodal structure, where the main mode corresponds to the general mode of moderate activity (20–60 in decadal sunspot numbers), while the secondary maximum represents a statistically different mode of low activity (decadal sunspot numbers below 20) corresponding to grand minima.

The question of whether the occurrence of grand minima in solar activity is a stochastic or chaotic process is important for understanding the action of the solar-dynamo machine. Even a simple deterministic numerical dynamo model can produce events comparable with grand minima (Brandenburg et al. 1989; Käpylä et al. 2016). Such models can also simulate a sequence of grand minima occurrences, which are irregular and seemingly chaotic (e.g., Covas et al. 1998; Jennings and Weiss 1991; Tobias et al. 1995). The presence of long-term dynamics in the dynamo process is often explained in terms of the α-effect, which, being a result of the electromotive force averaged over turbulent vortices, can contain a fluctuating part (e.g., Hoyng 1993; Ossendrijver et al. 1996) leading to irregularly occurring grand minima (e.g., Brandenburg and Spiegel 2008). The present dynamo models can reproduce almost all the observed features of the solar cycle under *ad hoc* assumptions (e.g., Pipin et al. 2012), although it is still unclear what leads to the observed variability. Most of these models predict that the occurrence of grand minima is a purely random "memoryless" Poisson-like process, with the probability of a grand minimum occurring being constant in time. This unambiguously leads to the exponential shape of the

waiting-time distribution (waiting time is the time interval between subsequent events) for grand minima.

Usoskin et al. (2007) performed a statistical analysis of grand minima occurrence time (Table 3) and concluded that their occurrence is not a result of long-term cyclic variations, but is defined by stochastic/chaotic processes. Moreover, waiting-time distribution deviates from the exponential law. This implies that the event occurrence is still random, but the probability is nonuniform in time and depends on the previous history. In the time series it is observed as a tendency of the events to cluster together with a relatively-short waiting time, while the clusters are separated by long event-free intervals (cf. Sect. 4.1). Such behaviour can be interpreted in different ways, e.g., self-organized criticality or processes related to the accumulation and release of energy. This poses a strong observational constraint on theoretical models aiming to explain the long-term evolution of solar activity (Sect. 4.4.1). However, as discussed by Moss et al. (2008) and Usoskin et al. (2009d), the observed feature can be an artefact of the small statistics (only a couple of dozens of grand minima are identified during the Holocene), making this result only indicative and waiting for a more detailed investigation.

A histogram of the durations of grand minima from Table 3 is shown in Fig. 25. The mean duration is 70 year but the distribution has enhanced probabilities at greater lengths of >100 years. The minima tend to be either of a short (30–90 years) duration similar to the Maunder minimum, or rather long (>100 years), similar to the Spörer minimum, in agreement with earlier conclusions (Stuiver and Braziunas 1989). Interestingly, if the idea of the 'extended' MM is considered (Vaquero and Trigo 2015), it would appear of the Spörer-minimum type. This suggests that grand minima correspond to a special state of the dynamo. Once falling into a grand minimum as a result of a stochastic/chaotic but non-Poisson process, the dynamo is "trapped" in this state and its behaviour is driven by deterministic intrinsic features.
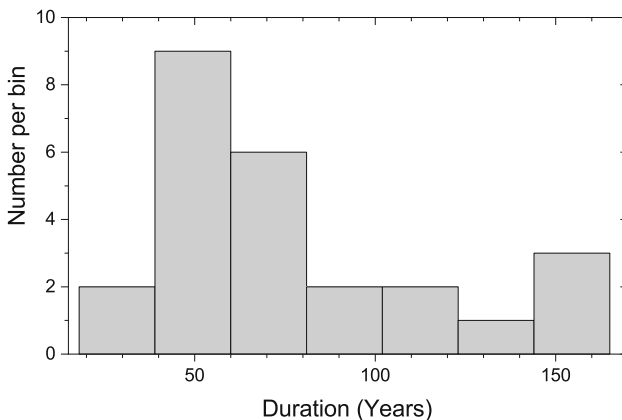

Fig. 25 Histogram of the duration of grand minima from Table 3

4.3 Grand maxima of solar activity

4.3.1 The modern episode of active sun

In the past several decades, we were living in a period of a very active sun with a level of activity that was the highest over the last few centuries covered by direct solar observation. The sunspot number was growing rapidly between 1900 and 1940, with nearly doubling average group sunspot number, and has remained at that high level until recently (see Fig. 1). Note that growth was related mostly to the increased cycle maximum amplitude, while sunspot activity always returns to a very low level around solar cycle minima. While the average group sunspot number (using ISN v.2) for the period 1879–1913 was around 56, it stands high at the level of 112 for 1945–1996. Therefore, the modern active sun episode, which started in the 1940s, can be regarded as the Modern grand maximum of solar activity, as opposed to a grand minimum (Wilson 1988b). As discussed by Clette et al. (2014, see their Figure 65), the number of spotless days during cycles 12–22 was half of that for another relatively high activity period ca. 1850. This again suggests the uniqueness of the Modern grand maximum on the centennial time scale. The reality of the Modern grand maximum was independently confirmed, e.g., by Zięba and Nieckarz (2014) who have shown, by studying active versus passive (spotless) days that cycles 17–23 were more active, compared to cycles 8–15.

Although uncertainties in sunspot numbers during the 18th and 19th centuries (see discussion in Sect. 2.2.1) make it a bit unclear on the centennial time scale, data on cosmogenic isotopes (Inceoglu et al. 2015; Solanki et al. 2004; Usoskin et al. 2016a) imply that such high-activity episodes occur seldom and aperiodically.

However, as we can securely say now, after very weak solar minima in 2008–2009 and 2019 (e.g., Gibson et al. 2011), solar activity has returned to its normal moderate level in cycles #24 and 25. Thus, the high activity episode known as the Modern grand maximum is over.

Is such high solar activity typical or is it something extraordinary? While it is broadly agreed that the modern active-sun episode is a special phenomenon, the question of how (a)typical such upward bumps are from "normal" activity is yet a topic of debate.

4.3.2 Grand maxima on a multi-millennial timescale

The question of how often grand maxima occur and how strong they are, cannot be studied using the 400-year-long series of direct observations. An increase in solar activity around 1200 AD, also related to the Medieval temperature optimum, is sometimes qualitatively regarded as a grand maximum (de Meyer 1998; Wilson 1988b), but its magnitude is lower than the modern maximum (e.g., Usoskin et al. 2003c; Wu et al. 2018b). Accordingly, it was not included in lists of grand maxima (Eddy 1977b; Inceoglu et al. 2015; Usoskin et al. 2007).

A quantitative analysis is only possible using proxy data, especially cosmogenic isotope records. Using a physics-based analysis of solar-activity series reconstructed

from [10]Be data from polar (Greenland and Antarctica) archives, Usoskin et al. (2003c, 2004) stated that the modern maximum is unique in the last millennium. This early result was confirmed by the most recent and precise reconstruction of sunspot activity based on ^{14}C annual data (Usoskin et al. 2021b). Using a similar analysis of the ^{14}C calibrated series, Solanki et al. (2004) found that the modern activity burst is not unique, but a very rare event, with the previous burst occurring about 8 millennia ago. An update (Usoskin et al. 2006a) of this result, using a more precise paleo-magnetic reconstruction by Korte and Constable (2005) since 5000 BC, suggests that an increase in solar activity comparable with the modern episode might have taken place around 2000 BC, i.e., around 4 millennia ago, in agreement with more recent studies by Steinhilber et al. (2012), Inceoglu et al. (2015) and Wu et al. (2018b). On the other hand, the definition of grand maxima is less robust than grand minima and is sensitive to other parameters such as geomagnetic field data or overall normalization (Usoskin et al. 2016a).

Keeping possible uncertainties in mind, let us consider a list of the grand maxima (defined as the 50-year smoothed sunspot number stably exceeding 50), identified for the last eleven millennia using cosmogenic isotope data, as shown in Table 4. A total

Table 4 Conservative list with approximate dates (in −BC/AD) of grand maxima in reconstructed solar activity (1—listed in Usoskin et al. (2007); 2—listed in Inceoglu et al. (2015); 3—listed in Usoskin et al. (2016a))

Center (−BC/AD)	Duration (years)	Comment
1970	80	Modern
505	50	2, 3
305	30	2, 3
−245	70	2, 3
−435	50	1–3
−2065	50	1–3
−2955	30	2, 3
−3170	100	1–3
−3405	50	2, 3
−3860	50	1–3
−6120	40	1–3
−6280	40	2, 3
−6515	70	1
−6710	40	1
−6865	50	1
−7215	30	1
−7660	80	1
−7780	20	1
−7850	20	1
−8030	50	1
−8350	70	1
−8915	190	1
−9375	130	1

of 23 grand maxima have been identified with a total duration of around 1400 years, suggesting that the sun spends around 12% of its time in an active state. A statistical analysis of grand-maxima–occurrence time suggests that they do not follow long-term cyclic variations, but a preferential clustering near highs of the Hallstatt cycle is observed (Usoskin et al. 2016a). The distribution of the waiting time between consecutive grand maxima is not unambiguously clear but also hints at a deviation from the exponential law. The duration of grand maxima has a smooth distribution, which nearly exponentially decreases towards longer intervals. Most of the reconstructed grand maxima (about 70%) were not longer than 50 years, and only five grand minima (including the modern one) have been longer than 70 years (cf. Barnard et al. 2011). Note, that the Modern grand maximum is over now and we are living during an epoch of moderate or even weak solar activity.

Grand maxima are not clearly defined and, in contrast to the grand minima, do not form a statistically distinguishable peak in the distribution (see Fig. 24). It is still unclear whether grand maxima correspond to a special state of the solar dynamo or rather to a tail of the regular mode. Although there are some indications for the former (Usoskin et al. 2016a), they are inconclusive.

4.4 Related implications

Reconstructions of long-term solar activity have different implications in related areas of science. The results, discussed in this overview, can be used in such diverse research disciplines as theoretical astrophysics, solar-terrestrial studies, paleo-climatology, and even archaeology and geology. We will not discuss all possible implications of long-term solar activity in great detail but only briefly mention them here.

4.4.1 Theoretical constrains

The basic principles of the occurrence of the 11-year Schwabe cycle are more-or-less understood in terms of the solar dynamo, which acts, in its classical form (e.g., Parker 1955), as follows (see detail in Charbonneau 2020). Differential rotation Ω produces a toroidal magnetic field from a poloidal one, while the so-called α-effect, associated with the helicity of the velocity field or Joy's law tilt of active regions, produces a poloidal magnetic field from a toroidal one. This classical model results in a quasi-periodic process in the form of propagation of a toroidal field pattern in the latitudinal direction (the "butterfly diagram"—see Fig. 2). As evident from observation, the solar cycle is far from being a strictly periodic phenomenon, with essential variations in the cycle length and especially in the amplitude, varying dramatically between nearly spotless grand minima and very large activity during grand maxima. The mere fact of such great variability, known from sunspot data, forced solar physicists to develop dynamo models further. Simple deterministic numerical dynamo models, developed on the basis of Parker's migratory dynamo, can simulate events, which are seemingly comparable with grand minima/maxima occurrence (e.g., Brandenburg et al. 1989). However, since variations in the solar-activity level, as deduced from cosmogenic isotopes, appear essentially nonperiodic and irregular, appropriate

models have been developed to reproduce irregularly-occurring grand minima (e.g., Covas et al. 1998; Jennings and Weiss 1991; Tobias et al. 1995). Models, including an *ad hoc* stochastic driver (Charbonneau 2001; Charbonneau et al. 2004; Choudhuri 1992; Käpylä et al. 2016; Mininni et al. 2001; Ossendrijver 2000; Schmitt et al. 1996; Weiss and Tobias 2000), are able to reproduce the great variability and intermittency found in the solar cycle (see the review by Charbonneau 2020). A recent statistical result of grand minima occurrence shows disagreement between observational data, depicting a degree of self-organization or "memory", and the above dynamo model, which predicts a pure Poisson occurrence rate for grand minima (see Sect. 4.2). This poses an important constraint on the dynamo theory, responsible for long-term solar-activity variations (Moss et al. 2008; Sokoloff 2004).

In general, the following additional constraints can be posed on dynamo models aiming to describe the long-term (during the past 11 000 years) evolution of solar magnetic activity.

– The sun spends about 70% of its time at moderate magnetic-activity levels, 15–20% of its time in a grand minimum and 10–15% in a grand maximum. Presently, since the beginning cycle #24 in 2008, the sun is in a state of moderate activity after the Modern grand maximum.
– Grand minima form a special, statistically significant mode of the solar dynamo. The existence of the grand maximum mode is hinted at but not conclusive.
– Occurrence of grand minima and maxima is not a result of long-term cyclic variations but is defined by stochastic or chaotic processes.
– Observed statistics of the occurrence of grand minima and maxima display deviation from a "memory-less" Poisson-like process, but tend to either cluster events together or produce long event-free periods. Grand minima and maxima tend to cluster around lows and highs of the $\approx$ 2400-year Hallstatt cycle, respectively. This can be interpreted in different ways, such as self-organized criticality (e.g., de Carvalho and Prado 2000), a time-dependent Poisson process (e.g., Wheatland 2003), or some memory in the driving process (e.g., Mega et al. 2003).
– Grand minima tend to be of two different types: short (40–70 years) minima of Maunder type and long (longer than 100 years) minima of Spörer type. Grand minima form a special statistically significant state of the dynamo.
– Duration of grand maxima resembles a random Poisson-like process, in contrast to grand minima.

4.4.2 Solar-terrestrial relations

The sun ultimately defines the climate on Earth supplying it with energy via radiation received by the terrestrial system, but the role of solar variability in climate variations is far from being clear. Solar variability can affect the Earth's environment and climate in different ways (see, e.g., reviews by Gray et al. 2010; Haigh 2007). The variability of total solar irradiance (TSI) measured during recent decades is known to be too small to explain observed climate variations (e.g., Foukal et al. 2006; Fröhlich 2006; Yeo et al. 2014). On the other hand, there are other ways solar variability may

affect the climate, e.g., an unknown long-term trend in TSI (Solanki and Krivova 2004; Wang et al. 2005) or a terrestrial amplifier of spectral irradiance variations (Haigh et al. 2010; Shindell et al. 1999). Uncertainties in the TSI/SSI reconstructions remain large (Egorova et al. 2018; Kopp and Shapiro 2021; Schmidt et al. 2012; Yeo et al. 2014), making it difficult to assess climate models on a long-term scale. Alternatively, an indirect mechanism is also driven by solar activity, such as the ionization of the atmosphere by CR (Usoskin and Kovaltsov 2006) or the global terrestrial current system (Golubenko et al. 2021; Tinsley and Zhou 2006) can modify atmospheric properties, in particular cloud cover or aerosols (Ney 1959; Svensmark 1998). Although the role of this direct mechanism is found to be small (Mironova et al. 2015), indirect effects of energetic particles may be still notable (e. g., Calisto et al. 2011; Gray et al. 2010; Martin-Puertas et al. 2012) and is currently considered as a potential solar forcing on climate (e.g., Jungclaus et al. 2017; Matthes et al. 2017).

Accordingly, improved knowledge of the solar driver's variability may help in disentangling various effects in the very complicated system that is the terrestrial climate (e.g., Gray et al. 2010). It is of particular importance to know the driving forces in the pre-industrial era, when all climate changes were natural. Knowledge of natural variability can lead to an improved understanding of anthropogenic effects upon the Earth's climate (e.g., Chiodo et al. 2016; Ineson et al. 2015).

Studies of the long-term solar-terrestrial relations are mostly phenomenological, lacking a clear quantitative physical mechanism. Therefore, more precise knowledge of past solar activity, especially since it is accompanied by continuous efforts of the paleo-climatic community on improving climatic data sets, is crucial for an improved understanding of the natural (including solar) variability of the terrestrial environment.

4.5 Summary

In this section, solar activity on a longer scale is discussed, based on recent reconstructions.

According to these reconstructions, the sun spent about 70% of its time during the Holocene, which is ongoing, in a normal state characterized by medium solar activity as we experience now. About 15–20% of the time the sun is in a grand minimum state, while 10–15% of the time has been taken up by periods of very high activity.

One of the main features of long-term solar activity is its irregular behaviour, which cannot be described by a combination of quasi-periodic processes as it includes an essentially random component.

Grand minima, whose representative is the Maunder minimum of the late 17th century, are typical solar phenomena. Approximately 25 grand minima can be robustly identified in solar activity reconstructions for the Holocene period. Their occurrence suggests that they appear not periodically, but tend to appear in clusters separated by 2000–2500 years (the Hallstatt cycle), and having a recurrence period of ≈ 210 years (Suess/de Vries cycle) within the clusters. Grand minima tend to be of two distinct types: short (40–70 years, Maunder-like) and longer (>100 years, Spörer-

like). The appearance of grand minima can be reproduced by modern stochastic-driven dynamo models to some extent, but some problems still remain to be resolved.

The recent level of solar activity (after the 1940s) was very high, corresponding to a grand maximum, which are typical but rare events in solar behaviour. However, this grand maximum has ceased after solar cycle 23. The duration of grand maxima resembles a random Poisson-like process, in contrast to grand minima.

These observational features of the long-term behaviour of solar activity have important implications, especially for the development of theoretical solar-dynamo models and for solar-terrestrial studies.

5 Solar energetic particles in the past

In addition to galactic cosmic rays, which are always present in the Earth's vicinity, solar energetic-particle (SEP) events with a greatly enhanced flux of less energetic particles in the interplanetary medium also occur sporadically (e.g., Desai and Giacalone 2016; Klecker et al. 2006; Reames 2021; Vainio et al. 2009). Strong SEP events often originate from CME-related shocks propagating in the solar corona and the interplanetary medium, which leads to an effective bulk acceleration of charged particles (e.g., Cane and Lario 2006; Gopalswamy et al. 2012). Although these particles are significantly less energetic than GCRs, they can occasionally be accelerated to an energy reaching up to several GeV or more, which is enough to initiate the atmospheric cascade. Peak intensity of SEP flux can be very high, up to 10^4 particles (with energy > 30 MeV) per cm^2 per second which is many orders of magnitude greater than that of GCR. The long-term (solar cycle) average flux (or fluence) of SEP is mostly defined by rare major events, which occur a few times per solar cycle, with only minor contributions from a large number of weak events (Shea
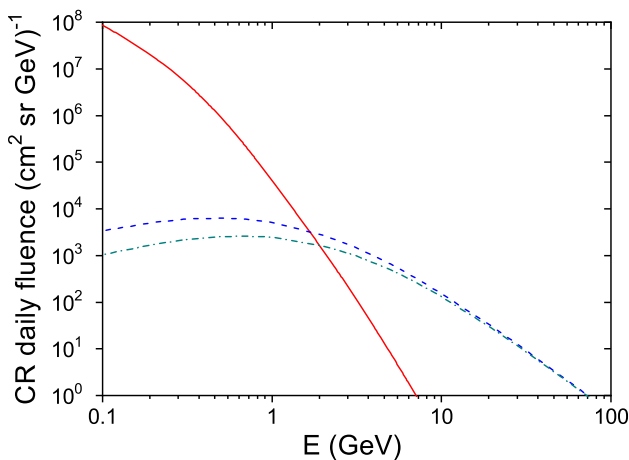

Fig. 26 Daily fluence of solar energetic particles for the day of 20-Jan-2005, GLE#69 (red curve—Raukunen et al. 2018) and galactic cosmic rays (dashed curves) for minimum (blue) and maximum (green) phases of a solar cycle

and Smart 1990, 2002). As an example, energy spectra of GCRs and SEPs are shown in Fig. 26 for the day of 20-Jan-2005, when one of the strongest directly observed SEP events (GLE#69) took place. Such SEPs dominate the low-energy section of cosmic rays (below hundreds of MeV of a particle's kinetic energy), which is crucial for the radiation environment, and play an important role in solar-terrestrial relations. For many reasons, it is important to know the variations of SEPs on long-term scales.

It is not straightforward to evaluate the average SEP flux even for the modern instrumental epoch of direct space-borne measurements (e.g., Mewaldt et al. 2007). For example, estimates for the average flux of SEPs with energy above 30 MeV (called F_{30} henceforth) for individual cycles may vary by an order of magnitude, from 7 cm^{-2} s^{-1} for cycle 24 up to 70 cm^{-2} s^{-1} for cycle 19 (Reedy 2012; Raukunen et al. 2022). Moreover, estimates of the SEP flux were quite uncertain during the earlier years of space-borne measurements because of two effects, which are hard to account for (e.g., Reeves et al. 1992; Tylka et al. 1997). One is related to the very high flux intensities of SEPs during the peak phase of events, when a detector can be saturated because of the dead-time effect (the maximum trigger rate of the detector is exceeded). The other is related to events with high-energy solar particles, which can penetrate into the detector through the walls of the collimator or the detector, leading to an enhanced effective acceptance cone with respect to the "expected" one. Since the SEP fluence is defined by major events, these effects may lead to an underestimate of the average flux of SEPs. A revisited analysis of the GOES instrumental data since 1984 has been made recently by Raukunen et al. (2022) using a re-calibration of the different energy channels.

The modern generation of detectors is better suited for measuring high fluxes. The average F_{30} flux for the last solar cycles is estimated as about 33 cm^{-2} s^{-1} for 1984–2019 (Raukunen et al. 2022).

5.1 Cosmogenic isotopes

SEP events can produce energetic particles which can initiate the atmospheric cascade and be detected by ground-based detectors – such events are called ground-level enhancements (GLE) and occur, on average, a dozen per solar cycle. Data for all known GLEs are collected at the International GLE Database (IGLED – https://gle.oulu.fi, Usoskin et al. 2020a). The strongest known GLE #5 occurred on 23-Feb-1956 as an up-to 5000% (x50) increase (above the GCR-related background) of the count rates of mid–high-latitude ground-based neutron monitors, and it was characterized by a very hard energy spectrum (Usoskin et al. 2020b). Accordingly, such energetic particles can produce cosmogenic isotopes in the atmosphere, but it remained unclear whether their amount is sufficient to make a detectable signal. The question about the possible rare occurrence of extreme SEP events on the millennial time scale is important not only from the theoretical point of view but also for the assessment of radiation risks for space-borne missions, especially manned ones. Usoskin et al. (2006b) suggested that a typical strong SEP (GLE) event leaves no distinguishable signature in the cosmogenic data. It was confirmed by a thorough analysis that none of the directly measured SEP(GLE) events can be even potentially

detected by the cosmogenic-isotope method (Mekhaldi et al. 2021; Usoskin et al. 2020b). A SEP event should be at least an order of magnitude stronger than GLE #5 to be detected by the cosmogenic proxy data. Such events are called extreme solar particle events (ESPE). Several attempts had been made earlier to find or at least put an upper limit on ESPEs occurrence from the cosmogenic isotope data (Lingenfelter and Hudson 1980; Usoskin et al. 2006b; Webber et al. 2007), but the result was grossly uncertain (Hudson 2010; Schrijver et al. 2012), mostly because of the large model uncertainties of the radionuclide production. In particular, Usoskin and Kovaltsov (2012) proposed a list of 23 ESPEs candidates based on a combined analysis of two ^{14}C and five ^{10}Be records over the last millennia. Later, only one of these candidates (around 775 AD—see below) has been confirmed as an ESPE, another one (ca. 1452 AD) was shown to be a signature of the Vanuatu volcanic eruption in Greenland ice cores, others were not confirmed.

While the response of ^{10}Be to a SEP event is typically a few-year-long peak, because of the relatively simple atmospheric transport/deposition (see Sect. 3.3.3), the response of ^{14}C has a typical shape shown in Fig. 27—with a sharp peak and exponential decay of the length of several decades, due to the carbon cycle (see Sect. 3.2.3).

5.1.1 The event of 774/5 AD: the worst case scenario?

The first ESPE was discovered by Miyake et al. (2012) as a large, 10–20‰ increase in biennially measured Δ^{14}C in a Japanese-cedar tree rings, as shown in Fig. 27. This event was later confirmed by annual ^{14}C data from a German oak tree (Usoskin et al. 2013), Russian and American tree samples (Jull et al. 2014), New Zealand trees
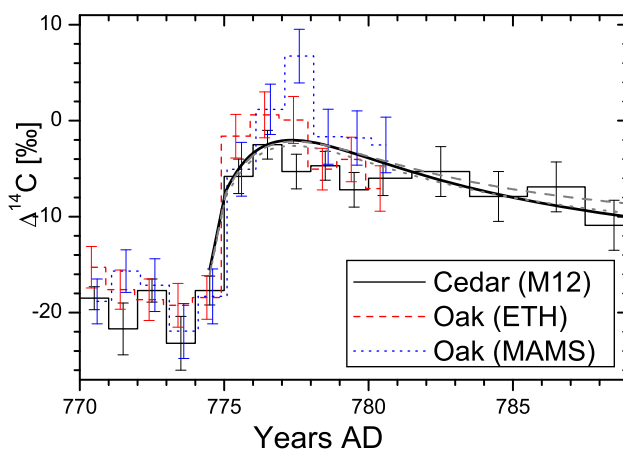

Fig. 27 Time profiles of the measured Δ^{14}C content in Japanese cedar (M12—Miyake et al. 2012) and German oak (ETH Zürich & Mannheim AMS—Usoskin et al. 2013) trees for the period around 775 AD. Smooth black and grey lines depict best-fit Δ^{14}C profiles, calculated using a family of realistic carbon-cycle models for an instantaneous injection of ^{14}C into the stratosphere (Usoskin and Kovaltsov 2012). Image after Usoskin et al. (2013)
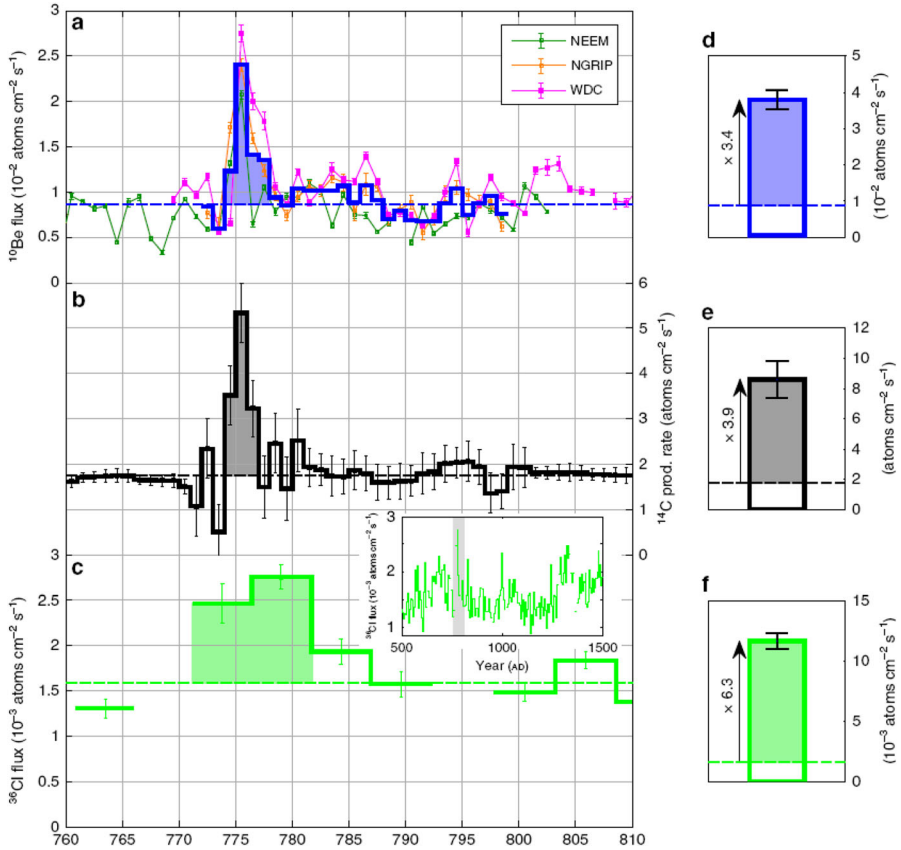
Fig. 28 Summary of the high-resolution cosmogenic data for the ESPE 774/5 AD. Panels a through c depict the time series of the ^{10}Be (time adjusted) depositional flux from the NEEM-2011-S1, NGRIP and WDC ice cores as well as the average flux (thick blue curve); modelled ^{14}C production rate; and the (time adjusted) depositional flux of ^{36}Cl, respectively. The dashed lines represent the background levels. The filled areas represent the estimated production enhancements caused by the ESPE event of 774/5 AD. Panels d through f show the summary isotope's production enhancements due to the ESPE above the estimated background levels. Image reproduced by permission from Mekhaldi et al. (2015), copyright by the authors

(Güttler et al. 2013), Poland (Rakowski et al. 2015), Finnish Lapland (Uusitalo et al. 2018), etc. also in ^{10}Be and ^{36}Cl ice-core records from Greenland and Antarctica (Mekhaldi et al. 2015; Miyake et al. 2015; Sigl et al. 2015), and also corals from the Chinese Sea (Liu et al. 2014). A summary of the data sets showing a highly significant increase in the cosmogenic-isotope production during the event of 774/5 AD is shown in Fig. 28 as analyzed by Mekhaldi et al. (2015).

When reporting the discovery, Miyake et al. (2012) initially suggested that the event was probably caused by γ-rays from an unknown nearby supernova as the observed increase was too strong for a SEP event. Various exotic scenarios of this event were proposed also by other researchers: a γ-ray burst (Hambaryan and Neuhäuser 2013; Pavlov et al. 2013); or even a cometary impact on Earth (Liu et al.

2014). However, these scenarios were undoubtedly rejected by a joint analysis of observed facts (Usoskin et al. 2013), viz. a significant increase of ^{10}Be production, which would have been absent in the case of γ-ray origin of the event (Pavlov et al. 2013); globally symmetric signal, specifically between Antarctic and Greenland ice cores (Sukhodolov et al. 2017), which is impossible to obtain from a point (beamed) source; full consistency between increases of different isotopes suggesting a relatively soft spectrum of the event (Mekhaldi et al. 2015; Sukhodolov et al. 2017); a possible polar enhancement of the ^{14}C signal as emphasized by Uusitalo et al. (2018) implying that the isotope production was mostly in the polar regions. All this says that the event was caused by a strong enhancement in the flux of energetic particles with a relatively soft spectrum impinging on Earth. Moreover, other similar events discovered later imply that such events are rare but not unique excluding very exotic scenarios. Considering the multitude of facts, it has been consensually established that the 774/5 AD increase in cosmogenic isotopes (aka *Miyake event*) was caused by an extreme SEP event, ESPE (Cliver et al. 2014; Eichler and Mordecai 2012; Mekhaldi et al. 2015; Melott and Thomas 2012; Thomas et al. 2013; Usoskin and Kovaltsov 2012; Usoskin et al. 2013).

Because of the processes of atmospheric transport and deposition of cosmogenic isotopes, the observed cosmogenic peak was delayed with respect to the time when the event had actually happened. Using different datasets, in particular, sub-annual ^{14}C data measured in trees from different regions with different tree-growing seasons, and models, it was shown that the event itself was short (shorter than a few months) and took place during the period of late Spring—Summer of 774 AD (Güttler et al. 2015; Sukhodolov et al. 2017; Uusitalo et al. 2018). This leads to a slight confusion in the event's name—the measured cosmogenic-isotope peak corresponds to the year 775 AD but the event per se took place in 774 AD. Accordingly, this ESPE is often called the 774/5 AD event, or Miyake event.

The fact that the ESPE was detected in different isotopes, which are sensitive to different energy ranges (see Fig. 9b) makes it possible to evaluate the energy spectrum of particles producing the event. Particularly important is the cosmogenic isotope ^{36}Cl sensitive to lower-energy particles. The first detailed analysis of the spectral shape of ESPE was performed by Mekhaldi et al. (2015) who estimated the ESPE spectrum and confirmed its solar origin. The estimate was based on an assumption that the spectrum must be very hard (Webber et al. 2007) leading to a slight underestimate of the event's strength. A more realistic method of spectral reconstruction, based on a database of the directly measured SEP spectra, leads to a slightly softer spectral estimate, comparable to the modern GLE events (Koldobskiy et al. 2023; Paleari et al. 2022). The reconstructed energy spectrum of the 774/5 AD ESPE is shown in Fig. 29 along with other major ESPE and three strong GLE events with different spectra—from soft to hard. One can see that the 774/5 AD event (as well as other ESPEs) was characterized by the energy spectrum typical for hard GLE events, but several orders of magnitude stronger. Roughly, the 774/5 AD was a factor 70 ± 30 stronger than the largest directly recorded GLE #5 making it really extreme (Usoskin et al. 2020b).
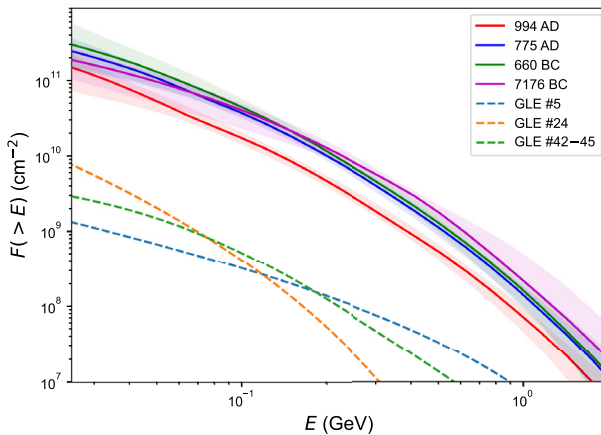
Fig. 29 Event-integrated (fluence) integral spectra for the four major ESPEs as denoted in the legend. Shaded areas depict the 68% confidence intervals. Dashed curves denote the integral spectra for three strong GLE events (Koldobskiy et al. 2021): the hard-spectrum GLE#5 (23-Feb-1956), soft-spectrum GLE#24 (04-Aug-1972) and a 'typical' series of GLE#42–45 (October–November 1989), as denoted in the legend

5.1.2 Other known ESPE events

Soon after the discovery of the 774/5 AD event, another ESPE was found (Miyake et al. 2013) as corresponding to the year 994 AD of the observed increase (the ESPE took place in 993 AD). The event was systematically analyzed by Mekhaldi et al. (2015) and shown to be another ESPE, similar to that of 774/5 AD but a factor of ≈ 1.5 weaker, yet 40 ± 20 times stronger than GLE #5. Several other ESPEs and candidates were discovered later: ESPE of ca. 660 BC (O'Hare et al. 2019; Park et al. 2017), 7176 BC (Brehm et al. 2022; Paleari et al. 2022) and 5259 BC (Brehm et al. 2022). These five events have been confirmed by multi-proxy analyses performed by different groups and can be considered real ESPEs. In addition, three event candidates observed only as $\Delta^{14}C$ increases still wait for independent confirmation: 5410 BC (Miyake et al. 2021), 1052 AD (Brehm et al. 2021; Terrasi et al. 2020) and 1279 AD (Brehm et al. 2021). The relative strength of these ESPEs and candidates is shown in Fig. 30 with respect to the strongest directly observed GLE#5. It is interesting that the three strongest events have exactly the same strength (within the error bars) and similar spectra (Fig. 29) while other confirmed events are somewhat smaller. This could indicate that the size of ESPEs may have an upper limit, but this is yet inconclusive.

The signatures of ESPEs are so strong and clearly visible in both ice-core ^{10}Be and tree-ring ^{14}C datasets that it is now used as a tie point (the point with an independently known date, e.g., volcanic eruption or, as in this case, the SEP event) for more precise dating of ice cores and archeological samples (e.g., Kuitems et al. 2022; Sigl et al. 2015).
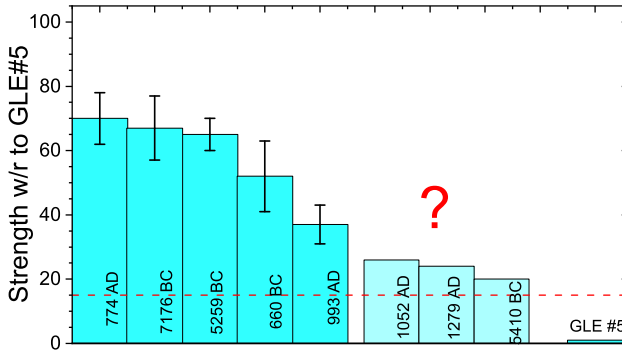
Fig. 30 The relative strength of ESPEs (darker blue) and candidates (light blue bars with the red question mark) given against the GLE#5 (23-Feb-1956, see Usoskin et al. 2020b) as the unity. The date of the event is denoted in the bars. The strength is given in the sense of the global ^{14}C production following estimates by Brehm et al. (2021)
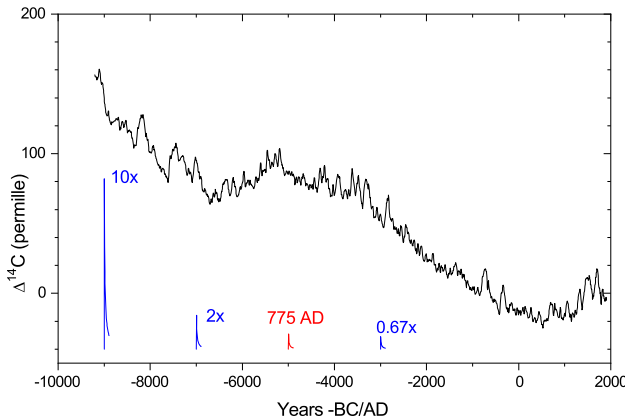

Fig. 31 The record (black) of Δ^{14}C (IntCal09 Reimer et al. 2009) throughout the Holocene, along with the expected signal in the decadal Δ^{14}C data from the actual (red) and scaled (blue, scaling factor denoted with 'x') 775 AD event. The "0.67x" peak roughly corresponds to the 994 AD event.

Do we expect that even stronger SEP events took place in the past? The 775 AD event was observed as the sharpest peak ($\approx 4\,‰$/yr) in the decadal ^{14}C IntCal dataset, while the smaller peak ($\approx 3.5\,‰$/yr) of the 994 AD was only barely seen in the IntCal data. Other found ESPEs were not greater than that (e.g., Paleari et al. 2022). Accordingly, an event stronger than that of 775 AD could be found only in a case of an unlikely random coincidence of the event itself with an incidental drop of ^{14}C caused by other reasons, masking the spike. In particular, an event twice as strong as the 775 AD one is hardly possible to occur since it would have produced a large spike in the IntCal data which could not be missed (see Fig. 31). Thus, the 775 AD event can securely serve as the worst-case scenario of the SEP event during the entire Holocene.
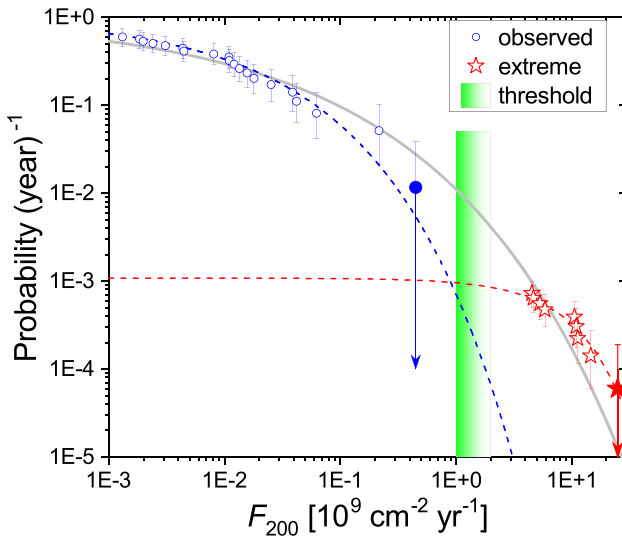
Fig. 32 Complementary cumulative probability density function (CCPDF—see text) of occurrence of annual SEP fluence (> 200 MeV) exceeding the given value F_{200}, as assessed from the data for the space era 1984–2019 (Raukunen et al. 2022,—blue circles) and cosmogenic isotope data (Fig. 30—red stars). Filled symbols depict conservative upper limits of F_{200}. Dashed curved illustrate possible distributions fitted separately to the direct F_{200} data (Weibull—blue curve) and to the proxy-based ESPE events (exponential—red). The grey curve depicts the Weibull distribution best fitted to the data (Usoskin et al. 2023). The vertical bar indicates the sensitivity threshold of the cosmogenic-isotope method to an ESPE on a 3σ-level (Usoskin et al. 2020b)

5.1.3 Occurrence rate

The complementary cumulative probability density function (CCPDF) of the occurrence (viz. the probability that the fluence of SEPs (> 200 MeV) during a randomly selected year exceeds a given F_{200} value) of strong SEP events, as revealed from the direct measurements and the cosmogenic-isotope data, is shown in Fig. 32. The blue dots are based on the revisited statistic of annual SEP fluences measured by GOES spacecraft from 1984–2019 (Raukunen et al. 2022), while red stars correspond to ESPEs (five confirmed events and three candidates as discussed in Sect. 5.1.2). Solid-filled symbols depict conservative upper limits for the fluence which is the double strongest directly observed (blue dot) or reconstructed from the proxy (star). A significant, a factor of ≈ 30, a gap exists between the directly measured and reconstructed events, leaving the question of their origin open (Usoskin and Kovaltsov 2021): whether the ESPE are *Black swans* or *Dragon kings*. A *Black swan* is an impactful event unexpected from the previous experience and/or common sense, but it can be explained a-posteriori in the frameworks of the existing knowledge once it happens (Taleb 2007). A *Dragon king* is an extremely impactful event (king) of the unknown nature (Dragon) which cannot be understood with the present knowledge even a-posteriori and requires new knowledge to be developed (Sornette and Ouillon 2012). In the contexts of ESPEs, this is translated to the question of whether the ESPEs represent the very far tail of rare extremely strong

SEP events formed due to a combination of favourable solar/heliospheric conditions as represented by the joint distribution in Fig. 32 (Black swan) or a new, yet unknown type of extreme eruptive events as illustrated in the Figure by dashed curves. Because of the instrumental gap between the two datasets (Mekhaldi et al. 2021; Usoskin et al. 2020b), it is unlikely that events in the intermediate range of $F_{200} \approx 10^9$ particles/cm^2 can be resolved by the proxy data to distinguish between different distributions.

The present paradigm is that ESPEs are black swans, viz. formed as the extreme tail of the 'normal' SEP events. This is consistent with the result of analyses of lunar-isotope proxy (Sect. 5.3) and stellar superflares (Sect. 5.2)—see discussion in Cliver et al. (2022).

5.2 Super-flares on sun-like stars

Nearly simultaneously with ESPEs, super-flares were discovered on sun-like stars using four years of observations by the *Kepler* telescope of thousands of stars (Maehara et al. 2012). Such super-flares have bolometric energy between 10^{34}–10^{36} erg which is a factor 25–2500 greater than the strongest directly observed solar flare of 4-Nov-2003 ($\approx 4.3 \cdot 10^{32}$ erg—Emslie et al. 2012). Even stronger flares are known on more active stars including faster rotating and younger stars and binary systems (e.g., Doyle et al. 1991), but the discovery of Maehara et al. (2012) was about super-flares on solar analogues without indications of binary or hot-Jupiter
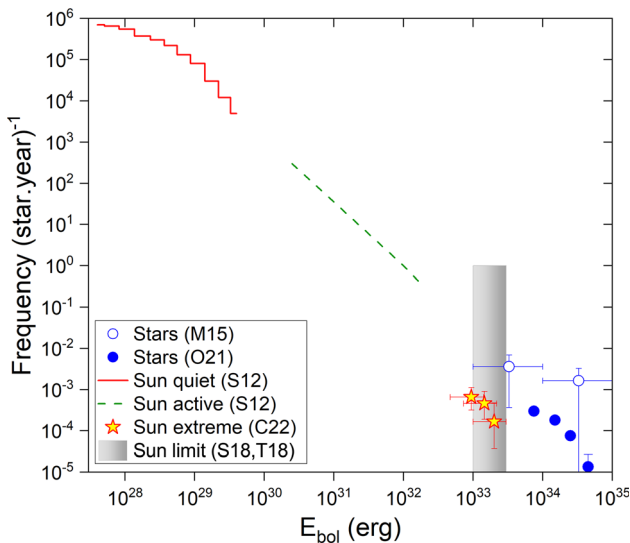

Fig. 33 CCPDF of occurrence of solar flares, as a function of their bolometric energy, for quite (red) and active (dashed green) sun, extreme events based on cosmogenic isotopes (stars), and two estimates of stellar super-flares (blue) statistics. The grey bar denotes the theoretical upper limit of the solar-flare strength. References are: S12—Schrijver et al. (2012); M15—Maehara et al. (2015); S18—Schmieder (2018); T18—Tschernitz et al. (2018); O21 – Okamoto et al. (2021); C22— Cliver et al. (2022)

companions. Although the question of how accurately the flaring stars correspond to our sun is still open with several surveys of parameters (Maehara et al. 2015; Notsu et al. 2019; Okamoto et al. 2021; Reinhold et al. 2020, 2021), it is generally accepted that sun can potentially produce super-flares, but the occurrence rate is still debated (see more details in Cliver et al. 2022).

The statistic (in the form of CCPDF) of solar and stellar flares is shown in Fig. 33. Again, as in the case of ESPEs, there is a gap between the observed solar flares ($E_{bol} \geq 4 \cdot 10^{32}$ erg) and stellar super-flares, while the distribution looks consistent.

The question of the possible relation between super-flares and ESPEs is presently open. It is likely that the two phenomena represent the same eruptive processes on the sun, but the occurrence rates and energy ranges mismatch. As shown in Fig. 33, ESPEs during the Holocene ($\approx$12 kyrs of data coverage) are an order of magnitude rarer and less energetic (the energy was indirectly estimated by Cliver et al. 2022) than the super-flares on sun-like stars ($\approx$20 kyears·stars). The origin of the mismatch is unknown, but several reasons are identified which can lead to it: a simple geometrical factor—only eruptive event located close to the West limb of the solar disc can produce major SEP events so that not each flare produces SEP events at Earth (e.g., Desai and Giacalone 2016; Vainio et al. 2009); the SEP acceleration mechanism—favourable conditions are needed for a flare or CME to effectively accelerate protons (e.g., Gopalswamy 2018); heliospheric transport of SEP—particle-wave-interaction feedback (called streaming limit) can saturate the flux of SEPs in the interplanetary space (Reames and Ng 2010; Reames 2021); or inconsistency between the sun and flaring 'sun-like' stars may exist, e.g., in the form of observational biases (active stars are likely to be analyzed) or other stellar parameters not accounted for (e.g., differential rotation rate, depth of the convection zone, meridional flow).

It is interesting that there are indications that even stellar coronal mass ejections and filament eruptions can be potentially detected (Namekata et al. 2021; Veronig et al. 2021).

5.3 Lunar rocks and regolith

Since SEPs and GCRs are characterized by significantly different energy spectra, they can be separated by a natural spectrometer making it possible to evaluate their fluxes independently. A spectrometer that is able to separate cosmic rays is lunar rocks. The Moon is not protected by the magnetosphere or atmosphere, and charged particles of all energies can reach its surface directly. Since the penetrating ability of such particles depends on their energy, the lunar rock/soil acts as a primitive integral spectrometer as illustrated in Fig. 34. Soft (low-energy) particles can penetrate into the soil and initiate nuclear reactions, producing cosmogenic isotopes there only in a shallow near-surface layer, which becomes thicker as the particle's energy increases. As the energy reaches several hundred MeV, a nucleonic cascade, similar to the one in the Earth's atmosphere, can develop at a depth below several tens of g/cm^2 and deeper. Thus, measuring cosmogenic isotopes at different depths in lunar cores can provide an estimate of the energy spectrum of cosmic-ray particles irradiating the
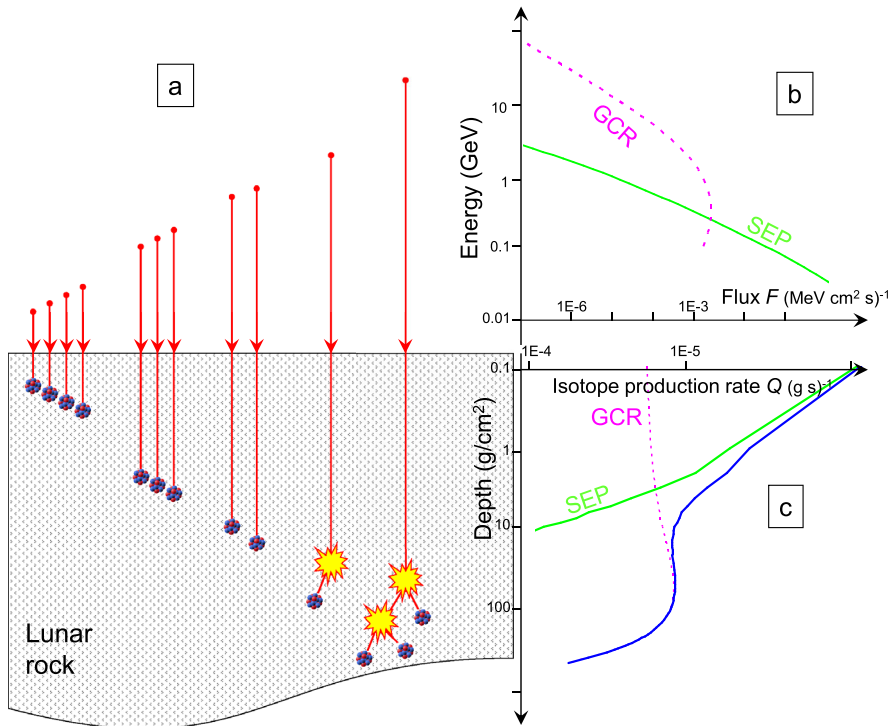
Fig. 34 Scheme of the lunar regolith acting as a primitive spectrometer. Panel a: Depending on the bombarding particle's energy (depicted as the length of the red bar in the upper part of the figure), the formation of cosmogenic isotope takes place at different depths (blue balls in the lower part). When the energy is high enough (> 100 MeV/nuc), a nucleonic cascade can be formed (yellow stars). Panel b: Typical energy spectra of GCR (magenta dashed curve) and SEP (green). Panel c: Typical depth profiles of the cosmogenic isotope production due to both GCR (magenta), SEP (green and their sum (blue)

lunar surface. Since the deep layers are affected only by GCR, one can estimate, by first measuring the isotope activity in deep layers, the average GCR flux and then estimate the expected contribution of GCR to the isotope production in the shallow layers. The difference between the measured isotope concentrations in the shallow layers and those expected from GCR can be ascribed to SEPs allowing for their spectrum estimate (see Fig. 34c).

A disadvantage of this approach is that lunar samples are not stratified and do not allow for temporal separation. The measured isotope activity is a balance between production and decay and, therefore, represents the production (and the ensuing flux) integrated over the lifetime of the isotope before the sample has been measured. However, using different isotopes with different lifetimes, one can evaluate the cosmic-ray flux integrated over different timescales.

Real data (in units of disintegrations per minute per kilogram) of cosmogenic ^{26}Al measured in several lunar cores and rocks are shown in Fig. 35. As seen, the contributions from GCR and SEP are clearly distinguishable by the depth so that the layers below $\approx$10 g/cm^2 are totally dominated by GCRs while the shallow layers are
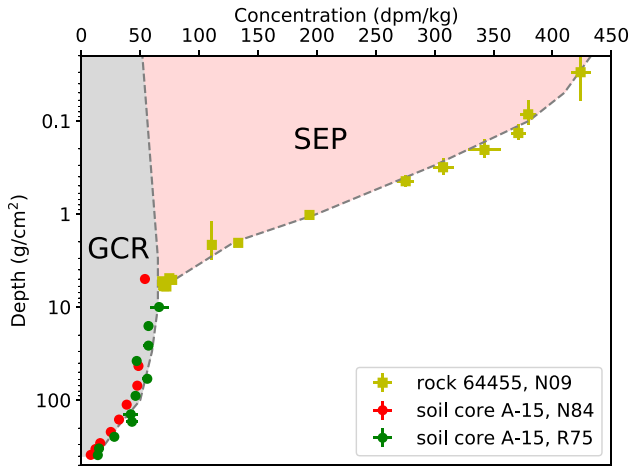
Fig. 35 Depth profile of the measured activity of ^{26}Al in several lunar samples (as denoted in the legend) as well the interpretation of the profile as presented in Fig. 34C. References are: (R75 – Rancitelli et al. 1975), (N84—Nishiizumi et al. 1984), (N09 – Nishiizumi et al. 2009). The plot is courtesy of S. Poluianov
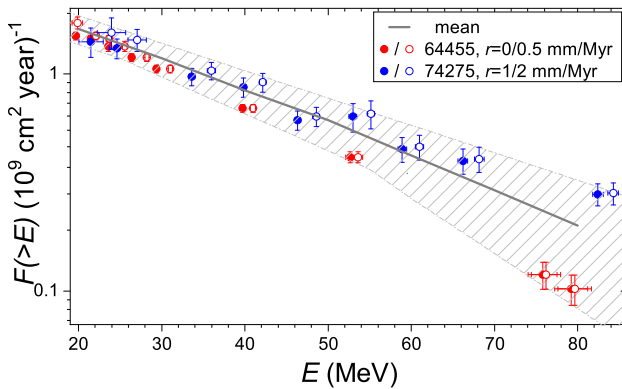

Fig. 36 Integral omnidirectional fluxes $F(>E)$ of SEPs averaged over a million of years reconstructed from ^{26}Al in lunar samples. Colored filled and open dots depict reconstructions based on different lunar samples and different assumptions on erosion rates. The thick line and the hatched area depict the mean spectrum and its full-range uncertainties. The plot is modified after Poluianov et al. (2018) where all the details about reconstructions can be found

dominated by SEPs. After subtracting the GCR contribution, the depth profile of the isotope's production can be converted into the integral spectrum of SEP averaged over the lifetime of the isotope.

Several such SEP flux reconstructions have been made in the past using measurements of different cosmogenic isotopes in lunar rocks, soil and deep-core samples brought to Earth by Apollo missions in the 1960–1970s (Miyake et al. 2020). An example of the most recent analysis (Poluianov et al. 2018) based on the data of ^{26}Al in several lunar samples is shown in Fig. 36. One can see that even considering possible uncertainties (e.g., the erosion rates) and multiple data samples,

Table 5 Estimates of 4π omni-directional integral (above 30 MeV) flux, F_{30} in [cm^2 s]$^{-1}$, of solar energetic particles, obtained from different sources

Timescale	Method	Source	Reference	F_{30} (cm^{-2} s^{-1})
$1984 - 2019$	Measurements	Space-borne	Raukunen et al. (2022)	33
$2009 - 2019$	Measurements	Space-borne	Raukunen et al. (2022)	7.4
10^4 yr	^{14}C	Lunar rock	Jull et al. (1998)	42
10^5 yr	^{41}Ca	Lunar rock	Fink et al. (1998)	56
5×10^5 yr	^{36}Cl	Lunar rock	Nishiizumi et al. (2009)	46
10^6 yr	^{26}Al	Lunar rock	Kohl et al. (1978)	25
10^6 yr	^{26}Al	Lunar rock	Grismore et al. (2001)	55
10^6 yr	^{26}Al	Lunar rock	Poluianov et al. (2018)	37
10^6 yr	^{10}Be, ^{26}Al	Lunar rock	Michel et al. (1996)	24
10^6 yr	^{10}Be, ^{26}Al	Lunar rock	Fink et al. (1998)	32
10^6 yr	^{10}Be, ^{26}Al	Lunar rock	Nishiizumi et al. (2009)	24
2×10^6 yr	^{10}Be, ^{26}Al	Lunar rock	Nishizumi et al. (1997)	≈ 35
5×10^6 yr	^{53}Mn	Lunar rock	Kohl et al. (1978)	25
2×10^6 yr	^{21}Ne, ^{22}Ne, ^{38}Ar	Lunar rock	Rao et al. (1994)	22

the reconstructed integral spectrum of SEP converges to a fairly narrow band. Similar efforts have been performed earlier using different isotopes and analysis methods as summarized in Table 5. All reconstructions with the Mega-year or shorter timescale yield the mean F_{30} value of 38 ± 4.5 (cm^2 sec)$^{-1}$, which is consistent (within the error bars) with the mean directly measured SEP flux over the last decades. The results on the $> 10^6$-yr timescale are more uncertain because of the poorly known corrosion rate. This gave rise to the paradigm that the modern SEP fluxes are fully representative of the Mega-year timescale (see Poluianov et al. 2018, and references therein). On the other hand, rare extreme-flux ESPEs also contribute to the long-term SEP flux, from ≈ 10 (only the known ESPEs during the Holocene) and up to 40 (cm^2 sec)$^{-1}$ (continuous distribution in Fig. 32) on the long-time average (Usoskin et al. 2022). This has led to a disagreement between the direct data, cosmogenic-isotope proxy and lunar-based reconstructions of the SEP fluxes. However, solar activity was unusually high between ca. 1940–2009 representing the Modern grand maxima which is not a typical solar activity level (Sect. 4.3). The mean SEP during the moderate solar cycle 24 (2009–2019), which is a typical one for long-term solar activity (e.g., Usoskin et al. 2016b), was only 7.4 (cm^2 sec)$^{-1}$ as shown in Table 5. This reconciles the disagreement and makes all three ways of the average SEP flux estimate consistent with each other (Usoskin et al. 2022).

5.4 Nitrate in polar ice is not a proxy for SEPs

It has been discussed earlier that another quantitative index of strong SEP events (with $F_{30} > 10^9$ cm^{-2}) might be related to nitrate (NO$_3^-$) records measured in polar ice cores (e.g., Dreschhoff and Zeller 1998; McCracken et al. 2001; Zeller and Dreschhoff 1995). However, it was shown (Duderstadt et al. 2016) that a realistic SEP event can hardly produce a sufficient amount of nitrate to leave a strong pulse-like signature in an ice core. As shown by several independent studies, no clear nitrate signal has been found for the strongest known solar events such as the Carrington event (September 1859) (Wolff et al. 2012; Usoskin and Kovaltsov 2012) or the extreme event of 774/5 AD (Mekhaldi et al. 2017; Sukhodolov et al. 2017). Thus, the nitrate record in polar ice cannot serve as an index of SEP events. On the other hand, it may be used to study the long-term variability of GCR (Traversi et al. 2012).

5.5 Summary

In this section, estimates of the averaged long-term flux of SEPs are discussed.

Measurements of cosmogenic isotopes with different lifetimes in lunar rocks and regolith allow one to make rough estimates of the SEP flux and even energy spectrum over different timescales. The directly space-borne-measured SEP flux averaged over the past decades is smaller than the lunar-rock-based estimates but fully consistent with those when extreme SEP events are also considered on longer timescales—up to millions of years.

Terrestrial cosmogenic isotope data in independently dated archives (tree trunks, ice cores) give a possibility to assess the occurrence rate of extreme SEP events on the time scales up to ten millennia. Measurements of nitrates in polar ice have been shown to be an invalid index of strong SEP events in the past. At present, five confirmed ESPEs and three candidates are known with the strongest one occurring in 774/5 AD (see Fig. 30), which can serve as the worst-case scenario for an extreme SEP event on the multi-millennial time scale. Other confirmed events are slightly smaller in size.

Presently, the statistics of the SEP events occurrence from both direct measurements for the last decades and terrestrial proxy-based extreme events on the multi-millennial time scale are consistent with the million-year averaged SEP flux derived from lunar-rock data.

6 Conclusions

This review presents the current state of the art in reconstruction and studies of long-term solar activity on a multi-millennial timescale.

Although the concept of solar activity is intuitively understandable as a deviation from the "quiet-sun" concept, there is no clear definition for it, and different indices have been proposed to quantify different aspects of variable solar activity. One of the most common and practical indices is the sunspot number, which forms the longest

available series of direct scientific observations. While all other indices have a high correlation with sunspot numbers, dominated by the 11-year Schwabe cycle, the relationship between them at other timescales (short- and long-term trends) may vary to a great extent.

On longer timescales, quantitative information on past solar activity can only be obtained using the methods based upon indirect proxy, i.e., quantitative parameters, which can be measured nowadays but represent the signatures, stored in natural archives, of different effects of solar magnetic activity in the past. Such traceable signatures can be related to nuclear or chemical effects caused by cosmic rays in the Earth's atmosphere, lunar rocks or meteorites. The most common proxy of solar activity is formed by data from the cosmogenic radionuclides, ^{10}Be and ^{14}C, produced by cosmic rays in the Earth's atmosphere and stored in independently-dated stratified natural archives, such as tree rings or ice cores. Using a fully developed physics-based model, it is now possible to reconstruct the temporal behaviour of solar activity in the past, over many millennia. The most robust results can be obtained for the Holocene epoch, which started more than 11,000 years ago, characterized by a stable climate which minimizes possible uncertainties in the reconstruction. An indirect verification of long-term solar-activity reconstructions supports their veracity and confirms that variations of cosmogenic nuclides on the long-term scale (centuries to millennia) during the Holocene make a solid basis for studies of solar variability in the past. However, such reconstructions may still contain systematic uncertainties related to unknown changes in the geomagnetic field or climate of the past, especially in the early part of the Holocene.

Cosmogenic isotopes in terrestrial archives reveal that the sun rarely produces extremely eruptive events, nearly two orders of magnitude stronger than anything we have experienced directly during the last decades. Although such ESPEs are rare (roughly once per 1–1.5 millennia) they contribute, due to their extreme strength, about half of the long-term averaged SEP flux. The SEP event of 774/5 AD, discovered using data from cosmogenic isotopes, was the strongest known event, which can serve as the worst-case scenario for the entire Holocene. Measurements of the concentration of different cosmogenic isotopes in lunar rocks make it possible to estimate the SEP flux on different timescales.

In general, the following main features are observed in the long-term evolution of solar magnetic activity.

– Solar activity is dominated by the 11-year Schwabe cycle on an interannual timescale. Some additional longer characteristic times can be found, including the centennial Gleissberg secular cycle, ≈210-year de Vries/Suess cycle, and a quasi-cycle of 2000–2400 years (Hallstatt cycle). However, all these cycles are intermittent and cannot be regarded as strict phase-locked periodicities.
– One of the main features of long-term solar activity is that it contains an essential chaotic/stochastic component, which leads to irregular variations and makes solar-activity predictions impossible for a scale exceeding one solar cycle.
– The sun spends about 70% of its time at moderate magnetic activity levels, about 15–20% of its time in a grand minimum and about 10–15% in a grand maximum.

- Grand minima are typical but rare phenomena in solar behaviour. They form a distinct mode of the solar dynamo. Their occurrence appears not periodically, but rather as the result of a chaotic process within clusters separated by the 2000–2500 years (around the lows of the Hallstatt cycle). Grand minima tend to be of two distinct types: short (Maunder-like) and longer (Spörer-like).
- The recent level of solar activity (after the 1940s) was very high, corresponding to a prolonged grand maximum, but it has ceased to the normal moderate level. Grand maxima are also rare and irregularly occurring events, though the exact rate of their occurrence is still a subject of debate.

These observational features of the long-term behaviour of solar activity have important implications, especially for the development of theoretical solar-dynamo models and for solar-terrestrial studies.

References

Abreu JA, Beer J, Steinhilber F, Tobias SM, Weiss NO (2008) For how long will the current grand maximum of solar activity persist? Geophys Res Lett 35:L20109. https://doi.org/10.1029/2008GL035442

Abreu JA, Beer J, Ferriz-Mas A, McCracken KG, Steinhilber F (2012) Is there a planetary influence on solar activity? Astron Astrophys 548:A88. https://doi.org/10.1051/0004-6361/201219997

Acero F, Gallego M, Garcia J, Usoskin I, Vaquero J (2018) Extreme value theory applied to the millennial sunspot number series. Astrophys J 853:80. https://doi.org/10.3847/1538-4357/aaa406

Adolphi F, Muscheler R (2016) Synchronizing the Greenland ice core and radiocarbon timescales over the Holocene–Bayesian wiggle-matching of cosmogenic radionuclide records. Clim Past 12:15–30. https://doi.org/10.5194/cp-12-15-2016

Agostinelli S, Allison J, Amako K, Apostolakis J, Araujo H, Arce P, Asai M, Axen D, Banerjee S, Barrand G, Behner F, Bellagamba L, Boudreau J, Broglia L, Brunengo A, Burkhardt H, Chauvie S, Chuma J, Chytracek R, Cooperman G, Cosmo G, Degtyarenko P, dell'Acqua A, Depaola G, Dietrich D, Enami R, Feliciello A, Ferguson C, Fesefeldt H, Folger G, Foppiano F, Forti A, Garelli S, Giani S, Giannitrapani R, Gibin D, Gómez Cadenas JJ, González I, Gracia Abril G, Greeniaus G, Greiner W, Grichine V, Grossheim A, Guatelli S, Gumplinger P, Hamatsu R, Hashimoto K, Hasui H, Heikkinen A, Howard A, Ivanchenko V, Johnson A, Jones FW, Kallenbach J, Kanaya N, Kawabata M, Kawabata Y, Kawaguti M, Kelner S, Kent P, Kimura A, Kodama T, Kokoulin R, Kossov M, Kurashige H, Lamanna E, Lampén T, Lara V, Lefebure V, Lei F, Liendl M, Lockman W, Longo F, Magni S, Maire M, Medernach E, Minamimoto K, Mora de Freitas P, Morita Y, Murakami K, Nagamatu M, Nartallo R, Nieminen P, Nishimura T, Ohtsubo K, Okamura M, O'Neale S, Oohata Y, Paech K, Perl J, Pfeiffer A, Pia MG, Ranjard F, Rybin A, Sadilov S, di Salvo E, Santin G, Sasaki T, Savvas N, Sawada Y, Scherer S, Sei S, Sirotenko V, Smith D, Starkov N, Stoecker H, Sulkimo J, Takahata M, Tanaka S, Tcherniaev E, Safai Tehrani E, Tropeano M, Truscott P, Uno H, Urban L, Urban P, Verderi M, Walkden A, Wander W, Weber H, Wellisch JP, Wenaus T, Williams DC, Wright D, Yamada T, Yoshida H, Zschiesche D (2003) Geant4-a simulation toolkit. Nucl Instr Meth Phys Res A 506:250–303

Aguilar M, Ali Cavasonza L, Ambrosi G, Arruda L, Attig N, Barao F, Barrin L, Bartoloni A, Başeğmez-du Pree S, Bates J, Battiston R, Behlmann M, Beischer B, Berdugo J, Bertucci B, Bindi V, de Boer W, Bollweg K, Borgia B, Boschini MJ, Bourquin M, Bueno EF, Burger J, Burger WJ, Burmeister S, Cai XD, Capell M, Casaus J, Castellini G, Cervelli F, Chang YH, Chen GM, Chen HS, Chen Y, Cheng L, Chou HY, Chouidou S, Choutko V, Chung CH, Clark C, Coignet G, Consolandi C, Contin A, Corti C, Cui Z, Dadzie K, Dai YM, Delgado C, Della Torre S, Demirköz MB, Derome L, Di Falco S, Di Felice V, Díaz C, Dimiccoli F, von Doetinchem P, Dong F, Donnini F, Duranti M, Egorov A, Eline A, Feng J, Fiandrini E, Fisher P, Formato V, Freeman C, Galaktionov Y, Gámez C, García-López RJ, Gargiulo C, Gast H, Gebauer I, Gervasi M, Giovacchini F, Gómez-Coral DM, Gong J, Goy C, Grabski V, Grandi D, Graziani M, Guo KH, Haino S, Han KC, Hashmani RK, He ZH, Heber B, Hsieh TH, Hu JY, Huang ZC, Hungerford W, Incagli M, Jang WY, Jia Y, Jinchi H, Kanishev K, Khiali B, Kim GN, Kirn T, Konyushikhin M, Kounina O, Kounine A, Koutsenko V, Kuhlman A, Kulemzin A, La Vacca G, Laudi E, Laurenti G, Lazzizzera I, Lebedev A, Lee HT, Lee SC, Leluc C, Li JQ, Li M, Li Q, Li S, Li TX, Li ZH, Light C, Lin CH, Lippert T, Liu Z, Lu SQ, Lu YS, Luebelsmeyer K, Luo JZ, Lyu SS, Machate M, Mañá C, Marín J, Marquardt J, Martin T, Martínez G, Masi N, Maurin D, Menchaca-Rocha A, Meng Q, Mo DC, Molero M, Mott P, Mussolin L, Ni JQ, Nikonov N, Nozzoli F, Oliva A, Orcinha M, Palermo M, Palmonari F, Paniccia M, Pashnin A, Pauluzzi M, Pensotti S, Phan HD, Plyaskin V, Pohl M, Porter S, Qi XM, Qin X, Qu ZY, Quadrani L, Rancoita PG, Rapin D, Reina Conde A, Rosier-Lees S, Rozhkov A, Rozza D, Sagdeev R, Schael S, Schmidt SM, Schulz von Dratzig A, Schwering G, Seo ES, Shan BS, Shi JY, Siedenburg T, Solano C, Song JW, Sonnabend R, Sun Q, Sun ZT, Tacconi M, Tang XW, Tang ZC, Tian J, Ting SCC, Ting SM, Tomassetti N, Torsti J, Tüysüz C, Urban T, Usoskin I, Vagelli V, Vainio R, Valente E, Valtonen E, Vázquez Acosta M, Vecchi M, Velasco M, Vialle JP, Wang LQ, Wang NH, Wang QL, Wang S, Wang X, Wang ZX, Wei J, Weng ZL, Wu H, Xiong RQ, Xu W, Yan Q, Yang Y, Yi H, Yu YJ, Yu ZQ, Zannoni M, Zhang C, Zhang F, Zhang FZ, Zhang JH, Zhang Z, Zhao F, Zheng ZM, Zhuang HL, Zhukov V, Zichichi A, Zimmermann N, Zuccon P, AMS Collaboration (2021) The Alpha Magnetic Spectrometer (AMS) on the international space station: Part II - Results from the first seven years. Phys Rep 894:1–116. https://doi.org/10.1016/j.physrep.2020.09.003

Aparicio AJP, Vaquero JM, Carrasco VMS, Gallego MC (2014) Sunspot numbers and areas from the madrid astronomical observatory (1876–1986). Sol Phys 289:4335–4349. https://doi.org/10.1007/s11207-014-0567-x. arXiv:1407.3104 [astro-ph.SR]

Argento DC, Reedy RC, Stone JO (2013) Modeling the earth's cosmic radiation. Nucl Instrum Methods B 294:464–469. https://doi.org/10.1016/j.nimb.2012.05.022

Arlt R (2008) Digitization of sunspot drawings by Staudacher in 1749–1796. Sol Phys 247:399–410. https://doi.org/10.1007/s11207-007-9113-4

Arlt R (2009) The butterfly diagram in the eighteenth century. Sol Phys 255:143–153. https://doi.org/10.1007/s11207-008-9306-5. arXiv:0812.2233

Arlt R, Abdolvand A (2011) First solar butterfly diagram from Schwabe's observations in 1825–1867. In: Choudhary DP, Strassmeier KG (eds) Physics of sun and star spots. IAU Symposium, vol S273. Cambridge University Press, Cambridge; New York, pp 286–289. https://doi.org/10.1017/S1743921311015390. arXiv:1010.3131 [astro-ph.SR]

Arlt R, Vaquero J (2020) Historical sunspot records. Living Rev Sol Phys 17:1. https://doi.org/10.1007/s41116-020-0023-y

Arlt R, Leussu R, Giese N, Mursula K, Usoskin I (2013) Sunspot positions and sizes for 1825–1867 from the observations by Samuel Heinrich Schwabe. Mon Not R Astron Soc 433:3165–3172. https://doi.org/10.1093/mnras/stt961. arXiv:1305.7400 [astro-ph.SR]

Asvestari E, Gil A, Kovaltsov GA, Usoskin IG (2017) Neutron monitors and cosmogenic isotopes as cosmic ray energy-integration detectors: effective yield functions, effective energy, and its dependence on the local interstellar spectrum. J Geophys Res (Space Phys) 122:9790–9802. https://doi.org/10.1002/2017JA024469

Asvestari E, Usoskin IG, Kovaltsov GA, Owens MJ, Krivova NA, Rubinetti S, Taricco C (2017b) Assessment of different sunspot number series using the cosmogenic isotope ^{44}Ti in meteorites. Mon Not Royal Astron Soc 467:1608–1613. https://doi.org/10.1093/mnras/stx190

Aulanier G, Démoulin P, Schrijver CJ, Janvier M, Pariat E, Schmieder B (2013) The standard flare model in three dimensions. II. Upper limit on solar flare energy. Astron Astrophys 549:A66. https://doi.org/10.1051/0004-6361/201220406. arXiv:1212.2086 [astro-ph.SR]

Balmaceda LA, Solanki SK, Krivova NA (2005) A cross-calibrated sunspot areas time series since 1874. Mem Soc Astron Ital 76:929–932

Baranyi T, Győri L, Ludmány A, Coffey HE (2001) Comparison of sunspot area data bases. Mon Not R Astron Soc 323:223–230. https://doi.org/10.1046/j.1365-8711.2001.04195.x

Bard E, Arnold M, Maurice P, Duplessy JC (1987) Measurements of bomb radiocarbon in the ocean by means of accelerator mass spectrometry: technical aspects. Nucl Instrum Methods B 29:297–301. https://doi.org/10.1016/0168-583X(87)90253-9

Bard E, Raisbeck GM, Yiou F, Jouzel J (1997) Solar modulation of cosmogenic nuclide production over the last millenium: comparison between ^{14}C and ^{10}Be records. Earth Planet Sci Lett 150:453–462. https://doi.org/10.1016/S0012-821X(97)00082-4

Barnard L, Lockwood M, Hapgood MA, Owens MJ, Davis CJ, Steinhilber F (2011) Predicting space climate change. Geophys Res Lett 38:L16103. https://doi.org/10.1029/2011GL048489

Basurah HM (2004) Auroral evidence for early high solar activities. Sol Phys 225:209–212. https://doi.org/10.1007/s11207-004-1372-8

Beer J (2000) Long-term indirect indices of solar variability. Space Sci Rev 94(1/2):53–66. https://doi.org/10.1023/A:1026778013901

Beer J, Siegenthaler U, Oeschger H, Andrée M, Bonani G, Suter M, Wolfli W, Finkel RC, Langway CC (1983) Temporal ^{10}Be Variations. In: Dea Durgaprasad (ed) 18th international cosmic ray conference, vol 9. TIFR, Bombay, pp 317–320

Beer J, Siegenthaler U, Oeschger H, Bonani G, Finkel RC (1988) Information on past solar activity and geomagnetism from Be-10 in the Camp Century ice core. Nature 331:675–679. https://doi.org/10.1038/331675a0

Beer J, Blinov A, Bonani G, Finkel RC, Hofmann HJ, Lehmann B, Oeschger H, Sigg A, Schwander J, Staffelbach T, Stauffer B, Suter M, Wötfli W (1990) Use of ^{10}Be in polar ice to trace the 11-year cycle of solar activity. Nature 347:164–166. https://doi.org/10.1038/347164a0

Beer J, Tobias S, Weiss N (1998) An active Sun throughout the Maunder minimum. Sol Phys 181:237–249. https://doi.org/10.1023/A:1005026001784

Beer J, Vonmoos MV, Muscheler R, McCracken KG, Mende W (2003) Heliospheric Modulation over the past 10,000 Years as derived from Cosmogenic Nuclides. In: Kajita T, Asaoka Y, Kawachi A, Matsubara Y, Sasaki M (eds) 28th international cosmic ray conference, vol 7. Universal Academy Press, Tokyo, Japan, pp 4147–4150

Beer J, McCracken KG, von Steiger R (2012) Cosmogenic radionuclides: theory and applications in the terrestrial and space environments, physics of earth and space environments, vol 26. Springer, Berlin, Heidelberg. https://doi.org/10.1007/978-3-642-14651-0

Belmaker R, Lazar B, Tepelyakov N, Stein M, Beer J (2008) ^{10}Be in Lake Lisan sediments—a proxy for production or climate? Earth Planet Sci Lett 269:447–456. https://doi.org/10.1016/j.epsl.2008.02.032

Benevolenskaya E (1998) Longitudinal structure of the double magnetic cycle. Sol Phys 181(2):479–489. https://doi.org/10.1023/A:1005077029797

Berggren AM, Beer J, Possnert G, Aldahan A, Kubik P, Christl M, Johnsen SJ, Abreu JA, Vinther BM (2009) A 600-year annual ^{10}Be record from the NGRIP ice core, Greenland. Geophys Res Lett 36: L11801. https://doi.org/10.1029/2009GL038004

Bezuglov MV, Malyshevsky VS, Malykhina TV, Torgovkin AV, Fomin GV, Shramenko BI (2012) Photonuclear channel of ^{7}Be production in the Earth's atmosphere. Phys Atom Nucl 75:393–397. https://doi.org/10.1134/S1063778812030040

Bhandari PA, Lal D, Rama D (1966) Stratospheric circulation studies based on natural and artificail radioactive tracer elements. Tellus 18:391–406. https://doi.org/10.3402/tellusa.v18i2-3.9390

Bisschoff D, Potgieter MS (2016) New local interstellar spectra for protons, helium and carbon derived from PAMELA and Voyager 1 observations. Astrophys Space Sci 361:48. https://doi.org/10.1007/s10509-015-2633-8. arXiv:1512.04836 [astro-ph.HE]

Bonino G, Cini-Castagnoli G, Bhandari N, Taricco C (1995) Behavior of the heliosphere over prolonged solar quiet periods by ^{44}Ti measurements in meteorites. Science 270:1648–1650. https://doi.org/10.1126/science.270.5242.1648

Bracewell RN (1986) Simulating the sunspot cycle. Nature 323:516–519. https://doi.org/10.1038/323516a0

Brandenburg A, Sokoloff D (2002) Local and Nonlocal Magnetic Diffusion and Alpha-Effect Tensors in Shear Flow Turbulence. Geophys Astrophys Fluid Dyn 96:319–344. https://doi.org/10.1080/03091920290032974. arXiv:astro-ph/0111568

Brandenburg A, Spiegel EA (2008) Modeling a Maunder minimum. Astron Nachr 329:351–358. https://doi.org/10.1002/asna.200810973. arXiv:0801.2156

Brandenburg A, Krause F, Meinel R, Moss D, Tuominen I (1989) The stability of nonlinear dynamos and the limited role of kinematic growth rates. Astron Astrophys 213:411–422

Bray RJ, Loughhead RE (1964) Sunspots, international astrophysics series, vol 7. Chapman & Hall, London

Brehm N, Bayliss A, Christl M, Synal H, Adolphi F, Beer J, Kromer B, Muscheler R, Solanki S, Usoskin I, Bleicher N, Bollhalder S, Tyers C, Wacker L (2021) Eleven-year solar cycles over the last millennium revealed by radiocarbon in tree rings. Nature Geosci 14:10–15. https://doi.org/10.1038/s41561-020-00674-0

Brehm N, Christl M, Knowles TDJ, Casanova E, Evershed R, Adolphi F, Muscheler R, Synal HA, Mekhaldi F, Paleari C, Leuschner HH, Bayliss A, Nicolussi K, Pichler T, Schlüchter C, Pearson C, Salzer M, Fonti P, Nievergelt D, Hantemirov R, Brown D, Usoskin I, Wacker L (2022) Tree-rings reveal two strong solar proton events in 7176 and 5259 BCE. Nature Commun 13:1196. https://doi.org/10.1038/s41467-022-28804-9

Brody J (2002) The enigma of sunspots. A story of discovery and scientific revolution. Floris Books, Edinburgh

Broeker WS, Peng TH (1986) Carbon cycle: 1985 Glacial to interglacial changes in the operation of the global carbon cycle. Radiocarbon 28:309–327

Brooke JM, Moss D (1994) Non-linear dynamos in torus geometry: transition to chaos. Mon Not R Astron Soc 266:733–739. https://doi.org/10.1093/mnras/266.3.733

Burger RA, Potgieter MS, Heber B (2000) Rigidity dependence of cosmic ray proton latitudinal gradients measured by Ulysses spacecraft: implications for the diffusion tensor. J Geophys Res 105:27,447-27,455. https://doi.org/10.1029/2000JA000153

Caballero-Lopez RA, Moraal H (2004) Limitations of the force field equation to describe cosmic ray modulation. J Geophys Res 109:A01101. https://doi.org/10.1029/2003JA010098

Calisto M, Usoskin I, Rozanov E, Peter T (2011) Influence of Galactic Cosmic Rays on atmospheric composition and dynamics. Atmos Chem Phys 11:4547–4556. https://doi.org/10.5194/acp-11-4547-2011

Cane HV, Lario D (2006) An introduction to CMEs and energetic particles. Space Sci Rev 123:45–56. https://doi.org/10.1007/s11214-006-9011-3

Carbonell M, Oliver R, Ballester JL (1993) On the asymmetry of solar activity. Astron Astrophys 274:497–504

Carbonell M, Oliver R, Ballester JL (1994) A search for chaotic behaviour in solar activity. Astron Astrophys 290:983–994

Carrasco VMS, Vaquero JM (2016) Sunspot observations during the Maunder minimum from the correspondence of John Flamsteed. Sol Phys 291:2493–2503. https://doi.org/10.1007/s11207-015-0839-0. arXiv:1601.02851 [astro-ph.SR]

Carrasco VMS, Vaquero JM, Gallego MC, Trigo RM (2013) Forty two years counting spots: Solar observations by D.E. Hadden during 1890–1931 revisited. New Astron 25:95–102. https://doi.org/10.1016/j.newast.2013.05.002

Carrasco VMS, Gallego MC, Arlt R, Vaquero JM (2020) Revisiting the amplitude of solar cycle 9: the case of sunspot observations by W.C. Bond. Sol Phys 295(9):127. https://doi.org/10.1007/s11207-020-01696-y

Carrasco VMS, Gallego MC, Vaquero JM (2020) Number of sunspot groups from the Galileo–Scheiner controversy revisited. Mon Not R Astron Soc 496(2):2482–2492. https://doi.org/10.1093/mnras/staa1633. arXiv:2103.10296 [astro-ph.SR]

Carrasco VMS, Gallego MC, Villalba Álvarez J, Vaquero JM, Hayakawa H (2021) Analyses of early sunspot records by Jean Tarde (1615–1617) and Jan Smogulecki (1621–1625). Sol Phys 296(11):170. https://doi.org/10.1007/s11207-021-01905-2

Carrasco VMS, Hayakawa H, Kuroyanagi C, Gallego MC, Vaquero JM (2021) Strong evidence of low levels of solar activity during the Maunder Minimum. Mon Not R Astron Soc 504(4):5199–5204. https://doi.org/10.1093/mnras/stab1155

Casas R, Vaquero JM, Vázquez M (2006) Solar Rotation in the 17th century. Sol Phys 234:379–392. https://doi.org/10.1007/s11207-006-0036-2

Castagnoli G, Lal D (1980) Solar modulation effects in terrestrial production of carbon-14. Radiocarbon 22:133–158

Cauquoin A, Raisbeck GM, Jouzel J, Bard E (2014) No evidence for planetary influence on solar activity 330 000 years ago. Astron Astrophys 561:A132. https://doi.org/10.1051/0004-6361/201322879

Charbonneau P (2001) Multiperiodicity, chaos, and intermittency in a reduced model of the solar cycle. Sol Phys 199:385–404

Charbonneau P (2020) Dynamo models of the solar cycle. Living Rev Sol Phys 17:4. https://doi.org/10.1007/s41116-020-00025-6

Charbonneau P (2022) External forcing of the solar dynamo. Front Astron Space Sci 9:853676. https://doi.org/10.3389/fspas.2022.853676

Charbonneau P, Dikpati M (2000) Stochastic fluctuations in a Babcock-Leighton model of the solar cycle. Astrophys J 543:1027–1043. https://doi.org/10.1086/317142

Charbonneau P, Blais-Laurier G, St-Jean C (2004) Intermittency and phase persistence in a Babcock-Leighton model of the solar cycle. Astrophys J Lett 616:L183–L186. https://doi.org/10.1086/426897

Chatzistergos T, Usoskin IG, Kovaltsov GA, Krivova NA, Solanki SK (2017) New reconstruction of the sunspot group numbers since 1739 using direct calibration and "backbone" methods. Astron Astrophys 602:A69. https://doi.org/10.1051/0004-6361/201630045. arXiv:1702.06183 [astro-ph.SR]

Chiodo G, García-Herrera R, Calvo N, Vaquero JM, Añel JA, Barriopedro D, Matthes K (2016) The impact of a future solar minimum on climate change projections in the Northern Hemisphere. Environ Res Lett 11(3):034015. https://doi.org/10.1088/1748-9326/11/3/034015

Chol-jun K, Kyong-phyong J (2022) Stable solar periodicities: the time stability. Mon Not R Astron Soc 511(1):1401–1407. https://doi.org/10.1093/mnras/stac134. arXiv:2011.14564 [astro-ph.SR]

Choudhuri AR (1992) Stochastic fluctuations of the solar dynamo. Astron Astrophys 253:277–285

Clark DH, Stephenson FR (1978) An interpretation of the pre-telescopic sunspot records from the orient. Quart J R Astron Soc 19:387–410

Clette F, Lefèvre L (2016) The new sunspot number: assembling all corrections. Sol Phys 291:2629–2651. https://doi.org/10.1007/s11207-016-1014-y

Clette F, Berghmans D, Vanlommel P, van der Linden RAM, Koeckelenbergh A, Wauters L (2007) From the Wolf number to the International Sunspot Index: 25 years of SIDC. Adv Space Res 40:919–928. https://doi.org/10.1016/j.asr.2006.12.045

Clette F, Svalgaard L, Vaquero JM, Cliver EW (2014) Revisiting the Sunspot Number. Space Sci Rev https://doi.org/10.1007/s11214-014-0074-2. arXiv:1407.3231 [astro-ph.SR]

Clette F, Lefèvre L, Chatzistergos T, Hayakawa H, Carrasco VM, Arlt R, Cliver EW, Dudok de Wit T, Friedli T, Karachik N, Kopp G, Lockwood M, Mathieu S, Muñoz-Jaramillo A, Owens M, Pesnell D, Pevtsov A, Svalgaard L, Usoskin IG, van Driel-Gesztelyi L, Vaquero JM (2023) Re-calibration of the sunspot number: status report. Sol Phys 298:44. https://doi.org/10.1007/s11207-023-02136-3

Cliver EW, Ling AG (2016) The discontinuity circa 1885 in the Group Sunspot Number. Solar Phys 291:2763–2784. https://doi.org/10.1007/s11207-015-0841-6

Cliver EW, Boriakoff V, Bounar KH (1998) Geomagnetic activity and the solar wind during the Maunder Minimum. Geophys Res Lett 25:897–900. https://doi.org/10.1029/98GL00500

Cliver EW, Tylka AJ, Dietrich WF, Ling AG (2014) On a solar origin for the cosmogenic nuclide event of 775 A.D. Astrophys J 781:32. https://doi.org/10.1088/0004-637X/781/1/32

Cliver EW, Schrijver CJ, Shibata K, Usoskin IG (2022) Extreme solar events. Living Rev Sol Phys 19:2. https://doi.org/10.1007/s41116-022-00033-8. arXiv:2205.09265 [astro-ph.SR]

Cooke DJ, Humble JE, Shea MA, Smart DF, Lund N, Rasmussen IL, Byrnak B, Goret P, Petrou N (1991) On cosmic-ray cut-off terminology. Nuovo Cimento C 14:213–234. https://doi.org/10.1007/BF02509357

Covas E, Tavakol R, Tworkowski A, Brandenburg A (1998) Axisymmetric mean field dynamos with dynamic and algebraic α-quenching. Astron Astrophys 329:350–360 arXiv:astro-ph/9709062

Damon PE, Sonett CP (1991) Solar and terrestrial components of the atmospheric ^{14}C variation spectrum. In: Sonett CP, Giampapa MS, Matthews MS (eds) The sun in time. University of Arizona Press, Tucson, pp 360–388

Damon PE, Lerman JC, Long A (1978) Temporal fluctuations of atmospheric ^{14}C: causal factors and implications. Annu Rev Earth Planet Sci 6:457–494. https://doi.org/10.1146/annurev.ea.06.050178.002325

de La Rue W, Stewart B, Loewy B (1871) Further investigations on planetary influence upon solar activity. Proc R Soc London Ser I 20:210–218

de Carvalho JX, Prado CPC (2000) Self-organized criticality in the Olami-Feder-Christensen model. Phys Rev Lett 84:4006–4009. https://doi.org/10.1103/PhysRevLett.84.4006

de Meyer F (1998) Modulation of the solar magnetic cycle. Sol Phys 181:201–219. https://doi.org/10.1023/A:1005079132329

Delaygue G, Bard E (2011) An Antarctic view of Beryllium-10 and solar activity for the past millennium. Climate Dyn 36:2201–2218. https://doi.org/10.1007/s00382-010-0795-1

Desai M, Giacalone J (2016) Large gradual solar energetic particle events. Living Rev Sol Phys 13:3. https://doi.org/10.1007/s41116-016-0002-5

Diercke A, Arlt R, Denker C (2015) Digitization of sunspot drawings by Spörer made in 1861–1894. Astron Nachr 336:53–62. https://doi.org/10.1002/asna.201412138. arXiv:1411.7790 [astro-ph.SR]

Donadini F, Korte M, Constable C (2010) Millennial variations of the geomagnetic field: from data recovery to field reconstruction. Space Sci Rev 155:219–246. https://doi.org/10.1007/s11214-010-9662-y

Donnelly RF, White OR, Livingston WC (1994) The solar Ca II K index and the Mg II core-to-wing ratio. Sol Phys 152:69–76. https://doi.org/10.1007/BF01473185

Dorman LI (2004) Cosmic rays in the Earth's atmosphere and underground. Kluwer Academic Publishers, Dordrecht. https://doi.org/10.1007/978-1-4020-2113-8

Doyle JG, Kellett BJ, Byrne PB, Avgoloupis S, Mavridis LN, Seiradakis JH, Bromage GE, Tsuru T, Makishima K, Makishima K, McHardy IM (1991) Simultaneous detection of a large flare in the X-ray and optical regions on the RS CVn-type star II Peg. Mon Not R Atron Soc 248:503. https://doi.org/10.1093/mnras/248.3.503

Dreschhoff GAM, Zeller EJ (1998) Ultra-high resolution nitrate in polar ice as indicator of past solar activity. Sol Phys 177:365–374. https://doi.org/10.1023/A:1004932530313

Duderstadt KA, Dibb JE, Schwadron NA, Spence HE, Solomon SC, Yudin VA, Jackman CH, Randall CE (2016) Nitrate ion spikes in ice cores not suitable as proxies for solar proton events. J Geophys Res 121:2994–3016. https://doi.org/10.1002/2015JD023805. arXiv:1511.03358 [physics.ao-ph]

Dudok de Wit T, Ermolli I, Haberreiter M, Kambezidis H, Lam M, Lilensten J, Matthes K, Mironova I, Schmidt H, Seppälä A, Tanskanen E, Tourpali K, Yair Y (2015) Earth's climate response to a changing Sun. EDP Science, Les Ulis Cedex A, France

Dudok de Wit T, Lefèvre L, Clette F (2016) Uncertainties in the sunspot numbers: estimation and implications. Sol Phys 291:2709–2731. https://doi.org/10.1007/s11207-016-0970-6. arXiv:1608.05261 [astro-ph.SR]

Eddy JA (1976) The Maunder minimum. Science 192:1189–1202. https://doi.org/10.1126/science.192.4245.1189

Eddy JA (1977) Climate and the changing sun. Climatic Change 1:173–190. https://doi.org/10.1007/BF01884410

Eddy JA (1977) The case of the missing sunspots. Sci Am 236:80–88. https://doi.org/10.1038/scientificamerican0577-80

Eddy JA (1983) The Maunder minimum: a reappraisal. Sol Phys 89:195–207. https://doi.org/10.1007/BF00211962

Eddy JA, Stephenson FR, Yau KKC (1989) On pre-telescopic sunspot records. Quart J R Astron Soc 30:65–73

Egorova T, Schmutz W, Rozanov E, Shapiro AI, Usoskin I, Beer J, Tagirov RV, Peter T (2018) Revised historical solar irradiance forcing. Astron Astrophys 615:A85. https://doi.org/10.1051/0004-6361/201731199. arXiv:1804.00287 [astro-ph.SR]

Eichler D, Mordecai D (2012) Comet encounters and carbon 14. Astrophys J Lett 761:L27. https://doi.org/10.1088/2041-8205/761/2/L27

Elsasser W, Nay EP, Winkler JR (1956) Cosmic-ray intensity and geomagnetism. Nature 178:1226–1227. https://doi.org/10.1038/1781226a0

Emslie AG, Dennis BR, Shih AY, Chamberlin PC, Mewaldt RA, Moore CS, Share GH, Vourlidas A, Welsch BT (2012) Global Energetics of thirty-eight large solar eruptive events. Astrophys J 759:71. https://doi.org/10.1088/0004-637X/759/1/71. arXiv:1209.2654 [astro-ph.SR]

Feynman J, Gabriel SB (1990) Period and phase of the 88-year solar cycle and the Maunder minimum: evidence for a chaotic Sun. Sol Phys 127:393–403. https://doi.org/10.1007/BF00152176

Field CV, Schmidt GA, Koch D, Salyk C (2006) Modeling production and climate-related impacts on ^{10}Be concentration in ice cores. J Geophys Res 111:D15107. https://doi.org/10.1029/2005JD006410

Fink D, Klein J, Middleton R, Vogt S, Herzog GF, Reedy RC (1998) ^{41}Ca, ^{26}Al, and ^{10}Be in lunar basalt 74275 and ^{10}Be in the double drive tube 74002/74001. Geochim Cosmochim Acta 62:2389–2402. https://doi.org/10.1016/S0016-7037(98)00134-3

Finkel RC, Nishiizumi K (1997) Beryllium 10 concentrations in the Greenland Ice Sheet Project 2 ice core from 3–40 ka. J Geophys Res 102:26,699-26,706. https://doi.org/10.1029/97JC01282

Foukal P (1996) The behavior of solar magnetic plages measured from Mt. Wilson observations between 1915–1984. Geophys Res Lett 23:2169–2172. https://doi.org/10.1029/96GL01356

Foukal P, Fröhlich C, Spruit H, Wigley TML (2006) Variations in solar luminosity and their effect on the Earth's climate. Nature 443:161–166. https://doi.org/10.1038/nature05072

Fraser-Smith AC (1987) Centered and eccentric geomagnetic dipoles and their poles, 1600–1985. Rev Geophys 25:1–16. https://doi.org/10.1029/RG025i001p00001

Frick P, Galyagin D, Hoyt DV, Nesme-Ribes E, Schatten KH, Sokoloff D, Zakharov V (1997) Wavelet analysis of solar activity recorded by sunspot groups. Astron Astrophys 328:670–681

Friedli TK (2020) Recalculation of the Wolf Series from 1877 to 1893. Sol Phys 295(6):72. https://doi.org/10.1007/s11207-020-01637-9

Fröhlich C (2006) Solar irradiance variability since 1978. Space Sci Rev 125:53–65. https://doi.org/10.1007/s11214-006-9046-5

Fröhlich C (2012) Total solar irradiance observations. Surv Geophys 33:453–473. https://doi.org/10.1007/s10712-011-9168-5

Garcia-Munoz M, Mason GM, Simpson JA (1975) The anomalous ^{4}He component in the cosmic-ray spectrum at $\lesssim$50 MeV per nucleon during 1972–1974. Astrophys J 202:265–275. https://doi.org/10.1086/153973

Genevey A, Gallet Y, Constable CG, Korte M, Hulot G (2008) ArcheoInt: an upgraded compilation of geomagnetic field intensity data for the past ten millennia. Geochem Geophys Geosyst 9:Q04038. https://doi.org/10.1029/2007GC001881

Gerber S, Joos F, Brügger P, Stocker TF, Mann ME, Sitch S, Scholze M (2002) Constraining temperature variations over the last millennium by comparing simulated and observed atmospheric CO_2. Climate Dyn 20:281–299

Gibson SE, de Toma G, Emery B, Riley P, Zhao L, Elsworth Y, Leamon RJ, Lei J, McIntosh S, Mewaldt RA, Thompson BJ, Webb D (2011) The whole heliosphere interval in the context of a long and structured solar minimum: an overview from Sun to Earth. Sol Phys 274:5–27. https://doi.org/10.1007/s11207-011-9921-4

Gleeson LJ, Axford WI (1968) Solar modulation of galactic cosmic rays. Astrophys J 154:1011–1026. https://doi.org/10.1086/149822

Gleissberg W (1939) A long-periodic fluctuation of the sun-spot numbers. Observatory 62:158–159

Gleissberg W (1948) A preliminary forecast of solar activity. Popular Astron 56:399

Gleissberg W (1952) Die Häufigkeit der Sonnenflecken. Akademie-Verlag, Berlin

Gleissberg W (1971) The probable behaviour of sunspot cycle 21. Sol Phys 21:240–245. https://doi.org/10.1007/BF00155794

Gnevyshev MN, Ohl A (1948) On the 22-year cycle of solar activity. Astron Zh 25:18–20

Golubenko K, Rozanov E, Kovaltsov G, Leppänen AP, Sukhodolov T, Usoskin I (2021) Application of CCM SOCOL-AERv2-BE to cosmogenic beryllium isotopes: description and validation for polar regions. Geosci Model Dev 14(12):7605–7620. https://doi.org/10.5194/gmd-14-7605-2021

Golubenko K, Rozanov E, Kovaltsov G, Usoskin I (2022) Zonal mean distribution of cosmogenic isotope (^{7}Be, ^{10}Be, ^{14}C, and ^{36}Cl) production in stratosphere and troposphere. J Geophys Res (Atmospheres) 127(16):e2022JD036726. https://doi.org/10.1029/2022JD036726

González-López A, Campuzano SA, Molina-Cardín A, Pavón-Carrasco FJ, De Santis A, Osete ML (2021) Characteristic periods of the paleosecular variation of the Earth's magnetic field during the Holocene from global paleoreconstructions. Phys Earth Planet Inter 312:106656. https://doi.org/10.1016/j.pepi.2021.106656

Gopalswamy N (2018) Chapter 2 - Extreme Solar Eruptions and their Space Weather Consequences. In: Buzulukova N (ed) Extreme Events in Geospace. Elsevier, pp 37–63. https://doi.org/10.1016/B978-0-12-812700-1.00002-9. arXiv:1709.03165

Gopalswamy N, Xie H, Yashiro S, Akiyama S, Mäkelä P, Usoskin IG (2012) Properties of ground level enhancement events and the associated solar eruptions during solar Cycle 23. Space Sci Rev 171:23–60. https://doi.org/10.1007/s11214-012-9890-4. arXiv:1205.0688 [astro-ph.SR]

Goslar T (2003) ^{14}C as an indicator of solar variability. PAGES News 11(2/3):12–14. http://www.pages-igbp.org/products/newsletters/nl2003_2a.pdf

Gough D (1981) On the seat of the solar cycle. In: Sofia S (ed) Variations of thesolar constant. NASA Conference Publication, vol 2191. pp 185–206. https://ntrs.nasa.gov/citations/19820009159

Gray LJ, Beer J, Geller M, Haigh JD, Lockwood M, Matthes K, Cubasch U, Fleitmann D, Harrison G, Hood L, Luterbacher J, Meehl GA, Shindell D, van Geel B, White W (2010) Solar influences on climate. Rev Geophys 48:RG4001. https://doi.org/10.1029/2009RG000282

Grieder PKF (2001) Cosmic rays at earth: researcher's reference manual and data book. Elsevier Science, Amsterdam, New York. https://doi.org/10.1016/B978-0-444-50710-5.X5000-3

Grinsted A, Moore JC, Jevrejeva S (2004) Application of the cross wavelet transform and wavelet coherence to geophysical time series. Nonlinear Proc Geophys 11:561–566

Grismore R, Llewellyn RA, Brown MD, Dowson ST, Cumblidge K (2001) Measurements of the concentrations of ^{26}Al in lunar rocks 15555 and 60025. Earth Planet Sci Lett 187:163–171. https://doi.org/10.1016/S0012-821X(01)00271-0

Güttler D, Beer J, Bleicher N, Boswijk G, Hogg AG, Palmer JG, Wacker L, Wunder J (2013) The 774/775 AD event in the southern hemisphere. In: Laboratory of Ion Beam Physics: Annual Report 2013. ETH, Zurich, p 33. http://www.ams.ethz.ch/publications/annual_reports/2013

Güttler D, Adolphi F, Beer J, Bleicher N, Boswijk G, Christl M, Hogg A, Palmer J, Vockenhuber C, Wacker L, Wunder J (2015) Rapid increase in cosmogenic ^{14}C in AD 775 measured in New Zealand kauri trees indicates short-lived increase in ^{14}C production spanning both hemispheres. Earth Planet Sci Lett 411:290–297. https://doi.org/10.1016/j.epsl.2014.11.048

Haigh JD (2007) The sun and the earth's climate. Living Rev Sol Phys 4:2. https://doi.org/10.12942/lrsp-2007-2

Haigh JD, Winning AR, Toumi R, Harder JW (2010) An influence of solar spectral variations on radiative forcing of climate. Nature 467:696–699. https://doi.org/10.1038/nature09426

Hale GE, Ellerman F, Nicholson SB, Joy AH (1919) The magnetic polarity of sun-spots. Astrophys J 49:153–178. https://doi.org/10.1086/142452

Hambaryan VV, Neuhäuser R (2013) A Galactic short gamma-ray burst as cause for the ^{14}C peak in AD 774/5. Mon Not R Astron Soc. https://doi.org/10.1093/mnras/sts378

Hanslmeier A, Brajša R, Čalogović J, Vršnak B, Ruždjak D, Steinhilber F, MacLeod CL, Ivezić Ž, Skokić I (2013) The chaotic solar cycle. II. Analysis of cosmogenic ^{10}Be data. Astron Astrophys 550:A6. https://doi.org/10.1051/0004-6361/201015215

Harvey KL, White OR (1999) What is solar cycle minimum? J Geophys Res 104(A9):19,759-19,764. https://doi.org/10.1029/1999JA900211

Hathaway DH (2015) The solar cycle. Living Rev Sol Phys 12:4. https://doi.org/10.1007/lrsp-2015-4

Hathaway DH, Wilson RM (2004) What the sunspot record tells us about space climate. Sol Phys 224:5–19. https://doi.org/10.1007/s11207-005-3996-8

Hayakawa H, Vaquero J, Ebihara Y (2018) Sporadic auroras near the geomagnetic equator: in the Philippines, on 27 October 1856. Ann Geophys 36(4):1153–1160. https://doi.org/10.5194/angeo-36-1153-2018. arXiv:1808.06608 [physics.space-ph]

Hayakawa H, Mitsuma Y, Ebihara Y, Miyake F (2019) The earliest candidates of auroral observations in Assyrian astrological reports: insights on solar activity around 660 BCE. Astrophys J Lett 884(1): L18. https://doi.org/10.3847/2041-8213/ab42e4. arXiv:1909.05498 [astro-ph.SR]

Hayakawa H, Stephenson FR, Uchikawa Y, Ebihara Y, Scott CJ, Wild MN, Willis DM (2019) The celestial sign in the Anglo-Saxon chronicle in the 770s: insights on contemporary solar activity. Sol Phys 294(4):42. https://doi.org/10.1007/s11207-019-1424-8. arXiv:1903.03075 [astro-ph.SR]

Hayakawa H, Iju T, Murata K, Besser BP (2021) Daniel Mögling's sunspot observations in 1626–1629: a manuscript reference for the solar activity before the Maunder minimum. Astrophys J 909(2):194. https://doi.org/10.3847/1538-4357/abdd34. arXiv:2102.04047 [astro-ph.SR]

Hayakawa H, Lockwood M, Owens M, Sôma M, Besser B, van Driel-Gesztelyi L (2021) Graphical evidence for the solar coronal structure during the Maunder minimum: comparative study of the total eclipse drawings in 1706 and 1715. J Space Weather Space Clim 11:1. https://doi.org/10.1051/swsc/2020035

He F, Wei Y, Maffei S, Livermore PW, Davies CJ, Mound J, Xu K, Cai S, Zhu R (2021) Equatorial auroral records reveal dynamics of the paleo-West Pacific geomagnetic anomaly. Proc Nat Acad Sci 118(20): e2026080118. https://doi.org/10.1073/pnas.2026080118

Heck D, Knapp J, Capdevielle J, Schatz G, Thouw T (1998) Corsika: a Monte Carlo code to simulate extensive air showers. In: FZKA 6019. Forschungszentrum, Karlsruhe

Heikkilä U, Beer J, Feichter J (2008) Modeling cosmogenic radionuclides ^{10}Be and ^{7}Be during the Maunder Minimum using the ECHAM5-HAM General Circulation Model. Atmos Chem Phys 8:2797–2809. https://doi.org/10.5194/acp-8-2797-2008

Heikkilä U, Beer J, Feichter J (2009) Meridional transport and deposition of atmospheric ^{10}Be. Atmos Chem Phys 9:515–527. https://doi.org/10.5194/acp-9-515-2009

Heikkilä U, Beer J, Abreu JA, Steinhilber F (2013) On the atmospheric transport and deposition of the cosmogenic radionuclides (^{10}Be): a review. Space Sci Rev 176:321–332. https://doi.org/10.1007/s11214-011-9838-0

Heilbron J (1999) The sun in the church: cathedrals as solar observatories. Harvard University Press, Harvard

Herbst K, Kopp A, Heber B, Steinhilber F, Fichtner H, Scherer K, Matthiä D (2010) On the importance of the local interstellar spectrum for the solar modulation parameter. J Geophys Res 115:D00I20. https://doi.org/10.1029/2009JD012557

Herbst K, Heber B, Kopp A, Sternal O, Steinhilber F (2012) The Local Interstellar Spectrum beyond the Heliopause: What can be Learned from Voyager in the Inner Heliosheath? Astrophys J 761:17. https://doi.org/10.1088/0004-637X/761/1/17

Horiuchi K, Minoura K, Kobayashi K, Nakamura T, Hatori S, Matsuzaki H, Kawai T (1999) Last-glacial to post-glacial ^{10}Be fluctuations in a sediment core from the Academician Ridge, Lake Baikal. Geophys Res Lett 26:1047–1050. https://doi.org/10.1029/1999GL900163

Horiuchi K, Ohta A, Uchida T, Matsuzaki H, Shibata Y, Motoyama H (2007) Concentration of ^{10}Be in an ice core from the Dome Fuji station, Eastern Antarctica: preliminary results from 1500 to 1810 yr AD. Nucl Instrum Methods B 259:584–587. https://doi.org/10.1016/j.nimb.2007.01.306

Horiuchi K, Uchida T, Sakamoto Y, Ohta A, Matsuzaki H, Shibata Y, Motoyama H (2008) Ice core record of ^{10}Be over the past millennium from Dome Fuji, Antarctica: a new proxy record of past solar activity and a powerful tool for stratigraphic dating. Quat Geochronology 3:253–261. https://doi.org/10.1016/j.quageo.2008.01.003

Hoyng P (1993) Helicity fluctuations in mean field theory: an explanation for the variability of the solar cycle? Astron Astrophys 272:321–339

Hoyt DV, Schatten K (1998) Group sunspot numbers: a new solar activity reconstruction. Sol Phys 179:189–219. https://doi.org/10.1023/A:1005007527816

Hoyt DV, Schatten KH (1996) How well was the sun observed during the Maunder minimum? Sol Phys 165:181–192. https://doi.org/10.1007/BF00149097

Hoyt DV, Schatten KH, Nesme-Ribes E (1994) The one hundredth year of Rudolf Wolf's death: do we have the correct reconstruction of solar activity? Geophys Res Lett 21:2067–2070. https://doi.org/10.1029/94GL01698

Hudson HS (2010) Solar flares add up. Nature Phys 6:637–638. https://doi.org/10.1038/nphys1764

Inceoglu F, Simoniello R, Knudsen VF, Karoff C, Olsen J, Turck-Chiéze S, Jacobsen BH (2015) Grand solar minima and maxima deduced from ^{10}Be and ^{14}C: magnetic dynamo configuration and polarity reversal. Astron Astrophys 577:A20

Ineson S, Maycock AC, Gray LJ, Scaife AA, Dunstone NJ, Harder JW, Knight JR, Lockwood M, Manners JC, Wood RA (2015) Regional climate impacts of a possible future grand solar minimum. Nature Commun 6:7535. https://doi.org/10.1038/ncomms8535

Jennings RL, Weiss NO (1991) Symmetry breaking in stellar dynamos. Mon Not R Astron Soc 252:249–260. https://doi.org/10.1093/mnras/252.2.249

Jiang J, Cameron RH, Schmitt D, Schüssler M (2011) The solar magnetic field since 1700. II. Physical reconstruction of total, polar and open flux. Astron Astrophys 528:A83. https://doi.org/10.1051/0004-6361/201016168. arXiv:1102.1270 [astro-ph.SR]

Jiang J, Zhang Z, Petrovay K (2023) Comparison of physics-based prediction models of solar cycle 25. J Atmos Sol-Terr Phys 243:106018. https://doi.org/10.1016/j.jastp.2023.106018

Jokipii JR, Levy EH (1977) Effects of particle drifts on the solar modulation of galactic cosmic rays. Astrophys J Lett 213:L85–L88. https://doi.org/10.1086/182415

de Jong AFM, Mook WG (1982) An anomalous Suess effect above Europe. Nature 298:641–644. https://doi.org/10.1038/298641a0

Joos F (1994) Imbalance in the budget. Nature 370:181–182. https://doi.org/10.1038/370181a0

Jull AJT, Cloudt S, Donahue DJ, Sisterson JM, Reedy RC, Masarik J (1998) ^{14}C depth profiles in Apollo 15 and 17 cores and lunar rock 68815. Geochim Cosmochim Acta 62:3025–3036. https://doi.org/10.1016/S0016-7037(98)00193-8

Jull AJT, Panyushkina IP, Lange TE, Kukarskih VV, Myglan VS, Clark KJ, Salzer MW, Burr GS, Leavitt SW (2014) Excursions in the ^{14}C record at AD 774–775 in tree rings from Russia and America. Geophys Res Lett 41:3004–3010. https://doi.org/10.1002/2014GL059874

Jungclaus JH, Bard E, Baroni M, Braconnot P, Cao J, Chini LP, Egorova T, Evans M, Fidel González-Rouco J, Goosse H, Hurtt GC, Joos F, Kaplan JO, Khodri M, Klein Goldewijk K, Krivova N, LeGrande AN, Lorenz SJ, Luterbacher J, Man W, Maycock AC, Meinshausen M, Moberg A, Muscheler R, Nehrbass-Ahles C, Otto-Bliesner BI, Phipps SJ, Pongratz J, Rozanov E, Schmidt GA, Schmidt H, Schmutz W, Schurer A, Shapiro AI, Sigl M, Smerdon JE, Solanki SK, Timmreck C, Toohey M, Usoskin IG, Wagner S, Wu CJ, Leng Yeo K, Zanchettin D, Zhang Q, Zorita E (2017) The PMIP4 contribution to CMIP6 - Part 3: the last millennium, scientific objective, and experimental design for the PMIP4 past1000 simulations. Geosci Model Dev 10(11):4005–4033. https://doi.org/10.5194/gmd-10-4005-2017

Kaiser Kudsk S, Knudsen M, Karoff C, Baittinger C, Misios S, Olsen J (2022) Solar variability between 650 CE and 1900 - Novel insights from a global compilation of new and existing high-resolution ^{14}C records. Quat Sci Rev 292:107617. https://doi.org/10.1016/j.quascirev.2022.107617

Käpylä MJ, Käpylä PJ, Olspert N, Brandenburg A, Warnecke J, Karak BB, Pelt J (2016) Multiple dynamo modes as a mechanism for long-term solar activity variations. Astron Astrophys 589:A56. https://doi.org/10.1051/0004-6361/201527002. arXiv:1507.05417 [astro-ph.SR]

Käpylä PJ, Mantere MJ, Brandenburg A (2012) Cyclic magnetic activity due to turbulent convection in spherical wedge geometry. Astrophys J Lett 755:L22. https://doi.org/10.1088/2041-8205/755/1/L22

Kigoshi K, Hasegawa H (1966) Secular variation of atmospheric radiocarbon concentration and its dependence on geomagnetism. J Geophys Res 71:1065–1071. https://doi.org/10.1029/JZ071i004p01065

Klecker B, Kunow H, Cane HV, Dalla S, Heber B, Kecskemety K, Klein KL, Kóta J, Kucharek H, Lario D, Lee MA, Popecki MA, Posner A, Rodriguez-Pacheco J, Sanderson T, Simnett GM, Roelof EC (2006) Energetic particle observations. Space Sci Rev 123:217–250. https://doi.org/10.1007/s11214-006-9018-9

Kleczek J (1952) Solar flare index calculations. Publ Centr Astron Inst Czechoslovakia 22:1

Knudsen MF, Riisager P, Donadini F, Snowball I, Muscheler R, Korhonen K, Pesonen LJ (2008) Variations in the geomagnetic dipole moment during the Holocene and the past 50 kyr. Earth Planet Sci Lett 272:319–329. https://doi.org/10.1016/j.epsl.2008.04.048

Koch D, Schmidt GA, Field CV (2006) Sulfur, sea salt, and radionuclide aerosols in GISS ModelE. J Geophys Res 111(D10):D06206. https://doi.org/10.1029/2004JD005550

Kocharov GE, Ostryakov VM, Peristykh AN, Vasil'ev VA (1995) Radiocarbon content variations and Maunder minimum of solar activity. Sol Phys 159:381–391. https://doi.org/10.1007/BF00686539

Kohl CP, Murrell MT, Russ III GP, Arnold JR (1978) Evidence for the constancy of the solar cosmic ray flux over the past ten million years: ^{53}Mn and ^{26}Al measurements. In: Lunar and Planetary Science IX. Geochim. Cosmochim. Acta Suppl., vol 10. Pergamon Press, New York, pp 2299–2310

Koldobskiy SA, Bindi V, Corti C, Kovaltsov G, Usoskin I (2019) Validation of the neutron monitor yield function using data from AMS-02 experiment 2011–2017. J Geophys Res (Space Phys) 124:2367–2379. https://doi.org/10.1029/2018JA026340

Koldobskiy SA, Raukunen O, Vainio R, Kovaltsov G, Usoskin I (2021) New reconstruction of event-integrated spectra (spectral fluences) for major solar energetic particle events. Astron Astrophys 647:A132. https://doi.org/10.1051/0004-6361/202040058

Koldobskiy SA, Kähkönen R, Hofer B, Krivova NA, Kovaltsov G, Usoskin I (2022a) Time lag between cosmic-ray and solar variability: sunspot numbers and open solar magnetic flux. Sol Phys 297(3):38. https://doi.org/10.1007/s11207-022-01970-1

Koldobskiy SA, Usoskin I, Kovaltsov G (2022b) Effective energy of cosmogenic isotope (^{10}Be, ^{14}C and ^{36}Cl) production by solar energetic particles and galactic cosmic rays. J Geophys Res Space Phys 127:e2021JA029919. https://doi.org/10.1029/2021JA029919

Koldobskiy S, Mekhaldi F, Kovaltsov G, Usoskin I (2023) Multiproxy reconstructions of integral energy spectra for extreme solar particle events of 7176 BCE, 660 BCE, 775 CE, and 994 CE. J Geophys Res (Space Phys) 128:e2022JA031186. https://doi.org/10.1029/2022JA031186

Kopp G, Shapiro A (2021) Irradiance variations of the sun and sun-like stars—overview of topical collection. Sol Phys 296(4):60. https://doi.org/10.1007/s11207-021-01802-8. arXiv:2102.06913 [astro-ph.SR]

Korte M, Constable CG (2005) The geomagnetic dipole moment over the last 7000 years—new results from a global model. Earth Planet Sci Lett 236:348–358. https://doi.org/10.1016/j.epsl.2004.12.031

Korte M, Constable CG (2006) Centennial to millennial geomagnetic secular variation. Geophys J Int 167:43–52. https://doi.org/10.1111/j.1365-246X.2006.03088.x

Korte M, Constable CG (2008) Spatial and temporal resolution of millennial scale geomagnetic field models. Adv Space Res 41:57–69. https://doi.org/10.1016/j.asr.2007.03.094

Korte M, Constable C, Donadini F, Holme R (2011) Reconstructing the Holocene geomagnetic field. Earth Planet Sci Lett 312:497–505. https://doi.org/10.1016/j.epsl.2011.10.031

Kovaltsov GA, Usoskin IG (2007) Regional cosmic ray induced ionization and geomagnetic field changes. Adv Geosci 13:31–35. https://doi.org/10.5194/adgeo-13-31-2007

Kovaltsov GA, Usoskin IG (2010) A new 3D numerical model of cosmogenic nuclide ^{10}Be production in the atmosphere. Earth Planet Sci Lett 291:182–188. https://doi.org/10.1016/j.epsl.2010.01.011

Kovaltsov GA, Usoskin IG, Mursula K (2004) An upper limit on sunspot activity during the Maunder minimum. Sol Phys 224:95–101. https://doi.org/10.1007/s11207-005-4281-6

Kovaltsov GA, Mishev A, Usoskin IG (2012) A new model of cosmogenic production of radiocarbon ^{14}C in the atmosphere. Earth Planet Sci Lett 337:114–120. https://doi.org/10.1016/j.epsl.2012.05.036. arXiv:1206.6974 [physics.ao-ph]

Kremliovsky MN (1994) Can we understand time scales of solar activity? Sol Phys 151:351–370. https://doi.org/10.1007/BF00679081

Kremliovsky MN (1995) Limits of predictability of solar activity. Solar Phys 159:371–380. https://doi.org/10.1007/BF00686538

Krivova N, Balmaceda L, Solanki S (2007) Reconstruction of solar total irradiance since 1700 from the surface magnetic flux. Astron Astrophys 467:335–346. https://doi.org/10.1051/0004-6361:20066725

Krivova N, Solanki S, Hofer B, Wu C, Usoskin I, Cameron R (2021) Modelling the evolution of the sun's open and total magnetic flux. Astron Astrophys. https://doi.org/10.1051/0004-6361/2021/40504

Křivský L (1984) Long-term fluctuations of solar activity during the last thousand years. Sol Phys 93:189–194. https://doi.org/10.1007/BF00156664

Křivský L, Pejml K (1988) Solar activity, aurorae and climate in Central Europe in the Last 1000 Years. Publ Astron Inst Czechoslovak Acad Sci 75:32

Kuitems M, Wallace BL, Lindsay C, Scifo A, Doeve P, Jenkins K, Lindauer S, Erdil P, Ledger PM, Forbes V, Vermeeren C, Friedrich R, Dee MW (2022) Evidence for European presence in the Americas in AD 1021. Nature 601(7893):388–391. https://doi.org/10.1038/s41586-021-03972-8

Kuklin GV (1976) Cyclical and secular variations of solar activity. In: Bumba V, Kleczek J (eds) Basic mechanisms of solar activity. IAU symposium, vol 71. D. Reidel, Dordrecht; Boston, pp 147–190. https://doi.org/10.1007/978-94-010-1481-6_16

Kurths J, Ruzmaikin AA (1990) On forecasting the sunspot numbers. Sol Phys 126:407–410. https://doi.org/10.1007/BF00153060

Lal D (1987) ^{10}Be in polar ice: data reflect changes in cosmic ray flux or polar meteorology. Geophys Res Lett 14:785–788. https://doi.org/10.1029/GL014i008p00785

Lal D, Peters B (1967) Cosmic ray produced radioactivity on the earth. In: Sittle K (ed) Kosmische Strahlung II / Cosmic Rays II Handbuch der Physik / Encyclopedia of Physics, vol 9. Springer, Berlin, pp 551–612. https://doi.org/10.1007/978-3-642-46079-1_7

Lal D, Suess HE (1968) The radioactivity of the atmosphere and hydrosphere. Annu Rev Nucl Sci 18:407–434. https://doi.org/10.1146/annurev.ns.18.120168.002203

Lal D, Jull AJT, Pollard D, Vacher L (2005) Evidence for large century time-scale changes in solar activity in the past 32 Kyr, based on in-situ cosmogenic ^{14}C in ice at Summit, Greenland. Earth Planet Sci Lett 234:335–349. https://doi.org/10.1016/j.epsl.2005.02.011

Lawrence JK, Cadavid AC, Ruzmaikin AA (1995) Turbulent and chaotic dynamics underlying solar magnetic variability. Astrophys J 455:366. https://doi.org/10.1086/176583

Lee EH, Ahn YS, Yang HJ, Chen KY (2004) The sunspot and auroral activity cycle derived from Korean historical records of the 11th 18th century. Sol Phys 224:373–386. https://doi.org/10.1007/s11207-005-5199-8

Letfus V (1999) Daily relative sunspot numbers 1749–1848: reconstruction of missing observations. Sol Phys 184:201–211. https://doi.org/10.1023/A:1005086320594

Letfus V (2000) Relative sunspot numbers in the first half of eighteenth century. Sol Phys 194:175–184. https://doi.org/10.1023/A:1005208223601

Leussu R, Usoskin IG, Arlt R, Mursula K (2013) Inconsistency of the Wolf sunspot number series around 1848. Astron Astrophys 559:A28. https://doi.org/10.1051/0004-6361/201322373. arXiv:1310.8443 [astro-ph.SR]

Licht A, Hulot G, Gallet Y, Thébault E (2013) Ensembles of low degree archeomagnetic field models for the past three millennia. Phys Earth Planet Inter 224:38–67. https://doi.org/10.1016/j.pepi.2013.08.007

Lingenfelter RE (1963) Production of carbon 14 by cosmic-ray neutrons. Rev Geophys Space Phys 1:35–55. https://doi.org/10.1029/RG001i001p00035

Lingenfelter RE, Hudson HS (1980) Solar particle fluxes and the ancient Sun. In: Pepin RO, Eddy JA, Merrill RB (eds) The ancient sun: fossil record in the earth, moon and meteorites. Pergamon Press, New York; Oxford, pp 69–79

Linker JA, Heinemann SG, Temmer M, Owens MJ, Caplan RM, Arge CN, Asvestari E, Delouille V, Downs C, Hofmeister SJ, Jebaraj IC, Madjarska MS, Pinto RF, Pomoell J, Samara E, Scolini C, Vršnak B (2021) Coronal hole detection and open magnetic flux. Astrophys J 918(1):21. https://doi.org/10.3847/1538-4357/ac090a. arXiv:2103.05837 [astro-ph.SR]

Liu Y, Zhang Z, Peng Z, Ling M, Shen C, Liu W, Sun X, Shen C, Liu K, Sun W (2014) Mysterious abrupt carbon-14 increase in coral contributed by a comet. Sci Rep 4:3728. https://doi.org/10.1038/srep03728

Lockwood M (2013) Reconstruction and prediction of variations in the open solar magnetic flux and interplanetary conditions. Living Rev Sol Phys 10:1–88. https://doi.org/10.12942/lrsp-2013-4

Lockwood M, Owens MJ (2014) Implications of the recent low solar minimum for the solar wind during the Maunder minimum. Astrophys J Lett 781:L7. https://doi.org/10.1088/2041-8205/781/1/L7

Lockwood M, Stamper R, Wild MN (1999) A doubling of the Sun's coronal magnetic field during the past 100 years. Nature 399:437–439. https://doi.org/10.1038/20867

Lockwood M, Owens MJ, Barnard L, Davis CJ, Steinhilber F (2011) The persistence of solar activity indicators and the descent of the Sun into Maunder Minimum conditions. Geophys Res Lett 38:L22105. https://doi.org/10.1029/2011GL049811

Lockwood M, Barnard L, Nevanlinna H, Owens MJ, Harrison RG, Rouillard AP, Davis CJ (2013) Reconstruction of geomagnetic activity and near-Earth interplanetary conditions over the past 167 yr - Part 1: A new geomagnetic data composite. Ann Geophys 31:1957–1977. https://doi.org/10.5194/angeo-31-1957-2013

Lockwood M, Owens MJ, Barnard L (2014) Centennial variations in sunspot number, open solar flux, and streamer belt width: 1. Correction of the sunspot number record since 1874. J Geophys Res Space Phys 119:5172–5182. https://doi.org/10.1002/2014JA019970

Lockwood M, Owens MJ, Barnard L (2014) Centennial variations in sunspot number, open solar flux, and streamer belt width: 2. Comparison with the geomagnetic data. J Geophys Res 119:5183–5192. https://doi.org/10.1002/2014JA019972

Lockwood M, Owens MJ, Barnard L, Scott CJ, Usoskin IG, Nevanlinna H (2016) Tests of sunspot number sequences: 2. Using geomagnetic and auroral data. Solar Phys 291:2811–2828. https://doi.org/10.1007/s11207-016-0913-2 arXiv:1605.01948 [astro-ph.SR]

Lockwood M, Owens MJ, Barnard L, Usoskin I (2016) An assessment of sunspot number data composites over 1845–2014. Astrophys J 824(1):54. https://doi.org/10.3847/0004-637X/824/1/54

Lockwood M, Owens MJ, Barnard L, Usoskin IG (2016) Tests of sunspot number sequences: 3. Effects of regression procedures on the calibration of historic sunspot data. Sol Phys 291:2829–2841. https://doi.org/10.1007/s11207-015-0829-2. arXiv:1510.07809 [astro-ph.SR]

Love JJ (2011) Secular trends in storm-level geomagnetic activity. Ann Geophys 29:251–262. https://doi.org/10.5194/angeo-29-251-2011

Lukianova R, Alekseev G, Mursula K (2009) Effects of station relocation in the aa index. J Geophys Res 114:A02105. https://doi.org/10.1029/2008JA013824

Maehara H, Shibayama T, Notsu S, Notsu Y, Nagao T, Kusaba S, Honda S, Nogami D, Shibata K (2012) Superflares on solar-type stars. Nature 485:478–481. https://doi.org/10.1038/nature11063

Maehara H, Shibayama T, Notsu S, Notsu Y, Honda S, Nogami D, Shibata K (2015) Statistical properties of superflares on solar-type stars based on 1-min cadence data. Earth Planets Space 67:59. https://doi.org/10.1186/s40623-015-0217-z. arXiv:1504.00074 [astro-ph.SR]

Martin-Puertas C, Matthes K, Brauer A, Muscheler R, Hansen F, Petrick C, Aldahan A, Possnert G, van Geel B (2012) Regional atmospheric circulation shifts induced by a grand solar minimum. Nature Geosci 5:397–401. https://doi.org/10.1038/ngeo1460

Masarik J, Beer J (1999) Simulation of particle fluxes and cosmogenic nuclide production in the Earth's atmosphere. J Geophys Res 104(D10):12,099-12,112. https://doi.org/10.1029/1998JD200091

Masarik J, Beer J (2009) An updated simulation of particle fluxes and cosmogenic nuclide production in the Earth's atmosphere. J Geophys Res 114(D13):D11103. https://doi.org/10.1029/2008JD010557

Matthes K, Funke B, Andersson ME, Barnard L, Beer J, Charbonneau P, Clilverd MA, Dudok de Wit T, Haberreiter M, Hendry A, Jackman CH, Kretzschmar M, Kruschke T, Kunze M, Langematz U, Marsh DR, Maycock AC, Misios S, Rodger CJ, Scaife AA, Seppälä A, Shangguan M, Sinnhuber M, Tourpali K, Usoskin I, van de Kamp M, Verronen PT, Versick S (2017) Solar forcing for CMIP6 (v3.2). Geosci Model Dev 10:2247–2302. https://doi.org/10.5194/gmd-10-2247-2017

Mayaud PN (1972) The aa indices: A 100-year series characterizing the magnetic activity. J Geophys Res 77:6870–6874. https://doi.org/10.1029/JA077i034p06870

McCracken K, Beer J (2007) Long-term changes in the cosmic ray intensity at Earth, 1428–2005. J Geophys Res 112(A11):A10101

McCracken KG (2004) Geomagnetic and atmospheric effects upon the cosmogenic ^{10}Be observed in polar ice. J Geophys Res 109(A18):A04101. https://doi.org/10.1029/2003JA010060

McCracken KG (2007) Heliomagnetic field near Earth, 1428–2005. J Geophys Res 112:A09106. https://doi.org/10.1029/2006JA012119

McCracken KG, Dreschhoff GAM, Zeller EJ, Smart DF, Shea MA (2001) Solar cosmic ray events for the period 1561–1994: 1. Identification in polar ice, 1561–1950. J Geophys Res 106:21,585-21,598. https://doi.org/10.1029/2000JA000237

McHargue LR, Damon PE (1991) The global beryllium 10 cycle. Rev Geophys 29:141–158. https://doi.org/10.1029/91RG00072

Mega MS, Allegrini P, Grigolini P, Latora V, Palatella L, Rapisarda A, Vinciguerra S (2003) Power-law time distribution of large earthquakes. Phys Rev Lett 90:188501. https://doi.org/10.1103/PhysRevLett.90.188501. arXiv:cond-mat/0212529

Mekhaldi F, Muscheler R, Adolphi F, Aldahan A, Beer J, McConnell J, Possnert G, Sigl M, Svensson A, Synal H, Welten K, Woodruff T (2015) Multiradionuclide evidence for the solar origin of the cosmic-ray events of AD 774/5 and 993/4. Nature Comm 6:8611. https://doi.org/10.1038/ncomms9611

Mekhaldi F, McConnell JR, Adolphi F, Arienzo MM, Chellman NJ, Maselli OJ, Moy AD, Plummer CT, Sigl M, Muscheler R (2017) No coincident nitrate enhancement events in polar ice cores following the largest known solar storms. J Geophys Res (Atm) 122(21):11,900-11,913. https://doi.org/10.1002/2017JD027325

Mekhaldi F, Adolphi F, Herbst K, Muscheler R (2021) The signal of solar storms embedded in cosmogenic radionuclides: detectability and uncertainties. J Geophys Res (Space Phys) 126:e2021JA029351. https://doi.org/10.1029/2021JA029351

Melott AL, Thomas BC (2012) Causes of an AD 774–775 ^{14}C increase. Nature 491:E1–E2. https://doi.org/10.1038/nature11695. arXiv:1212.0490 [astro-ph.EP]

Mendoza B (1997) Geomagnetic activity and wind velocity during the Maunder minimum. Ann Geophys 15:397–402. https://doi.org/10.1007/s00585-997-0397-3

Mewaldt RA, Cohen CMS, Mason GM, Haggerty DK, Desai MI (2007) Long-term fluences of solar energetic particles from H to Fe. Space Sci Rev 130:323–328. https://doi.org/10.1007/s11214-007-9200-8

Michel R, Neumann S (1998) Interpretation of cosmogenic nuclides in meteorites on the basis of accelerator experiments and physical model calculations. Proc Indian Acad Sci (Earth Planet Sci) 107:441–457

Michel R, Leya I, Borges L (1996) Production of cosmogenic nuclides in meteoroids: accelerator experiments and model calculations to decipher the cosmic ray record in extraterrestrial matter. Nucl Instrum Methods B 113:434–444. https://doi.org/10.1016/0168-583X(95)01345-8

Mikaloff Fletcher SE, Gruber N, Jacobson AR, Doney SC, Dutkiewicz S, Gerber M, Follows M, Joos F, Lindsay K, Menemenlis D, Mouchet A, Müller SA, Sarmiento JL (2006) Inverse estimates of anthropogenic CO_2 uptake, transport, and storage by the ocean. Global Biogeochem Cycles 20: GB2002. https://doi.org/10.1029/2005GB002530

Mininni PD, Gómez DO, Mindlin GB (2000) Stochastic relaxation oscillator model for the solar cycle. Phys Rev Lett 85:5476–5479. https://doi.org/10.1103/PhysRevLett.85.5476

Mininni PD, Gómez DO, Mindlin GB (2001) Simple model of a stochastically excited solar dynamo. Sol Phys 201:203–223. https://doi.org/10.1023/A:1017515709106

Mininni PD, Gómez DO, Mindlin GB (2002) Biorthogonal decomposition techniques unveil the nature of the irregularities observed in the solar cycle. Phys Rev Lett 89(6):061101. https://doi.org/10.1103/PhysRevLett.89.061101

Mironova IA, Aplin KL, Arnold F, Bazilevskaya GA, Harrison RG, Krivolutsky AA, Nicoll KA, Rozanov EV, Turunen E, Usoskin IG (2015) Energetic particle influence on the Earth's atmosphere. Space Sci Rev 194:1–96. https://doi.org/10.1007/s11214-015-0185-4

Mishev A, Koldobskiy S, Kovaltsov G, Gil A, Usoskin I (2020) Updated neutron-monitor yield function: bridging between in-situ and ground-based cosmic ray measurements. J Geophys Res (Space Phys) 125:e2019JA027433. https://doi.org/10.1029/2019JA027433

Miyahara H, Masuda K, Muraki Y, Furuzawa H, Menjo H, Nakamura T (2004) Cyclicity of solar activity during the Maunder minimum deduced from radiocarbon content. Sol Phys 224:317–322. https://doi.org/10.1007/s11207-005-6501-5

Miyahara H, Masuda K, Muraki Y, Kitagawa H, Nakamura T (2006) Variation of solar cyclicity during the Spoerer Minimum. J Geophys Res 111(A10):A03103. https://doi.org/10.1029/2005JA011016

Miyahara H, Sokoloff D, Usoskin IG (2006) The solar cycle at the Maunder minimum epoch. In: Ip WH, Duldig M (eds) Advances in Geosciences, Vol. 2: Solar Terrestrial (ST). World Scientific, Singapore; Hackensack, NJ, pp 1–20

Miyahara H, Kitazawa K, Nagaya K, Yokoyama Y, Matsuzaki H, Masuda K, Nakamura T, Muraki Y (2010) Is the Sun heading for another Maunder Minimum? Precursors of the grand solar minima. J Cosmol 8:1970–1982

Miyake F, Nagaya K, Masuda K, Nakamura T (2012) A signature of cosmic-ray increase in ad 774–775 from tree rings in Japan. Nature 486:240–242. https://doi.org/10.1038/nature11123

Miyake F, Masuda K, Nakamura T (2013) Another rapid event in the carbon-14 content of tree rings. Nature Commun 4:1748. https://doi.org/10.1038/ncomms2783

Miyake F, Suzuki A, Masuda K, Horiuchi K, Motoyama H, Matsuzaki H, Motizuki Y, Takahashi K, Nakai Y (2015) Cosmic ray event of A.D. 774–775 shown in quasi-annual ^{10}Be data from the Antarctic Dome Fuji ice core. Geophys Res Lett 42:84–89. https://doi.org/10.1002/2014GL062218

Miyake F, Usoskin I, Poluianov S (eds) (2020) Extreme solar particle storms: the hostile sun. IOP Publishing, Bristol. https://doi.org/10.1088/2514-3433/ab404a

Miyake F, Panyushkina IP, Jull AJT, Adolphi F, Brehm N, Helama S, Kanzawa K, Moriya T, Muscheler R, Nicolussi K, Oinonen M, Salzer M, Takeyama M, Tokanai F, Wacker L (2021) A single year cosmic ray event at 5410 BCE registered in ^{14}C of tree rings. Geophys Res Lett 48:e2021GL093419. https://doi.org/10.1029/2021GL093419

Moraal H, Stoker PH (2010) Long-term neutron monitor observations and the 2009 cosmic ray maximum. J Geophys Res 115:A12109. https://doi.org/10.1029/2010JA015413

Morfill GE, Scheingraber H, Voges W, Sonett CP (1991) Sunspot number variations—stochastic or chaotic. In: Sonett CP, Giampapa MS, Matthews MS (eds) The sun in time. University of Arizona Press, Tucson, pp 30–58

Moss D, Brandenburg A, Tavakol R, Tuominen I (1992) Stochastic effects in mean-field dynamos. Astron Astrophys 265:843–849

Moss D, Sokoloff D, Usoskin IG, Tutubalin V (2008) Solar grand minima and random fluctuations in dynamo parameters. Sol Phys 250:221–234. https://doi.org/10.1007/s11207-008-9202-z. arXiv:0806. 3331

Mossman JE (1989) A comprehensive search for sunspots without the aid of a telescope, 1981–1982. Quart J R Astron Soc 30:59–64

Muñoz-Jaramillo A, Vaquero J (2019) Visualization of the challenges and limitations of the long-term sunspot number record. Nature Astron 3:205–211. https://doi.org/10.1038/s41550-018-0638-2

Mundt MD, Maguire WB II, Chase RRP (1991) Chaos in the sunspot cycle: analysis and prediction. J Geophys Res 96:1705–1716. https://doi.org/10.1029/90JA02150

Mursula K, Martini D (2006) Centennial increase in geomagnetic activity: latitudinal differences and global estimates. J Geophys Res 111:A08209. https://doi.org/10.1029/2005JA011549

Mursula K, Usoskin IG, Kovaltsov GA (2001) Persistent 22-year cycle in sunspot activity: evidence for a relic solar magnetic field. Sol Phys 198:51–56. https://doi.org/10.1023/A:1005218414790

Mursula K, Usoskin IG, Kovaltsov GA (2003) Reconstructing the long-term cosmic ray intensity: linear relations do not work. Ann Geophys 21:863–867. https://doi.org/10.5194/angeo-21-863-2003

Muscheler R, Joos F, Beer J, Müller SA, Vonmoos M, Snowball I (2007) Solar activity during the last 1000 yr inferred from radionuclide records. Quat Sci Rev 26:82–97. https://doi.org/10.1016/j.quascirev. 2006.07.012

Nagaya K, Kitazawa K, Miyake F, Masuda K, Muraki Y, Nakamura T, Miyahara H, Matsuzaki H (2012) Variation of the Schwabe cycle length during the grand solar minimum in the 4th century BC deduced from radiocarbon content in tree rings. Sol Phys 280:223–236. https://doi.org/10.1007/s11207-012-0045-2

Nagovitsyn YA (1997) A nonlinear mathematical model for the solar cyclicity and prospects for reconstructing the solar activity in the past. Astron Lett 23:742–748

Namekata K, Maehara H, Honda S, Notsu Y, Okamoto S, Takahashi J, Takayama M, Ohshima T, Saito T, Katoh N, Tozuka M, Murata KL, Ogawa F, Niwano M, Adachi R, Oeda M, Shiraishi K, Isogai K, Seki D, Ishii TT, Ichimoto K, Nogami D, Shibata K (2021) Probable detection of an eruptive filament from a superflare on a solar-type star. Nature Astron 6:241–248. https://doi.org/10.1038/s41550-021-01532-8. arXiv:2112.04808 [astro-ph.SR]

Nandy D (2021) Progress in solar cycle predictions: sunspot cycles 24–25 in perspective. Sol Phys 296 (3):54. https://doi.org/10.1007/s11207-021-01797-2. arXiv:2009.01908 [astro-ph.SR]

Nandy D, Martens PH, Obridko V, Dash S, Georgieva K (2021) Solar evolution and extrema: current state of understanding of long-term solar variability and its planetary impacts. Prog Earth Planet Sci 8 (1):40. https://doi.org/10.1186/s40645-021-00430-x

Nataf HC (2022) Tidally synchronized solar dynamo: a rebuttal. Sol Phys 297(8):107. https://doi.org/10. 1007/s11207-022-02038-w. arXiv:2206.14809 [astro-ph.SR]

Nevalainen J, Usoskin IG, Mishev A (2013) Eccentric dipole approximation of the geomagnetic field: application to cosmic ray computations. Adv Space Res 52:22–29. https://doi.org/10.1016/j.asr.2013. 02.020

Nevanlinna H (1995) Auroral observations in Finland—visual sightings during the 18th and 19th centuries. J Geomag Geoelectr 47:953–960. https://doi.org/10.5636/jgg.47.953

Nevanlinna H (2004) Historical space climate data from Finland: compilation and analysis. Sol Phys 224:395–405. https://doi.org/10.1007/s11207-005-3749-8

Nevanlinna H (2004) Results of the Helsinki magnetic observatory 1844–1912. Ann Geophys 22:1691–1704. https://doi.org/10.5194/angeo-22-1691-2004

Newton HW (1928) The Sun's cycle of activity. Quart J R Meteorol Soc 54(227):161–174

Ney EP (1959) Cosmic radiation and the weather. Nature 183:451–452. https://doi.org/10.1038/183451a0

Nilsson A, Holme R, Korte M, Suttie N, Hill M (2014) Reconstructing Holocene geomagnetic field variation: new methods, models and implications. Geophys J Int 198:229–248. https://doi.org/10. 1093/gji/ggu120

Nishiizumi K, Arnold JR, Klein J, Middleton R (1984) Al-26 depth profile in Apollo 15 drill core. Earth Planet Sci Lett 70:164–168. https://doi.org/10.1016/0012-821X(84)90002-5

Nishiizumi K, Arnold JR, Kohl CP, Caffee MW, Masarik J, Reedy RC (2009) Solar cosmic ray records in lunar rock 64455. Geochim Cosmochim Acta 73:2163–2176. https://doi.org/10.1016/j.gca.2008.12.021

Nishizumi K, Caffee MW, Arnold JR (1997) ^{10}Be from the active Sun. In: Lunar and Planetary Science XXVIII. Lunar and Planetary Institute, Houston

Notsu Y, Maehara H, Honda S, Hawley S, Davenport J, Namekata K, Notsu S, Ikuta K, Nogami D, Shibata K (2019) Do Kepler superflare stars really include slowly rotating sun-like stars? – results using APO 3.5 m telescope spectroscopic observations and Gaia-DR2 data. Astrophys J 876(1):58. https://doi.org/10.3847/1538-4357/ab14e6

O'Brien K (1979) Secular variations in the production of cosmogenic isotopes in the Earth's atmosphere. J Geophys Res 84:423–431. https://doi.org/10.1029/JA084iA02p00423

O'Brien K, Burke GDP (1973) Calculated cosmic ray neutron monitor response to solar modulation of galactic cosmic rays. J Geophys Res 78:3013–3019. https://doi.org/10.1029/JA078i016p03013

Oeschger H, Siegenthaler U, Schotterer U, Gugelmann A (1974) A box diffusion model to study the carbon dioxide exchange in nature. Tellus 27:168–192

Ogurtsov MG (2004) new evidence for long-term persistence in the Sun's activity. Sol Phys 220:93–105. https://doi.org/10.1023/B:sola.0000023439.59453.e5

Ogurtsov MG, Nagovitsyn YA, Kocharov GE, Jungner H (2002) Long-period cycles of the Sun's activity recorded in direct solar data and proxies. Sol Phys 211:371–394. https://doi.org/10.1023/A:1022411209257

Oguti T, Egeland A (1995) Auroral occurrence in Norwegian archives. J Geomag Geoelectr 47:353–359. https://doi.org/10.5636/jgg.47.353

O'Hare P, Mekhaldi F, Adolphi F, Raisbeck G, Aldahan A, Anderberg E, Beer J, Christl M, Fahrni S, Synal HA, Park J, Possnert G, Southon J, Bard E, Aster Team, Muscheler R (2019) Multiradionuclide evidence for an extreme solar proton event around 2,610 B.P. (660 BC). Proc Nat Acad Sci 116 (13):5961–5966. https://doi.org/10.1073/pnas.1815725116

Okamoto S, Notsu Y, Maehara H, Namekata K, Honda S, Ikuta K, Nogami D, Shibata K (2021) Statistical properties of superflares on solar-type stars: results using all of the Kepler primary mission data. Astrophys J 906(2):72. https://doi.org/10.3847/1538-4357/abc8f5. arXiv:2011.02117 [astro-ph.SR]

Oliver R, Ballester JL (1996) Rescaled range analysis of the asymmetry of solar activity. Sol Phys 169:215–224. https://doi.org/10.1007/BF00153842

Oliver R, Ballester JL (1998) Is there memory in solar activity? Phys Rev E 58:5650–5654. https://doi.org/10.1103/PhysRevE.58.5650

Ossendrijver MAJ (2000) The dynamo effect of magnetic flux tubes. Astron Astrophys 359:1205–1210

Ossendrijver MAJ, Hoyng P, Schmitt D (1996) Stochastic excitation and memory of the solar dynamo. Astron Astrophys 313:938–948

Ossendrijver MAJH (2003) The solar dynamo. Astron Astrophys Rev 11:287–367. https://doi.org/10.1007/s00159-003-0019-3

Ostriakov VM, Usoskin IG (1990) On the dimension of solar attractor. Sol Phys 127:405–412. https://doi.org/10.1007/BF00152177

Ostryakov VM, Usoskin IG (1990) Correlation dimensions of structured signals. Sov Tech Phys Lett 16:658–659

Owens MJ, Usoskin IG, Lockwood M (2012) Heliospheric modulation of galactic cosmic rays during grand solar minima: past and future variations. Geophys Res Lett 39:L19102. https://doi.org/10.1029/2012GL053151

Owens MJ, Cliver E, McCracken KG, Beer J, Barnard L, Lockwood M, Rouillard A, Passos D, Riley P, Usoskin I, Wang YM (2016) Near-Earth heliospheric magnetic field intensity since 1750: 2. Cosmogenic radionuclide reconstructions. J Geophys Res 121:6064–6074. https://doi.org/10.1002/2016JA022550

Owens MJ, Lockwood M, Riley P, Linker J (2017) Sunward Strahl: a method to unambiguously determine open solar flux from in situ spacecraft measurements using suprathermal electron data. J Geophys Res (Space Phys) 122:10980–10989. https://doi.org/10.1002/2017JA024631

Özgüç A, Ataç T, Rybák J (2003) Temporal variability of the flare index (1966–2001). Sol Phys 214:375–396. https://doi.org/10.1023/A:1024225802080

Paleari C, Mekhaldi F, Adolphi F, Christl M, Vockenhuber C, Gautschi P, Beer J, Brehm N, Erhardt T, Synal H, Wacker LFW, Muscheler R (2022) Cosmogenic radionuclides reveal an extreme solar particle storm near a solar minimum 9125 years bp. Nature Commun 13:214. https://doi.org/10.1038/s41467-021-27891-4

Panchev S, Tsekov M (2007) Empirical evidences of persistence and dynamical chaos in solar terrestrial phenomena. J Atmos Sol-Terr Phys 69:2391–2404. https://doi.org/10.1016/j.jastp.2007.07.011

Panovska S, Korte M, Constable CG (2019) One hundred thousand years of geomagnetic field evolution. Rev Geophys 57(4):1289–1337. https://doi.org/10.1029/2019RG000656

Park J, Southon J, Fahrni S, Creasman PP, Mewaldt R (2017) Relationship between solar activity and 14C peaks in AD 775, AD 994, and 660 BC. Radiocarbon 59:1147–1156

Parker EN (1955) Hydromagnetic dynamo models. Astrophys J 122:293–314. https://doi.org/10.1086/146087

Parker EN (1965) The passage of energetic charged particles through interplanetary space. Planet Space Sci 13:9–49. https://doi.org/10.1016/0032-0633(65)90131-5

Passos D, Nandy D, Hazra S, Lopes I (2014) A solar dynamo model driven by mean-field alpha and Babcock-Leighton sources: fluctuations, grand-minima-maxima, and hemispheric asymmetry in sunspot cycles. Astron Astrophys 563:A18. https://doi.org/10.1051/0004-6361/201322635. arXiv:1309.2186 [astro-ph.SR]

Pavlov AK, Blinov AV, Konstantinov AN, Ostryakov VM, Vasilyev GI, Vdovina MA, Volkov PA (2013) AD 775 pulse of cosmogenic radionuclides production as imprint of a Galactic gamma-ray burst. Mon Notes R Astron Soc 435:2878–2884. https://doi.org/10.1093/mnras/stt1468

Pavón-Carrasco FJ, Osete ML, Torta JM, De Santis A (2014) A geomagnetic field model for the Holocene based on archaeomagnetic and lava flow data. Earth Planet Sci Lett 388:98–109. https://doi.org/10.1016/j.epsl.2013.11.046

Pavón-Carrasco FJ, Gómez-Paccard M, Campuzano S, González-Rouco J, Osete ML (2018) Multi-centennial fluctuations of radionuclide production rates are modulated by the Earth's magnetic field. Sci Rep 8:9820. https://doi.org/10.1038/s41598-018-28115-4

Pedro JB, Heikkilä UE, Smith AM, Klekociuk A, van Ommen TD, Curran MAJ (2011) Beryllium-10 transport to Antarctica: results from seasonally resolved observations and modeling. J Geophys Res 116:D23120. https://doi.org/10.1029/2011JD016530

Peristykh AN, Damon PE (1998) Modulation of atmospheric ^{14}C concentration by the solar wind and irradiance components of the Hale and Schwabe solar cycles. Sol Phys 177:343. https://doi.org/10.1023/A:1004982321191

Peristykh AN, Damon PE (2003) Persistence of the Gleissberg 88-year solar cycle over the last $\sim$ 12,000 years: Evidence from cosmogenic isotopes. J Geophys Res 108:1003. https://doi.org/10.1029/2002JA009390

Pesnell WD (2012) Solar cycle predictions (Invited Review). Sol Phys 281:507–532. https://doi.org/10.1007/s11207-012-9997-5

Pesnell WD (2016) Predictions of solar cycle 24: How are we doing? Space Weather 14(1):10–21. https://doi.org/10.1002/2015SW001304

Pesnell WD, Schatten KH (2018) An early prediction of the amplitude of solar cycle 25. Sol Phys 293(7):112. https://doi.org/10.1007/s11207-018-1330-5

Petrovay K (2020) Solar cycle prediction. Living Rev Sol Phys 17:2. https://doi.org/10.1007/s41116-020-0022-z. arXiv:1907.02107 [astro-ph.SR]

Pipin VV, Sokoloff DD, Usoskin IG (2012) Variations of the solar cycle profile in a solar dynamo with fluctuating dynamo governing parameters. Astron Astrophys 542:A26. https://doi.org/10.1051/0004-6361/201118733. arXiv:1112.6218 [astro-ph.SR]

Poluianov S, Usoskin IG (2014) Critical analysis of a hypothesis of the planetary tidal influence on solar activity. Sol Phys 289:2333–2342. https://doi.org/10.1007/s11207-014-0475-0. arXiv:1401.3547 [astro-ph.EP]

Poluianov S, Kovaltsov GA, Usoskin IG (2018) Solar energetic particles and galactic cosmic rays over millions of years as inferred from data on cosmogenic ^{26}Al in lunar samples. Astron Astrophys 618:A96. https://doi.org/10.1051/0004-6361/201833561. arXiv:1807.10153 [astro-ph.SR]

Poluianov SV, Kovaltsov GA, Mishev AL, Usoskin IG (2016) Production of cosmogenic isotopes ^{7}Be, ^{10}Be, ^{14}C, ^{22}Na, and ^{36}Cl in the atmosphere: Altitudinal profiles of yield functions. J Geophys Res (Atm) 121:8125–8136. https://doi.org/10.1002/2016JD025034. arXiv:1606.05899 [astro-ph.EP]

Polygiannakis J, Preka-Papadema P, Moussas X (2003) On signal-noise decomposition of time-series using the continuous wavelet transform: application to sunspot index. Mon Not R Astron Soc 343:725–734. https://doi.org/10.1046/j.1365-8711.2003.06705.x. arXiv:physics/0301030

Potgieter M (2013) Solar modulation of cosmic rays. Living Rev Sol Phys 10:3. https://doi.org/10.12942/lrsp-2013-3. arXiv:1306.4421 [physics.space-ph]

Price CP, Prichard D, Hogenson EA (1992) Do the sunspot numbers form a 'chaotic' set? J Geophys Res 97:19,113-19,120. https://doi.org/10.1029/92JA01459

Pulkkinen T (2007) Space weather: terrestrial perspective. Living Rev Sol Phys 4:1. https://doi.org/10.12942/lrsp-2007-1

Raisbeck GM, Yiou F, Fruneau M, Loiseaux JM, Lieuvin M, Ravel JC (1981) Cosmogenic ^{10}Be/^{7}Be as a probe of atmospheric transport processes. Geophys Res Lett 8:1015–1018. https://doi.org/10.1029/GL008i009p01015

Raisbeck GM, Yiou F, Jouzel J, Petit JR (1990) ^{10}Be and δ^2H in Polar Ice Cores as a Probe of the Solar Variability's Influence on Climate. Philos Trans R Soc London, Ser A 330:463–469. https://doi.org/10.1098/rsta.1990.0027

Rakowski AZ, Krapiec M, Huels M, Pawlyta J, Dreves A, Meadows J (2015) Increase of radiocarbon concentration in tree rings from Kujawy (SE Poland) around AD 774–775. Nucl Instrum Methods Phys Res B 361:564–568. https://doi.org/10.1016/j.nimb.2015.03.035

Rancitelli LA, Fruchter JS, Felix WD, Perkins RW, Wogman NA (1975) Cosmogenic isotope production in Apollo deep-core samples. Lunar Planet Sci Conf Proc 6:1891–1899

Rao MN, Garrison DH, Bogard DD, Reedy RC (1994) Determination of the flux and energy distribution of energetic solar protons in the past 2 Myr using lunar rock 68815. Geochim Cosmochim Acta 58:4231–4245. https://doi.org/10.1016/0016-7037(94)90275-5

Raukunen O, Vainio R, Tylka AJ, Dietrich WF, Jiggens P, Heynderickx D, Dierckxsens M, Crosby N, Ganse U, Siipola R (2018) Two solar proton fluence models based on ground level enhancement observations. J Space Weather Space Clim 8(27):A04. https://doi.org/10.1051/swsc/2017031

Raukunen O, Usoskin I, Koldobskiy S, Kovaltsov G, Vainio R (2022) Annual integral solar proton fluences for 1984–2019. Astron Astrophys 665:A65. https://doi.org/10.1051/0004-6361/202243736

Reames DV (2021) Solar energetic particles. Lecture Notes in Physics, vol 978. Springer, Cham. https://doi.org/10.1007/978-3-030-66402-2

Reames DV, Ng CK (2010) Streaming-limited intensities of solar energetic particles on the intensity plateau. Astrophys J 723:1286–1293. https://doi.org/10.1088/0004-637X/723/2/1286

Reedy RC (2012) Update on Solar-Proton Fluxes During the Last Five Solar Activity Cycles. In: 43rd Lunar and Planetary Science Conference. vol 43. Lunar and Planetary Institute, Houston. http://www.lpi.usra.edu/meetings/lpsc2012/pdf/1285.pdf

Reeves GD, Cayton TE, Gary SP, Belian RD (1992) The great solar energetic particle events of 1989 observed from geosynchronous orbit. J Geophys Res 97:6219–6226. https://doi.org/10.1029/91JA03102

Reimer P, Austin W, Bard E, Bayliss A, Blackwell P, Ramsey C, Butzin M, Cheng H, Edwards R, Friedrich M, Grootes P, Guilderson T, Hajdas I, Heaton T, Hogg A, Hughen K, Kromer B, Manning S, Muscheler R, Palmer J, Pearson C, van der Plicht J, Reimer R, Richards D, Scott E, Southon J, Turney C, Wacker L, Adolphi F, Buentgen U, Capano M, Fahrni S, Fogtmann-Schulz A, Friedrich R, Koehler P, Kudsk S, Miyake F, Olsen J, Reinig F, Sakamoto M, Sookdeo A, Talamo S (2020) The IntCal20 northern hemisphere radiocarbon age calibration curve (0–55 cal KBP). Radiocarbon 62 (4):725–757. https://doi.org/10.1017/RDC.2020.41

Reimer PJ, Baillie MGL, Bard E, Bayliss A, Beck JW, Blackwell PG, Ramsey CB, Buck CE, Burr GS, Edwards RL, Friedrich M, Grootes PM, Guilderson TP, Hajdas I, Heaton TJ, Hogg AG, Hughen KA, Kaiser KF, Kromer B, McCormac FG, Manning SW, Reimer RW, Richards DA, Southon JR, Talamo S, Turney CSM, van der Plicht J, Weyhenmeyer CE (2009) IntCal09 and Marine09 radiocarbon age calibration curves, 0–50,000 years cal BP. Radiocarbon 51(4):1111–1150. https://doi.org/10.1017/S0033822200034202

Reimer PJ, Bard E, Bayliss A, Beck JW, Blackwell PG, Ramsey CB, Buck CE, Cheng H, Edwards RL, Friedrich M, Grootes PM, Guilderson TP, Haflidason H, Hajdas I, Hatte C, Heaton TJ, Hoffmann DL, Hogg AG, Hughen KA, Kaiser KF, Kromer B, Manning SW, Niu M, Reimer RW, Richards DA, Scott EM, Southon JR, Staff RA, Turney CSM, van der Plicht J (2013) IntCal13 and Marine13 radiocarbon age calibration curves 0–50000 years cal BP. Radiocarbon 55(4):1869–1887. https://doi.org/10.2458/azu_js_rc.55.16947

Reinhold T, Shapiro AI, Solanki SK, Montet B, Krivova NA, Cameron RH, Amazo-Gómez EM (2020) The Sun is less active than other solar-like stars. Science 368(6490):518–521. https://doi.org/10.1126/science.aay3821. arXiv:2005.01401 [astro-ph.SR]

Reinhold T, Shapiro AI, Witzke V, Nèmec NE, Işık E, Solanki SK (2021) Where have all the solar-like stars gone? rotation period detectability at various inclinations and metallicities. Astrophys J Lett 908 (2):L21. https://doi.org/10.3847/2041-8213/abde46. arXiv:2101.11426 [astro-ph.SR]

Ribes JC, Nesme-Ribes E (1993) The solar sunspot cycle in the Maunder minimum AD1645 to AD1715. Astron Astrophys 276:549–563

Rigozo NR, Echer E, Vieira LEA, Nordemann DJR (2001) Reconstruction of wolf sunspot numbers on the basis of spectral characteristics and estimates of associated radio flux and solar wind parameters for the last millennium. Sol Phys 203:179–191. https://doi.org/10.1023/A:1012745612022

Roth R, Joos F (2013) A reconstruction of radiocarbon production and total solar irradiance from the Holocene ^{14}C and CO_2 records: implications of data and model uncertainties. Clim Past 9:1879–1909. https://doi.org/10.5194/cp-9-1879-2013

Rozelot JP (1994) On the stability of the 11-year solar cycle period (and a few others). Sol Phys 149:149–154. https://doi.org/10.1007/BF00645186

Rozelot JP (1995) On the chaotic behaviour of the solar activity. Astron Astrophys 297:L45–L48

Ruth U, Barnola JM, Beer J, Bigler M, Blunier T, Castellano E, Fischer H, Fundel F, Huybrechts P, Kaufmann P, Kipfstuhl S, Lambrecht A, Morganti A, Oerter H, Parrenin F, Rybak O, Severi M, Udisti R, Wilhelms F, Wolff EW (2007) 'EDML1': a chronology for the EPICA deep ice core from Dronning Maud Land, Antarctica, over the last 150 000 years. Clim Past 3:475–484. https://doi.org/10.5194/cp-3-475-2007

Ruzmaikin A, Feynman J, Robinson P (1994) Long-term persistence of solar activity. Sol Phys 149:395–403. https://doi.org/10.1007/BF00690625

Ruzmaikin AA (1981) The solar cycle as a strange attractor. Comments Astrophys 9:85–93

Rybanský M, Rušin V, Minarovjech M, Klocok L, Cliver EW (2005) Reexamination of the coronal index of solar activity. J Geophys Res 110(A9):8106. https://doi.org/10.1029/2005JA011146

Sabine CL, Feely RA, Gruber N, Key RM, Lee K, Bullister JL, Wanninkhof R, Wong CS, Wallace DWR, Tilbrook B, Millero FJ, Peng TH, Kozyr A, Ono T, Rios AF (2004) The oceanic sink for anthropogenic CO_2. Science 305:367–371. https://doi.org/10.1126/science.1097403

Salakhutdinova II (1999) Identifying the quasi-regular and stochastic components of solar cyclicity and their properties. Sol Phys 188:377–396. https://doi.org/10.1023/A:1005265229175

Sarychev AP, Roshchina EM (2009) Comparison of three solar activity indices based on sunspot observations. Solar Syst Res 43:151–157. https://doi.org/10.1134/S0038094609020087

Schaefer B (1997) Improvements for the AAVSO sunspot number. J Am Assoc Variale Star Observ 26 (1):47–49

Schlamminger L (1990) Aurora borealis during the Maunder minimum. Mon Not R Astron Soc 247:67–69

Schmalz S, Stix M (1991) An αΩ dynamo with order and chaos. Astron Astrophys 245:654–661

Schmidt GA, Jungclaus JH, Ammann CM, Bard E, Braconnot P, Crowley TJ, Delaygue G, Joos F, Krivova NA, Muscheler R, Otto-Bliesner BL, Pongratz J, Shindell DT, Solanki SK, Steinhilber F, Vieira LEA (2012) Climate forcing reconstructions for use in PMIP simulations of the Last Millennium (v1.1), Geosci Model Dev 5:185–191. https://doi.org/10.5194/gmd-5-185-2012. http://www.geosci-model-dev.net/5/185/2012/

Schmieder B (2018) Extreme solar storms based on solar magnetic field. J Atmos Solar-Terr Phys 180:46–51. https://doi.org/10.1016/j.jastp.2017.07.018. arXiv:1708.01790 [astro-ph.SR]

Schmitt D, Schüssler M, Ferriz-Mas A (1996) Intermittent solar activity by an on-off dynamo. Astron Astrophys 311:L1–L4

Schmutz W (2021) Changes in the Total Solar Irradiance and climatic effects. J Space Weather Space Clim 11:40. https://doi.org/10.1051/swsc/2021016

Schove DJ (1955) The sunspot cycle, 649 B.C. to A.D. 2000. J Geophys Res 60:127–146. https://doi.org/10.1029/JZ060i002p00127

Schove DJ (1979) Sunspot turning-points and aurorae since A.D. 1510. Sol Phys 63:423–432. https://doi.org/10.1007/BF00174546

Schove DJ (1983) Sunspot, auroral, radiocarbon and climatic fluctuations since 7000 BC. Ann Geophys 1:391–396

Schrijver CJ, Beer J, Baltensperger U, Cliver EW, Güdel M, Hudson HS, McCracken KG, Osten RA, Peter T, Soderblom DR, Usoskin IG, Wolff EW (2012) Estimating the frequency of extremely energetic

solar events, based on solar, stellar, lunar, and terrestrial records. J Geophys Res 117:A08103. https://doi.org/10.1029/2012JA017706

Schröder W (1992) On the existence of the 11-year cycle in solar and auroral activity before and after the so-called Maunder minimum. J Geomag Geoelectr 44:119–128. https://doi.org/10.5636/jgg.44.119

Schüssler M, Caligari P, Ferriz-Mas A, Moreno-Insertis F (1994) Instability and eruption of magnetic flux tubes in the solar convection zone. Astron Astrophys 281:L69–L72

Schüssler M, Schmitt D, Ferriz-Mas A (1997) Long-term variation of solar activity by a dynamo based on magnetic flux tubes. In: Schmieder B, del Toro Iniesta JC, Vázquez M (eds) 1st advances in solar physics euroconference: advances in the physics of sunspots. ASP conference series, vol 118. Astronomical Society of the Pacific, San Francisco, pp 39–44

Schwabe H (1844) Sonnenbeobachtungen im Jahre (1843). Von Herrn Hofrath Schwabe in Dessau. Astron Nachr 21(15):233. https://doi.org/10.1002/asna.18440211505

Scuderi LA (1990) Oriental sunspot observations and volcanism. Quart J R Astron Soc 31:109–120

Sello S (2000) Wavelet entropy as a measure of solar cycle complexity. Astron Astrophys 363:311–315 arXiv:astro-ph/0005334

Senthamizh Pavai V, Arlt R, Dasi-Espuig M, Krivova NA, Solanki SK (2015) Sunspot areas and tilt angles for solar cycles 7–10. Astron Astrophys 584:A73. https://doi.org/10.1051/0004-6361/201527080. arXiv:1508.07849 [astro-ph.SR]

Serre T, Nesme-Ribes E (2000) Nonlinear analysis of solar cycles. Astron Astrophys 360:319–330

Shapley AH (1949) Reduction of sunspot-number observations. Publ Astron Soc Pac 61(358):13. https://doi.org/10.1086/126109

Shea MA, Smart DF (1990) A summary of major solar proton events. Sol Phys 127:297–320. https://doi.org/10.1007/BF00152170

Shea MA, Smart DF (2002) Solar proton event patterns: the rising portion of five solar cycles. Adv Space Res 29:325–330. https://doi.org/10.1016/S0273-1177(01)00592-0

Shibata K, Isobe H, Hillier A, Choudhuri AR, Maehara H, Ishii TT, Shibayama T, Notsu S, Notsu Y, Nagao T, Honda S, Nogami D (2013) Can Superflares Occur on Our Sun? Publ Astron Soc Japan 65. https://doi.org/10.1093/pasj/65.3.49. arXiv:1212.1361 [astro-ph.SR]

Shindell D, Rind D, Balachandran N, Lean JL, Lonergan P (1999) Solar cycle variability, ozone, and climate. Science 284:305–308. https://doi.org/10.1126/science.284.5412.305

Siegenthaler U, Heimann M, Oeschger H (1980) ^{14}C variations caused by changes in the global carbon cycle. Radiocarbon 22:177–191

Sigl M, Winstrup M, McConnell JR, Welten KC, Plunkett G, Ludlow F, Büntgen U, Caffee M, Chellman N, Dahl-Jensen D, Fischer H, Kipfstuhl S, Kostick C, Maselli OJ, Mekhaldi F, Mulvaney R, Muscheler R, Pasteris DR, Pilcher JR, Salzer M, Schüpbach S, Steffensen JP, Vinther BM, Woodruff TE (2015) Timing and climate forcing of volcanic eruptions for the past 2,500 years. Nature 523:543–549. https://doi.org/10.1038/nature14565

Silverman SM (1992) Secular variation of the aurora for the past 500 years. Rev Geophys 30:333–351. https://doi.org/10.1029/92RG01571

Silverman SM (2006) Comparison of the aurora of September 1/2, 1859 with other great auroras. Adv Space Res 38:136–144. https://doi.org/10.1016/j.asr.2005.03.157

Siscoe GL (1980) Evidence in the auroral record for secular solar variability. Rev Geophys Space Phys 18:647–658. https://doi.org/10.1029/RG018i003p00647

Siscoe GL, Verosub KL (1983) High medieval auroral incidence over China and Japan: implications for the medieval site of the geomagnetic pole. Geophys Res Lett 10:345–348. https://doi.org/10.1029/GL010i004p00345

Snow M, McClintock WE, Woods TN, White OR, Harder JW, Rottman G (2005) The Mg II Index from SORCE. Sol Phys 230:325–344. https://doi.org/10.1007/s11207-005-6879-0

Snowball I, Muscheler R (2007) Palaeomagnetic intensity data: an Achilles heel of solar activity reconstructions. Holocene 17:851–859. https://doi.org/10.1177/0959683607080531

Sokoloff D (2004) The Maunder minimum and the solar dynamo. Sol Phys 224:145–152. https://doi.org/10.1007/s11207-005-4176-6

Sokoloff D, Nesme-Ribes E (1994) The Maunder minimum: a mixed-parity dynamo mode? Astron Astrophys 288:293–298

Solanki SK, Krivova NA (2004) Solar irradiance variations: from current measurements to long-term estimates. Sol Phys 224:197–208. https://doi.org/10.1007/s11207-005-6499-8

Solanki SK, Schüssler M, Fligge M (2000) Evolution of the Sun's large-scale magnetic field since the Maunder minimum. Nature 408:445–447. https://doi.org/10.1038/35044027

Solanki SK, Scüssler M, Fligge M (2002) Secular variation of the Sun's magnetic flux. Astron Astrophys 383:706–712. https://doi.org/10.1051/0004-6361:20011790

Solanki SK, Usoskin IG, Kromer B, Schüssler M, Beer J (2004) Unusual activity of the Sun during recent decades compared to the previous 11,000 years. Nature 431:1084–1087. https://doi.org/10.1038/nature02995

Sonett CP (1983) The great solar anomaly ca. 1780–1800: an error in compiling the record? J Geophys Res 88:3225–3228. https://doi.org/10.1029/JA088iA04p03225

Sonett CP, Finney SA (1990) The spectrum of radiocarbon. Philos Trans R Soc London, Ser A 330:413–425. https://doi.org/10.1098/rsta.1990.0022

Soon WWH, Yaskell SH (2003) The Maunder minimum and the variable sun-earth connection. World Scientific, Singapore, River Edge, NJ

Sornette D, Ouillon G (2012) Dragon-kings: mechanisms, statistical methods and empirical evidence. Europ Phys J Spec Top 205. https://doi.org/10.1140/epjst/e2012-01559-5. arXiv:1205.1002 [nlin.AO]

Stefani F, Giesecke A, Weier T (2019) A model of a tidally synchronized solar dynamo. Sol Phys 294 (5):60. https://doi.org/10.1007/s11207-019-1447-1. arXiv:1803.08692 [astro-ph.SR]

Steig EJ, Polissar PJ, Stuiver M, Grootes PM, Finkel RC (1996) Large amplitude solar modulation cycles of ^{10}Be in Antarctica: Implications for atmospheric mixing processes and interpretation of the ice core record. Geophys Res Lett 23:523–526. https://doi.org/10.1029/96GL00255

Steinhilber F, Beer J, Fröhlich C (2009) Total solar irradiance during the Holocene. Geophys Res Lett 36: L19704. https://doi.org/10.1029/2009GL040142

Steinhilber F, Abreu JA, Beer J, McCracken KG (2010) Interplanetary magnetic field during the past 9300 years inferred from cosmogenic radionuclides. J Geophys Res 115:A01104. https://doi.org/10.1029/2009JA014193

Steinhilber F, Abreu JA, Beer J, Brunner I, Christl M, Fischer H, Heikkilä U, Kubik PW, Mann M, McCracken KG, Miller H, Miyahara H, Oerter H, Wilhelms F (2012) 9400 years of cosmic radiation and solar activity from ice cores and tree rings. Proc Natl Acad Sci USA 109(16):5967–5971. https://doi.org/10.1073/pnas.1118965109

Stephenson FR, Willis DM, Hallinan TJ (2004) Aurorae: the earliest datable observation of the aurora borealis. Astron Geophys 45:6.15-6.17. https://doi.org/10.1046/j.1468-4004.2003.45615.x

Stuiver M (1961) Variations in radiocarbon concentration and sunspot activity. J Geophys Res 66:273–276. https://doi.org/10.1029/JZ066i001p00273

Stuiver M, Braziunas TF (1989) Atmospheric ^{14}C and century-scale solar oscillations. Nature 338:405–408. https://doi.org/10.1038/338405a0

Stuiver M, Braziunas TF (1993) Sun, ocean, climate and atmospheric $^{14}CO_2$: an evaluation of casual and spectral relationships. Holocene 3(4):289–305. https://doi.org/10.1177/095968369300300401

Stuiver M, Pollach H (1977) Discussion: reporting of ^{14}C data. Radiocarbon 19:355–363

Stuiver M, Quay PD (1980) Changes in atmospheric carbon-14 attributed to a variable sun. Science 207:11–19. https://doi.org/10.1126/science.207.4426.11

Stuiver M, Braziunas TF, Becker B, Kromer B (1991) Climatic, solar, oceanic, and geomagnetic influences on late-glacial and Holocene atmospheric $^{14}C/^{12}$ Change. Quat Res 35:1–24. https://doi.org/10.1016/0033-5894(91)90091-I

Suess HE (1955) Radiocarbon concentration in modern wood. Science 122:415–417. https://doi.org/10.1126/science.122.3166.415-a

Suess HE (1980) The radiocarbon record in tree rings of the last 8000 years. Radiocarbon 22:200–209

Sukhodolov T, Usoskin I, Rozanov E, Asvestari E, Ball W, Curran M, Fischer H, Kovaltsov G, Miyake F, Peter T, Plummer C, Schmutz W, Severi M, Traversi R (2017) Atmospheric impacts of the strongest known solar particle storm of 775 AD. Sci Rep 7:45257. https://doi.org/10.1038/srep45257

Svalgaard L (2012) How well do we know the sunspot number? Proc IAU 286:27–33. https://doi.org/10.1017/S1743921312004590

Svalgaard L, Cliver EW (2005) The IDV index: its derivation and use in inferring long-term variations of the interplanetary magnetic field strength. J Geophys Res 110(A9):A12103. https://doi.org/10.1029/2005JA011203

Svalgaard L, Schatten KH (2016) Reconstruction of the sunspot group number: the Backbone method. Sol Phys 291:2653–2684. https://doi.org/10.1007/s11207-015-0815-8. arXiv:1506.00755 [astro-ph.SR]

Svalgaard L, Cliver EW, Le Sager P (2004) IHV: a new long-term geomagnetic index. Adv Space Res 34:436–439. https://doi.org/10.1016/j.asr.2003.01.029

Svensmark H (1998) Influence of Cosmic Rays on Earth's Climate. Phys Rev Lett 81:5027–5030. https://doi.org/10.1103/PhysRevLett.81.5027

Sweeney C, Gloor E, Jacobson AR, Key RM, McKinley G, Sarmiento JL, Wanninkhof R (2007) Constraining global air-sea gas exchange for CO_2 with recent bomb ^{14}C measurements. Global Biogeochem Cycles 21:GB2015. https://doi.org/10.1029/2006GB002784

Taleb N (2007) The Black Swan: the impact of the highly improbable. Random House, New York

Tans PP, de Jong AFM, Mook WG (1979) Natural atmospheric ^{14}C variation and the Suess effect. Nature 280:826–828. https://doi.org/10.1038/280826a0

Tapping KF (1987) Recent solar radio astronomy at centimeter wavelengths: the temporal variability of the 10.7-cm flux. J Geophys Res 92:829–838. https://doi.org/10.1029/JD092iD01p00829

Tapping KF, Charrois DP (1994) Limits to the accuracy of the 10.7 cm flux. Sol Phys 150:305–315. https://doi.org/10.1007/BF00712892

Taricco C, Bhandari N, Cane D, Colombetti P, Verma N (2006) Galactic cosmic ray flux decline and periodicities in the interplanetary space during the last 3 centuries revealed by ^{44}Ti in meteorites. J Geophys Res 111:A08102. https://doi.org/10.1029/2005JA011459

Tassoul JL, Tassoul M (2004) A concise history of solar and stellar physics. Princeton University Press, Princeton

Temmer M, Veronig A, Hanslmeier A (2002) Hemispheric sunspot numbers R_n and R_s: catalogue and N-S asymmetry analysis. Astron Astrophys 390:707–715. https://doi.org/10.1051/0004-6361:20020758. arXiv:astro-ph/0208436

Terrasi F, Marzaioli F, Buompane R, Passariello I, Porzio G, Capano M, Helama S, Oinonen M, Nöjd P, Uusitalo J, Jull A, Panyushkina I, Baisan CMM, Varga T, Kovaltsov G, Poluianov S, Usoskin I (2020) Can the ^{14}c production in 1055 CE be affected by by SN1054? Radiocarbon 62(5):1403–1418. https://doi.org/10.1017/RDC.2020.58

Thomas BC, Melott AL, Arkenberg KR, Snyder BR (2013) Terrestrial effects of possible astrophysical sources of an AD 774–775 increase in ^{14}C production. Geophys Res Lett 40:1237–1240. https://doi.org/10.1002/grl.50222

Tinsley BA, Zhou L (2006) Initial results of a global circuit model with variable stratospheric and tropospheric aerosols. J Geophys Res 111(D10):D16205. https://doi.org/10.1029/2005JD006988

Tobias SM, Weiss NO, Kirk V (1995) Chaotically modulated stellar dynamos. Mon Not R Astron Soc 273:1150–1166. https://doi.org/10.1093/mnras/273.4.1150

Toptygin IN (1985) Cosmic rays in interplanetary magnetic fields. Geophysics and astrophysics monographs. Kluwer Academic Publishers, Dordrecht. https://doi.org/10.1007/978-94-009-5257-7

Tovar I, Aparicio AJP, Carrasco VMS, Gallego MC, Vaquero JM (2021) Analysis of solar diameter measurements made at the Basilica of San Petronio during and after the Maunder Minimum. Astrophys J 912(2):122. https://doi.org/10.3847/1538-4357/abefdb

Traversi R, Usoskin IG, Solanki SK, Becagli S, Frezzotti M, Severi M, Stenni B, Udisti R (2012) Nitrate in polar ice: a new tracer of solar variability. Sol Phys 280:237–254. https://doi.org/10.1007/s11207-012-0060-3

Tschernitz J, Veronig A, Thalmann J, Hinterreiter J, Pötzi W (2018) Reconnection fluxes in eruptive and confined flares and implications for superflares on the Sun. Astrophys J 853(1):41. https://doi.org/10.3847/1538-4357/aaa199. arXiv:1712.04701 [astro-ph.SR]

Tylka AJ, Dietrich WF, Boberg PR (1997) Probability distribution of high-energy solar-heavy-ion fluxes from IMP-8: 1973–1996. IEEE Trans Nucl Sci 44:2140–2149. https://doi.org/10.1109/23.659029

Usoskin I, Kovaltsov G (2021) Mind the gap: new precise ^{14}C data indicate the nature of extreme solar particle events. Geophys Res Lett 48(17):e94848. https://doi.org/10.1029/2021GL094848

Usoskin I, Mursula K, Kovaltsov G (2001) Was one sunspot cycle lost in late XVIII century? Astron Astrophys 370:L31–L34. https://doi.org/10.1051/0004-6361:20010319

Usoskin I, Mursula K, Solanki S, Schüssler M, Kovaltsov G (2002) A physical reconstruction of cosmic ray intensity since 1610. J Geophys Res 107(A11):1374. https://doi.org/10.1029/2002JA009343

Usoskin I, Kovaltsov G, Kiviaho W (2021a) Robustness of solar-cycle empirical rules across different series including an updated ADF sunspot group series. Sol Phys 296:13. https://doi.org/10.1007/s11207-020-01750-9. arXiv:2012.08415

Usoskin IG, Koldobskiy SA, Poluianov SV, Raukunen O, Vainio R, Kovaltsov GA (2023) Consistency of the average flux of solar energetic particles over timescales of years to megayears. Astron Astrophys Lett 670:L22. https://doi.org/10.1051/0004-6361/202245810

Usoskin IG (2011) Cosmic rays and climate forcing. Mem Soc Astron Ital 82:937–942

Usoskin IG (2017) A history of solar activity over millennia. Living Rev Sol Phys 14:3. https://doi.org/10.1007/s41116-017-0006-9

Usoskin IG, Kovaltsov GA (2004) Long-term solar activity: direct and indirect study. Sol Phys 224:37–47. https://doi.org/10.1007/s11207-005-3997-7

Usoskin IG, Kovaltsov GA (2006) Cosmic ray induced ionization in the atmosphere: full modeling and practical applications. J Geophys Res 111:D21206. https://doi.org/10.1029/2006JD007150

Usoskin IG, Kovaltsov GA (2008) Production of cosmogenic ^{7}Be isotope in the atmosphere: full 3D modelling. J Geophys Res 113:D12107. https://doi.org/10.1029/2007JD009725

Usoskin IG, Kovaltsov GA (2012) Occurrence of extreme solar particle events: assessment from historical proxy data. Astrophys J 757:92. https://doi.org/10.1088/0004-637X/757/1/92. arXiv:1207.5932 [astro-ph.SR]

Usoskin IG, Kromer B (2005) Reconstruction of the ^{14}C production rate from measured relative abundance. Radiocarbon 47:31–37

Usoskin IG, Mursula K, Kovaltsov GA (2000) Cyclic behaviour of sunspot activity during the Maunder minimum. Astron Astrophys 354:L33–L36

Usoskin IG, Mursula K, Kovaltsov GA (2001) Heliospheric modulation of cosmic rays and solar activity during the Maunder Minimum. J Geophys Res 106:16039–16046. https://doi.org/10.1029/2000JA000105

Usoskin IG, Mursula K, Kovaltsov GA (2002) Lost sunspot cycle in the beginning of Dalton minimum: New evidence and consequences. Geophys Res Lett 29:36–1. https://doi.org/10.1029/2002GL015640

Usoskin IG, Mursula K, Kovaltsov GA (2003) Reconstruction of monthly and yearly group sunspot numbers from sparse daily observations. Sol Phys 218:295–305. https://doi.org/10.1023/B:SOLA.0000013029.99907.97

Usoskin IG, Mursula K, Kovaltsov GA (2003) The lost sunspot cycle: reanalysis of sunspot statistics. Astron Astrophys 403:743–748. https://doi.org/10.1051/0004-6361:20030398

Usoskin IG, Solanki SK, Schüssler M, Mursula K, Alanko K (2003) Millennium-scale sunspot number reconstruction: evidence for an unusually active Sun since the 1940s. Phys Rev Lett 91:211101. https://doi.org/10.1103/PhysRevLett.91.211101. arXiv:astro-ph/0310823

Usoskin IG, Mursula K, Solanki SK, Schüssler M, Alanko K (2004) Reconstruction of solar activity for the last millennium using ^{10}Be data. Astron Astrophys 413:745–751. https://doi.org/10.1051/0004-6361:20031533. arXiv:astro-ph/0309556

Usoskin IG, Alanko-Huotari K, Kovaltsov GA, Mursula K (2005) Heliospheric modulation of cosmic rays: monthly reconstruction for 1951–2004. J Geophys Res 110:A12108. https://doi.org/10.1029/2005JA011250

Usoskin IG, Solanki SK, Korte M (2006) Solar activity reconstructed over the last 7000 years: the influence of geomagnetic field changes. Geophys Res Lett 33:8103. https://doi.org/10.1029/2006GL025921

Usoskin IG, Solanki SK, Kovaltsov GA, Beer J, Kromer B (2006) Solar proton events in cosmogenic isotope data. Geophys Res Lett 33:L08107. https://doi.org/10.1029/2006GL026059

Usoskin IG, Solanki SK, Taricco C, Bhandari N, Kovaltsov GA (2006) Long-term solar activity reconstructions: direct test by cosmogenic ^{44}Ti in meteorites. Astron Astrophys 457:L25–L28. https://doi.org/10.1051/0004-6361:20065803

Usoskin IG, Solanki SK, Kovaltsov GA (2007) Grand minima and maxima of solar activity: new observational constraints. Astron Astrophys 471:301–309. https://doi.org/10.1051/0004-6361:20077704. arXiv:0706.0385

Usoskin IG, Field CV, Schmidt GA, Leppänen AP, Aldahan A, Kovaltsov GA, Possnert G, Ungar RK (2009) Short-term production and synoptic influences on atmospheric ^{7}Be concentrations. J Geophys Res 114(D13):D06108. https://doi.org/10.1029/2008JD011333

Usoskin IG, Horiuchi K, Solanki SK, Kovaltsov GA, Bard E (2009) On the common solar signal in different cosmogenic isotope data sets. J Geophys Res 114(A13):A03112. https://doi.org/10.1029/2008JA013888

Usoskin IG, Mursula K, Arlt R, Kovaltsov GA (2009) A solar cycle lost in 1793–1800: early sunspot observations resolve the old mystery. Astrophys J Lett 700:L154–L157. https://doi.org/10.1088/0004-637X/700/2/L154. arXiv:0907.0063 [astro-ph.SR]

Usoskin IG, Sokoloff D, Moss D (2009) Grand minima of solar activity and the mean-field dynamo. Sol Phys 254:345–355. https://doi.org/10.1007/s11207-008-9293-6

Usoskin IG, Mironova IA, Korte M, Kovaltsov GA (2010) Regional millennial trend in the cosmic ray induced ionization of the troposphere. J Atmos Sol-Terr Phys 72:19–25. https://doi.org/10.1016/j.jastp.2009.10.003

Usoskin IG, Bazilevskaya GA, Kovaltsov GA (2011) Solar modulation parameter for cosmic rays since 1936 reconstructed from ground-based neutron monitors and ionization chambers. J Geophys Res 116:A02104. https://doi.org/10.1029/2010JA016105

Usoskin IG, Kromer B, Ludlow F, Beer J, Friedrich M, Kovaltsov GA, Solanki SK, Wacker L (2013) The AD775 cosmic event revisited: the Sun is to blame. Astron Astrophys 552:L3. https://doi.org/10.1051/0004-6361/201321080. arXiv:1302.6897 [astro-ph.SR]

Usoskin IG, Hulot G, Gallet Y, Roth R, Licht A, Joos F, Kovaltsov GA, Thébault E, Khokhlov A (2014) Evidence for distinct modes of solar activity. Astron Astrophys 562:L10. https://doi.org/10.1051/0004-6361/201423391. arXiv:1402.4720 [astro-ph.SR]

Usoskin IG, Arlt R, Asvestari E, Hawkins E, Käpylä M, Kovaltsov GA, Krivova N, Lockwood M, Mursula K, O'Reilly J, Owens M, Scott CJ, Sokoloff DD, Solanki SK, Soon W, Vaquero JM (2015) The Maunder minimum (1645–1715) was indeed a grand minimum: a reassessment of multiple datasets. Astron Astrophys 581:A95. https://doi.org/10.1051/0004-6361/201526652. arXiv:1507.05191 [astro-ph.SR]

Usoskin IG, Gallet Y, Lopes F, Kovaltsov GA, Hulot G (2016) Solar activity during the Holocene: the Hallstatt cycle and its consequence for grand minima and maxim. Astron Astrophys 587:A150. https://doi.org/10.1051/0004-6361/201527295

Usoskin IG, Kovaltsov GA, Lockwood M, Mursula K, Owens M, Solanki SK (2016) A new calibrated sunspot group series since 1749: statistics of active day fractions. Sol Phys 291:2685–2708. https://doi.org/10.1007/s11207-015-0838-1. arXiv:1512.06421 [astro-ph.SR]

Usoskin IG, Gil A, Kovaltsov GA, Mishev AL, Mikhailov VV (2017) Heliospheric modulation of cosmic rays during the neutron monitor era: calibration using PAMELA data for 2006–2010. J Geophys Res (Space Phys) 122:3875–3887. https://doi.org/10.1002/2016JA023819. arXiv:1705.07197 [physics.space-ph]

Usoskin IG, Koldobskiy S, Kovaltsov GA, Gil A, Usoskina I, Willamo T, Ibragimov A (2020a) Revised GLE database: Fluences of solar energetic particles as measured by the neutron-monitor network since 1956. Astron Astrophys 640:A17. https://doi.org/10.1051/0004-6361/202038272

Usoskin IG, Koldobskiy SA, Kovaltsov GA, Rozanov EV, Sukhodolov TV, Mishev AL, Mironova IA (2020b) Revisited reference solar proton event of 23 February 1956: assessment of the cosmogenic-isotope method sensitivity to extreme solar events. J Geophys Res (Space Phys) 125(6):e27921. https://doi.org/10.1029/2020JA027921. arXiv:2005.10597 [astro-ph.SR]

Usoskin IG, Solanki SK, Krivova N, Hofer B, Kovaltsov GA, Wacker L, Brehm N, Kromer B (2021b) Solar cyclic activity over the last millennium reconstructed from annual ^{14}C data. Astron Astrophys 649:A141. https://doi.org/10.1051/0004-6361/202140711

Uusitalo J, Arppe L, Hackman T, Helama S, Kovaltsov G, Mielikäinen K, Mäkinen H, Nöjd P, Palonen V, Usoskin I, Oinonen M (2018) Solar superstorm of AD 774 recorded subannually by Arctic tree rings. Nature Commun 9:3495. https://doi.org/10.1038/s41467-018-05883-1

Vainio R, Desorgher L, Heynderickx D, Storini M, Flückiger E, Horne RB, Kovaltsov GA, Kudela K, Laurenza M, McKenna-Lawlor S, Rothkaehl H, Usoskin IG (2009) Dynamics of the Earth's particle radiation environment. Space Sci Rev 147:187–231. https://doi.org/10.1007/s11214-009-9496-7

Vaquero JM (2007) Historical sunspot observations: a review. Adv Space Res 40:929–941. https://doi.org/10.1016/j.asr.2007.01.087. arXiv:astro-ph/0702068

Vaquero JM, Trigo RM (2015) Redefining the limit dates for the Maunder Minimum. New Astron 34:120–122

Vaquero JM, Vázquez M (2009) The Sun recorded through history: scientific data extracted from historical documents. Astrophysics and Space Science Library, vol 361. Springer, New York. https://doi.org/10.1007/978-0-387-92790-9

Vaquero JM, Gallego MC, García JA (2002) A 250-year cycle in naked-eye observations of sunspots. Geophys Res Lett 29:58–1. https://doi.org/10.1029/2002GL014782

Vaquero JM, Trigo RM, Gallego MC (2005) A 'lost' sunspot observation in 1785. Astron Nachr 326:112–114. https://doi.org/10.1002/asna.200410343

Vaquero JM, Trigo RM, Gallego MC, Moreno-Corral MA (2007) Two early sunspots observers: Teodoro de Almeida and José Antonio Alzate. Sol Phys 240:165–175. https://doi.org/10.1007/s11207-006-0264-5

Vaquero JM, Gallego MC, Usoskin IG, Kovaltsov GA (2011) Revisited sunspot data: a new scenario for the onset of the Maunder minimum. Astrophys J Lett 731:L24. https://doi.org/10.1088/2041-8205/731/2/L24. arXiv:1103.1520 [astro-ph.SR]

Vaquero JM, Trigo RM, Gallego MC (2012) A simple method to check the reliability of annual sunspot number in the historical period 1610–1847. Sol Phys 277:389–395. https://doi.org/10.1007/s11207-011-9901-8. arXiv:1111.2633 [astro-ph.SR]

Vaquero JM, Gutiérrez-López S, Szelecka A (2014) A note on the relationship between sunspot numbers and active days. Adv Space Res 53:1180–1183. https://doi.org/10.1016/j.asr.2014.01.029. arXiv:1401.7037 [astro-ph.SR]

Vaquero JM, Kovaltsov GA, Usoskin IG, Carrasco VMS, Gallego MC (2015) Level and length of cyclic solar activity during the maunder minimum as deduced from the active day statistics. Astron Astrophys 577:A71. https://doi.org/10.1051/0004-6361/201525962

Vaquero JM, Svalgaard L, Carrasco VMS, Clette F, Lefèvre L, Gallego MC, Arlt R, Aparicio AJP, Richard JG, Howe R (2016) A revised collection of sunspot group numbers. Sol Phys 291:3061–3074. https://doi.org/10.1007/s11207-016-0982-2. arXiv:1609.04882 [astro-ph.SR]

Vasiliev SS, Dergachev VA (2002) The ∼2400-year cycle in atmospheric radiocarbon concentration: bispectrum of ^{14}C data over the last 8000 years. Ann Geophys 20:115–120. https://doi.org/10.5194/angeo-20-115-2002

Vasiliev SS, Dergachev VA, Raspopov OM, Jungner H (2012) Long-term variations in the flux of cosmogenic isotope ^{10}Be over the last 10000 years: variations in the geomagnetic field and climate. Geomagn Aeron 52:121–128. https://doi.org/10.1134/S001679321201015X

Vázquez M, Vaquero JM (2010) Aurorae observed at the Canary Islands. Sol Phys 267:431–444. https://doi.org/10.1007/s11207-010-9650-0

Veronig AM, Odert P, Leitzinger M, Dissauer K, Fleck NC, Hudson HS (2021) Indications of stellar coronal mass ejections through coronal dimmings. Nature Astron 5:697–706. https://doi.org/10.1038/s41550-021-01345-9. arXiv:2110.12029 [astro-ph.SR]

Vieira LEA, Solanki SK, Krivova NA, Usoskin IG (2011) Evolution of the solar irradiance during the Holocene. Astron Astrophys 531:A6. https://doi.org/10.1051/0004-6361/201015843. arXiv:1103.4958 [astro-ph.SR]

Viereck RA, Puga LC (1999) The NOAA Mg II core-to-wing solar index: construction of a 20-year time series of chromospheric variability from multiple satellites. J Geophys Res 104:9995–10006. https://doi.org/10.1029/1998JA900163

Vitinsky YI (1965) Solar activity forecasting. Israel Program for Scientific Translations, Jerusalem

Vitinsky YI, Kopecky M, Kuklin GV (1986) Statistics of sunspot activity. Nauka, Moscow (In Russian)

Vogt S, Herzog GF, Reedy RC (1990) Cosmogenic nuclides in extraterrestrial materials. Rev Geophys 28:253–275. https://doi.org/10.1029/RG028i003p00253

Vonmoos MV, Beer J, Muscheler R (2006) Large variations in Holocene solar activity: constraints from ^{10}Be in the Greenland Ice Core Project ice core. J Geophys Res 111(A10):A10105. https://doi.org/10.1029/2005JA011500

Vos EE, Potgieter MS (2015) New modeling of galactic proton modulation during the minimum of solar cycle 23/24. Astrophys J 815:119. https://doi.org/10.1088/0004-637X/815/2/119

Voss H, Kurths J, Schwarz U (1996) Reconstruction of grand minima of solar activity from Δ^{14}C data: linear and nonlinear signal analysis. J Geophys Res 101:15,637-15,644. https://doi.org/10.1029/96JA00542

Waldmeier M (1935) Neue Eigenschaften der Sonnenflecken Kurve. Astron Mitt Z 6:105–130

Waldmeier M (1939) Die Zonenwanderung der Sonnenflecken. Astron Mitt Zurich 14:470–481

Waldmeier M (1961) The sunspot-activity in the years 1610–1960. Schulthess u. Co. / Swiss Federal Observatory, Zürich

Wang YM, Sheeley NR Jr (2012) The solar wind and interplanetary field during very low amplitude sunspot cycles. Astrophys J 764:90. https://doi.org/10.1088/0004-637X/764/1/90

Wang YM, Lean J, Sheeley NR Jr (2005) Modeling the Sun's magnetic field and irradiance since 1713. Astrophys J 625:522–538. https://doi.org/10.1086/429689

Webber WR, Higbie PR (2003) Production of cosmogenic Be nuclei in the Earth's atmosphere by cosmic rays: its dependence on solar modulation and the interstellar cosmic ray spectrum. J Geophys Res 108:1355. https://doi.org/10.1029/2003JA009863

Webber WR, Higbie PR (2009) Galactic propagation of cosmic ray nuclei in a model with an increasing diffusion coefficient at low rigidities: a comparison of the new interstellar spectra with Voyager data in the outer heliosphere. J Geophys Res 114:A02103. https://doi.org/10.1029/2008JA013689

Webber WR, Higbie PR, McCracken KG (2007) Production of the cosmogenic isotopes ^{3}H, ^{7}Be, ^{10}Be, and ^{36}Cl in the Earth's atmosphere by solar and galactic cosmic rays. J Geophys Res 112:A10106. https://doi.org/10.1029/2007JA012499

Webber WR, Cummings AC, McDonald FB, Stone EC, Heikkila B, Lal N (2008) Galactic cosmic ray H and He nuclei energy spectra measured by Voyagers 1 and 2 near the heliospheric termination shock in positive and negative solar magnetic polarity cycles. J Geophys Res 113(A12):A10108. https://doi.org/10.1029/2008JA013395

Weiss NO, Tobias SM (2000) Physical causes of solar activity. Space Sci Rev 94:99–112. https://doi.org/10.1023/A:1026790416627

Weiss NO, Cattaneo F, Jones CA (1984) Periodic and aperiodic dynamo waves. Geophys Astrophys Fluid Dyn 30:305–341. https://doi.org/10.1080/03091928408219262

Weisshaar E, Cameron RH, Schüssler M (2023) No evidence for synchronization of the solar cycle by a "clock". Astron Astrophys 671:A87. https://doi.org/10.1051/0004-6361/202244997

Wheatland MS (2003) The coronal mass ejection waiting-time distribution. Sol Phys 214:361–373. https://doi.org/10.1023/A:1024222511574. arXiv:astro-ph/0303019

Willamo T, Usoskin IG, Kovaltsov GA (2017) Updated sunspot group number reconstruction for 1749–1996 using the active day fraction method. Astron Astrophys 601:A109. https://doi.org/10.1051/0004-6361/201629839. arXiv:1705.05109 [astro-ph.SR]

Willamo T, Usoskin IG, Kovaltsov GA (2018) A test of the active-day fraction method of sunspot group number calibration: dependence on the level of solar activity. Sol Phys 293(4):69. https://doi.org/10.1007/s11207-018-1292-7. arXiv:1803.10501 [astro-ph.SR]

Willis DM, Stephenson FR (2001) Solar and auroral evidence for an intense recurrent geomagnetic storm during December in AD 1128. Ann Geophys 19:289–302. https://doi.org/10.5194/angeo-19-289-2001

Willis DM, Easterbrook MG, Stephenson FR (1980) Seasonal variation of oriental sunspot sightings. Nature 287:617–619. https://doi.org/10.1038/287617a0

Willis DM, Davda VN, Stephenson FR (1996) Comparison between oriental and occidental sunspot observations. Quart J R Astron Soc 37:189–229

Willis DM, Wild MN, Warburton JS (2016) Re-examination of the daily number of sunspot groups for the royal observatory, Greenwich (1874–1885). Sol Phys 291:2519–2552. https://doi.org/10.1007/s11207-016-0856-7

Wilson PR (1994) Solar and stellar activity cycles, Cambridge astrophysics series, vol 24. Cambridge University Press, Cambridge; New York

Wilson RM (1988) Bimodality and the hale cycle. Sol Phys 117:269–278. https://doi.org/10.1007/BF00147248

Wilson RM (1988) On the long-term secular increase in sunspot number. Sol Phys 115:397–408. https://doi.org/10.1007/BF00148736

Wilson RM (1998) A comparison of Wolf's reconstructed record of annual sunspot number with Schwabe's observed record of 'clusters of spots' for the interval of 1826–1868. Sol Phys 182:217–230. https://doi.org/10.1023/A:1005046820210

Wittmann AD, Xu ZT (1987) A catalogue of sunspot observations from 165 BC to AD 1684. Astron Astrophys Suppl 70:83–94

Wolff EW, Bigler M, Curran MAJ, Dibb JE, Frey MM, Legrand M, McConnell JR (2012) The Carrington event not observed in most ice core nitrate records. Geophys Res Lett 39:L08503. https://doi.org/10.1029/2012GL051603

Wu CJ, Krivova NA, Solanki SK, Usoskin IG (2018) Solar total and spectral irradiance reconstruction over the last 9000 years. Astron Astrophys 620:A120. https://doi.org/10.1051/0004-6361/201832956. arXiv:1811.03464 [astro-ph.SR]

Wu CJ, Usoskin IG, Krivova N, Kovaltsov GA, Baroni M, Bard E, Solanki SK (2018) Solar activity over nine millennia: a consistent multi-proxy reconstruction. Astron Astrophys 615:A93. https://doi.org/10.1051/0004-6361/201731892. arXiv:1804.01302 [astro-ph.SR]

Yau KKC, Stephenson FR (1988) A revised catalog of far eastern observations of sunspots (165 BC to AD 1918). Quart J R Astron Soc 29:175–197

Yeo KL, Krivova NA, Solanki SK (2014) Solar cycle variation in solar irradiance. Space Sci Rev 186:137–167. https://doi.org/10.1007/s11214-014-0061-7. arXiv:1407.4249 [astro-ph.SR]

Yiou F, Raisbeck GM, Baumgartner S, Beer J, Hammer C, Johnsen S, Jouzel J, Kubik PW, Lestringuez J, Stiévenard M, Suter M, Yiou P (1997) Beryllium 10 in the Greenland ice core project ice core at Summit, Greenland. J Geophys Res 102:26,783-26,794. https://doi.org/10.1029/97JC01265

Yule GU (1927) On a method of investigating periodicities in disturbed series, with special reference to Wolfer's sunspot numbers. Philos Trans R Soc London Ser A 226:267–298. https://doi.org/10.1098/rsta.1927.0007

Zeller EJ, Dreschhoff GAM (1995) Anomalous nitrate concentrations in polar ice cores—do they result from solar particle injections into the polar atmosphere? Geophys Res Lett 22:2521–2524. https://doi.org/10.1029/95GL02560

Zharkova VV, Shepherd SJ, Popova E, Zharkov SI (2015) Heartbeat of the Sun from Principal Component Analysis and prediction of solar activity on a millenium timescale. Sci Rep 5:15689. https://doi.org/10.1038/srep15689

Zhentao X (1990) Solar observations in ancient china and solar variability. Philos Trans R Soc London Ser A 330:513–516. https://doi.org/10.1098/rsta.1990.0032

Zięba S, Nieckarz Z (2014) Sunspot time series: passive and active intervals. Sol Phys 289:2705–2726. https://doi.org/10.1007/s11207-014-0498-6

Zolotova NV, Ponyavin DI (2011) Enigma of the solar cycle 4 still not resolved. Astrophys J 736:115. https://doi.org/10.1088/0004-637X/736/2/115

Zolotova NV, Ponyavin DI (2015) The Maunder minimum is not as grand as it seemed to be. Astrophys J 800:42. https://doi.org/10.1088/0004-637X/800/1/42

Authors and Affiliations

Ilya G. Usoskin[1] (ORCID)

✉ Ilya G. Usoskin
   ilya.usoskin@oulu.fi

1   Space Physics and Astronomy Research Unit and Sodankylä Geophysical Observatory (Oulu unit), University of Oulu, 90014 Oulu, Finland